TC
1501
.N6
no.1

NOAA Technical Memorandum OTES 01

MONTE CARLO SIMULATIONS OF THE EFFECTS OF UNDERWATER PROPAGATION ON THE PENETRATION AND DEPTH MEASUREMENT BIAS OF AN AIRBORNE LASER BATHYMETER

Rockville, Md.
March 1981

U.S. DEPARTMENT OF COMMERCE / National Oceanic and Atmospheric Administration / Ocean Technology and Engineering Services

NOAA CENTRAL LIBRARY
1315 East West Highway
2nd Floor, SSMC3, E/OC4
Silver Spring, MD 20910-3281

TC
1501
.N6
no.1

NOAA Technical Memorandum OTES 01

MONTE CARLO SIMULATIONS OF THE EFFECTS OF UNDERWATER PROPAGATION ON THE PENETRATION AND DEPTH MEASUREMENT BIAS OF AN AIRBORNE LASER BATHYMETER

Gary C. Guenther
Engineering Development Office

Robert W. L. Thomas
EG&G/Washington Analytical Services
Center, Inc.

Rockville, Md.
March 1981

LIBRARY
APR 2 5 1994
N.O.A.A.
U.S. Dept. of Commerce

UNITED STATES
DEPARTMENT OF COMMERCE
Malcolm Baldrige, Secretary

National Oceanic and
Atmospheric Administration
James P. Walsh, Acting Administrator

Ocean Technology and
Engineering Services
M. E. Ringenbach, Director

Mention of a commercial company or product does not constitute an endorsement by NOAA (OA/OTES). Use for publicity or advertising purposes of information from this publication concerning proprietary products or the tests of such products is not authorized.

CONTENTS

FIGURES

ABSTRACT

This report documents the results of a Monte Carlo simulation of underwater light pulse propagation for a geometry applicable to airborne lidar. Actual lidar bottom return pulses will vary considerably in shape and arrival time depending on the water depth, the scanner nadir angle, the incident laser pulse width, the optical properties of the water, the airborne system signal processing electronics, and the depth determining algorithm or procedure. These perturbations of the return signals will cause depth measurement biases which can be considerably larger than the International Hydrographic Bureau shallow water accuracy requirement. The first step in the estimation of these bias errors is the determination of the impulse response functions of the medium for various permutations of the relevant optical parameters. An output data set consisting of 640 impulse response functions has been generated which provides the basic results of this phase of the investigation.

In general, bias error predictions can be used as bias error correctors which, when applied to the raw depth measurements during post-flight data processing, will significantly reduce the magnitude of the errors. Example bias predictor/correctors have been calculated from the impulse responses alone. These predictors, which are valid only for the case where the impulse response temporal width is very long compared to the incident laser pulse width (i.e., deep water) and where the signals are processed linearly with a fractional amplitude threshold for the depth determining algorithm, are reported and discussed for a wide range of nadir angle, optical depth, single-scatter albedo, and depth algorithm threshold fraction.

The bias predictors are necessarily parameterized on their driving, inherent optical properties (i.e., beam attenu-

ation coefficient and single-scattering albedo). Neither of these optical properties will be directly measured in the field as part of a typical airborne survey. It is thus necessary to provide continuous estimates of their values based solely on specially processed, ancillary flight data, or to restrict operational parameters in such a way that the resulting biases are small enough to permit ad hoc correction. A preliminary discussion of the required data and how one might make these determinations is reported.

1.0 INTRODUCTION

A Monte Carlo simulation program has been developed and exercised to model airborne lidar depth measurement biases caused by radiative transfer processes for impulse laser inputs to a water column. The water parameters and system constraints of the computation are appropriate to airborne laser hydrography systems presently under consideration for use in coastal waters.

Earlier analytical computations by Thomas and Guenther (1979) have indicated the possibility of a significant bias on the deep side for operations of the system at nadir. This bias arises from the multipath transport mechanism by which the laser radiation penetrates the water and is subsequently reflected back through the water to the receiver. This is the so-called "pulse stretching" effect. The impact of this effect on the estimated depth is influenced both by the temporal profile of the incident laser pulse and the return pulse processing electronics, but the key to the quantification of the effect is the generation of a set of response functions for the medium which characterize the temporal history of radiation reaching the receiver for an impulse input.

Monte Carlo simulation is the only practical method of generating the impulse response functions. If other theories existed for computing these functions, they would have to be subjected to simulation validation before we could be confident that the generated function was appropriate to the specified inherent properties of the water column. The Monte Carlo results have been successfully validated (see Section 2.4) by comparing certain basic outputs with previously documented relationships from the literature such as the ratio of diffuse to beam attenuation coefficients versus single-scattering albedo (Gordon et al. 1975, Timofeyeva 1972).

Section 2.0 contains a detailed description of the relevant physical processes, the mechanics of the simulation, the form and utility of the results, and the validation criteria. Section 3.0 describes the results obtained from analysis of the simulation outputs. Subsections discuss the energy and power relationships and the impulse response and depth measurement bias results which are presented in two basic sections: first a sensitivity study in which each of the major parameters is varied in turn against a representative background of the remaining parameters; and second, a selection of cases of special interest.

Depth measurement bias predictions are parameterized on inherent water properties (such as beam attenuation coefficient and single-scattering albedo) and system constraints. <u>If</u> these parameters are known or can be estimated, the bias <u>predictions</u> obtained from the simulation can be suitably modified to account for depth dependence and system electronics and applied to field data as "bias correctors" to reduce the magnitude of the raw biases in post-processing. This technique is considered mandatory if international hydrographic accuracy standards are to be met. Estimation of the relevant inherent water parameters from ancillary airborne lidar data poses a serious problem which will strongly impact system data processing requirements. Preliminary analyses and conclusions in this area are reported in Section 4.0 which describes the protocol which will be required to actually perform bias corrections. Overall conclusions follow in Section 5.0.

2.0 SIMULATION OF THE TRANSPORT OF LIGHT THROUGH THE WATER

2.1 The Relevant Physical Processes

A schematic illustration of the radiation transport relevant to a bathymetric lidar is given in Fig. 1. The laser pulse is incident on a region of the surface whose size depends on the altitude of the aircraft and the beam divergence. Each segment of the beam or ray is diverted by refraction at the surface this contributes to somewhat increased divergence beneath the surface.

Within the water the two principal mechanisms of interest are scattering and absorption. The path of a typical photon that might be received after reflection at the bottom is illustrated. It will be observed that the path involves a number of scattering events, and at each one of these events there is a certain probability of absorption. Thus the received photons have not only been scattered in an appropriate direction but also have avoided absorption within the transit path.

Some of the incident photons will be scattered back to the surface without reflection at the bottom; if these reach the receiver they contribute to the so-called volume backscattering. In a lidar system, the energy reflected from the bottom must be sufficiently large for it is to be detected in the presence of this volume backscattering.

2.2 The Simulation Method

In the Monte Carlo approach we model the transport of representative photons through a homogeneous water column to the bottom. A schematic diagram of the simulation geometry is given in Fig. 2. We consider photons incident on the surface at time t=0 in a direction making an angle ψ with the nadir. The surface at the point of incidence is considered to be horizontal so that the nadir angle of transport immediately beneath the surface is given by Snell's Law,

$$\sin\phi = \frac{\sin\psi}{\mu}, \qquad (1)$$

where μ is the refractive index of water (1.33). In this treatment all deviations of the incident ray arising from surface wave slopes have been neglected. The random pointing or "beam steering" errors caused by surface waves must be treated separately as a depth measurement precision loss.

In treating the scattering events in the water, paths between successive scatterings are exponentially distributed with a constant mean free path. That is, we assume that the distance L covered between scattering is distributed as

$$p(L)dL = \frac{1}{q} e^{-\frac{L}{q}} dL, \qquad (2)$$

where q is the mean free path.

Such a distribution is achieved by setting

$$L = -q\ell n\ \rho, \qquad (3)$$

where ρ is a rectangularly distributed random number in the interval (0,1).

Traditionally, the mean free path for radiation transport through water has been described through a parameter called the "narrow-beam attenuation coefficient" (α). The narrow-beam attenuation is comprised of two components, scattering and absorption, as illustrated in Fig. 3. If "s" is the scattering coefficient and "a" is the absorption coefficient, then

$$\alpha = a + s. \tag{4}$$

If a beam of intensity I_0 is incident on a column of water, then the amount that remains unscattered and also not absorbed after travelling a distance L is $I_0 \exp(-\alpha L)$. Thus the mean free path, q, is equal to α^{-1}.

The vertical "optical depth" of the medium, defined as the number of mean free path lengths required to vertically traverse the medium to the bottom for a depth D, is D/q which is equal to αD.

The "albedo for single scattering," ω_0, is defined as the average fraction of the incident energy at any scattering event that is not absorbed; i.e.,

$$\omega_0 = \frac{\alpha - a}{\alpha} = \frac{s}{\alpha}. \tag{5}$$

For typical coastal waters ω_0 is believed to range from about 0.55 to 0.9. In the simulations, photons are not actually eliminated by absorption as they might be in the real world. Rather, we represent the behavior of a photon ensemble by retaining a photon weight (initially unity) and multiplying it by the single-scattering albedo, ω_0, at each scattering event. In this way we can conveniently accumulate results for several values of ω_0 at the same time.

Photons are considered to change direction at all scattering events as illustrated in Fig. 4. The scattering angle θ from the incident direction is generated according to the "phase function", $P(\theta)$, which defines the probability that the photon will scatter into a unit solid angle between θ and $\theta+d\theta$. Since the solid angle between θ and $\theta+d\theta$ is $2\pi \sin\theta \, d\theta$, the probability of occurence of θ in θ to $\theta+d\theta$ is

$$P'(\theta)\, d\theta = 2\pi \sin\theta \, P(\theta)\, d\theta . \quad (6)$$

Typical phase functions for water exhibit a very strong forward scattering effect (Petzold 1972) as will be discussed in Section 3.1. The phase functions increase by a factor of more than 1000 as the scattering angle diminishes from 10° to 0.1°. The physical reason for this phenomenon appears to be the proximity of the refractive index of the scattering agent to that of the ambient water (Gordon 1974). (Note that if the refractive indices were identical there would be no scattering, and the phase function would be a delta function at zero degrees).

The value of each scattering angle, θ_k, is generated by solving the equation

$$\int_0^{\theta_k} p'(\theta)\, d\theta = 4\pi\, \rho \, , \quad (7)$$

where ρ is a rectangularly distributed random number between 0 and 1. This equation is solved by linear interpolation within a look-up table of the value of the integral as a function of θ_k.

The parameters, αD, ω_0, and $P(\theta)$ are the "inherent" description of the transport medium characterics required for the simulation. The relationships between these parameters and the parameters governing the "apparent" properties of the medium have been discussed by Gordon, Brown, and Jacobs (1975). The most important parameter of the apparent properties is K, the so-called "diffuse oceanographic attenuation coefficient", which is defined as the fractional rate of decay of the downwelling flux (i.e., the sum of all radiation reaching a given depth) as the depth is increased. For small depths, K depends on both the depth itself and the angle of incidence of the radiation at the surface; but for larger depths these dependences become very small. K is properly measured at or corrected to nadir entry. The ratio, K/α, is a monotonically decreasing function of ω_0 which has a value of unity when ω_0 is zero and which decreases towards zero as ω_0 tends to unity. There is a small dependence on the phase function, but this is not significant for realistic coastal waters.

The lengths of the photon paths for the photons reaching the bottom are summed to allow an evaluation of the associated time delay. The minimum time of transit to the bottom is

$$t_w = \frac{D}{c_w} , \tag{8}$$

where c_w is the velocity of light in water. The "time delay" for paths of length L_i is then computed as

$$t_D = \frac{1}{c_w}\left(\sum_{i=1}^{n} L_i - D\right) \quad . \tag{9}$$

By repeating this computation for a large number of downwelling photons we can compute the downwelling impulse response function $d(t_D)$ as a histogram representing the probability distribution of arrival times of incident photons at the bottom.

An important gain in the information content of the results arises from the realization that, for given values of αD and ω_0, all temporal results scale linearly with the depth, D. This is illustrated in Fig. 5 where we show representative photon paths for two cases with the same αD but with different values of D. The photon paths for the two cases are geometrically "similar" so that the fractional time delays t_D/t_w, are identical. Therefore the absolute time delays scale linearly with D, and one set of simulated results can be used to determine absolute results for all depths.

In order to increase the efficiency of the simulations further, we sample the times of first crossings of a number of intermediate levels on the way to the bottom. The intermediate levels are characterized by the appropriate values of αD, and, since the medium is homogeneous, the value of D in the simulation scales linearly with αD. Because of the above scaling law we are able to arbitrarily set to unity the depth D_{max} corresponding to the largest value of αD, namely, αD_{max}, so that in the computations the value of q is $(\alpha D_{max})^{-1}$.

The impulse response that is finally needed from the simulations is that for radiation returning to a distant receiver co-located with the source. Our early attempts to obtain this result were based on concepts of "virtual photon" sampling similar to those developed by Holland, Thomas and Pearce (1977). The basic idea in this approach is illustrated in Fig. 6. Each event (i.e., scattering or absortion) in the track of the real photon offers an opportunity for radiation to be directed towards the receiver, and if a photon were scattered in the correct direction it would have a finite probability of being appropriately refracted at the surface and entering the receiver. Thus at each scattering event we compute a receiver sample value by multiplying the residual photon weight by two factors:

1. the probability P_1 of scattering into unit solid angle in the direction required for refraction at the surface and into the receiver; and

2. the probability P_2 that the photon would survive the transit to the receiver without scattering or absorption.

Virtual photon sampling is of considerable value in many cases where there is a very low probability of actually receiving or detecting an input photon. In this case a very large number of photon tracks might have to be simulated before a single photon would be sampled and, of course, a much longer simulation still would be required to generate a statistically meaningful sample.

In the case of laser bathymetry simulation, however, we experienced difficulty in computing a result that was reproducible when using different seeds for the random number generator. This problem was tracked to the fact that a small number of samples exhibited very large weights associated with very large values of the probability, P_1. These situations arose when there was only a small deviation required in the path of the real photon to generate the virtual photon path. Since the phase function increases very rapidly for small angles, the few cases with small angle scattering could dominate the entire signal.

We attempted to alleviate this problem through the use of "importance" sampling (Hammersley and Handscomb 1965). In this technique, the photons reflected at the bottom are distributed in a region close to paths required for transit to the receiver, and appropriate renormalizing factors are applied. This did increase the information concerning those photons with very large weights but failed to provide a significant improvement in reproducibility. We were therefore forced to establish a less direct method of estimating the receiver response function -- one that does not involve the sampling of virtual photons.

With this in mind we developed a procedure based on a "reciprocity" principal (Chandrasekhar 1960) which states the <u>statistical</u> description of downwelling paths is identical to that of the upwelling paths. This is not declaration that the downwelling and upwelling paths are the same, but rather that the simulated downwelling photon tracks can be regarded as representative for both cases. Thus the computed impulse response $d(t_D)$ for downwelling transport forms the basis for the determination of the two way impulse response.

<u>If</u> the bottom reflection were regarded as isotropic, then reflection into a given solid angle in every direction would be equally likely. In this case we could estimate the receiver response function by regarding $d(t_D)$ to be the distribution function describing <u>both</u> downwelling and upwelling radiation. Very little data exists on the actual directional reflectivity of the ocean bottom, so we chose the traditional approach of assuming that the bottom is a Lambertian reflector; i.e., that the probability of reflection at a zenith angle Z is proportional to cos Z. This type of reflection results in a uniformly bright appearance of the illuminated surface independent of the viewing angle in the absence of the turbid medium. The Lambertian type of reflection results in a modified upwelling distribution $u(t_D)$ compiled by multiplying the samples of $d(t_D)$ by cos Z where Z, in this case, is the nadir angle of the photon arriving at the ocean floor. The sampled function $u(t_D)$, is considered to characterize the airborne receiver response for photons released from the bottom (all at time t=0). Just as for $d(t_D)$, the minimum time for any sample $u(t_D)$ is t_W given by Eq. (8).

Finally, we compute the receiver response function r(T) at a time T following the earliest possible round trip return. We note that if this return arises from downwelling photons with a time delay t_1, then the value of t_2, the time delay required for the upwelling path, is $T-t_1$. Thus the value of r(T) can be expressed by the integration of the product of $d(t_1)$ and $u(t_2)$ over all such cases:

$$r(T) = \int_0^T d(t_1)\, u(T-t_1)\, dt_1. \tag{10}$$

This is, of course, the convolution of u over d. The functions u and d are actually constructed by discrete samples during an interval $\Delta \cdot t_w$ where Δ is a small fraction (typically 0.005), and t_w, as before, is the vertical transit time for unscattered photons. The function r(t) is then constructed for discrete values of $T = nt_w\Delta$ (where n is an integer) by the following digital convolution of d and u:

$$r(n) = \sum_{m=1}^{n} d(m)\, u(n-m+1), \tag{11}$$

where d(m) is the sample of d collected such that

$$(m-1)t_w\Delta \leq t_D < m\, t_w\Delta, \tag{12}$$

and similarly for u(m). The value of r computed in this way has an associated time unit of $t_w\Delta$.

The act of convolving the functions d and u is an integration, and, as such, it has the effect of reducing the magnitude of statistical noise in the resulting function. It has been found that the function r(T) is acceptably reproducible for simulations of as low as 10,000 photons when the program is rerun with different starting random numbers; this adds confidence to the results.

When the time increment Δ is set to 0.005, the maximum time delay sampled is $0.25\ t_w$ ($=50\ t_w\Delta$). This means that only that part of the return occurring with a time delay (over the vertical two-way transit time) less than one quarter of the depth transit time is generated. This is normally the region within which the peak of the return power occurs, but, for large values of αD and large nadir angles, larger values of Δ must be used. Specifically, $\Delta=0.01$ was employed in these cases. The restriction of considering only the delay times up to $0.25\ t_w$ or $0.50\ t_w$ is important in limiting the simulation time requirements since any photons that were delayed by more than these amounts (compared to radiation travelling vertically downwards) can be eliminated from the simulations.

The depth measurement bias errors are estimated by applying fractional threshold detectors to the computed receiver response function, $r(T)$. The "reference time", T_R, for this computation is the time delay for radiation travelling unscattered (at the refraction angle ϕ) to the bottom and then being reflected back along the same path. This time delay is

$$T_R = 2t_w\ (\sec\phi-1). \tag{13}$$

For the nadir case, of course, ϕ is zero, so that T_R is zero. Thus only positive (deep) errors in depth estimates can be contributed by propagation effects in this case. For the off-nadir cases, however, both positive and negative errors can occur. Negative (shallow) errors arise from a favoring of paths closer to vertical, since these are the ones for which absorption is less likely to occur. This is the so-called "undercutting" effect where bottom reflection occurs predominately "beneath" the unscattered ray, and a significant amount of energy is returned <u>before</u> the reference delay time, T_R, as illustrated in Fig. 7.

Although a specific receiver field of view is not directly applied in the simulation, an effective field-of-view restriction is caused by the truncation of paths which have been judged to be excessively long (by the previously mentioned time increment criterion). This restriction applies only to photons which would have arrived in the trailing edge of the impulse response and in no way affects the leading edge or the peak power. Thus, the effective field of view is large but considerably less than unlimited, and probably represents a fairly realistic situation.

2.3 Interpretation of The Results

2.3.1 Energy and Peak Power Relationships

The simulations generate impulse response functions for the receiver as a function of the albedo for single scattering, ω_0, and the vertical optical depth, αD. All results are normalized such that

1. the input energy is unity,

2. the depth transit time is unity, and

3. the sampling interval is Δ.

The reported peak power value P_r is the sampled energy for a time interval that in the real world is $t_w\Delta$. Thus, if r_{max} is the peak power in units of energy/second, we have

$$r_{max} = \frac{P_r}{t_w \Delta} \ . \tag{14}$$

A separate set of simulations was performed for nadir entry with much larger values of Δ such that the time delay 50Δ includes virtually all of the return. This allows the estimation of the total return energy, R, where

$$R = \int_0^\infty r(T)\ dT, \tag{15}$$

for unit input energy.

In practice, of course, the input laser pulse is not an impulse but is distributed over time. Let s(t) represent the laser output power as a function of time (in watts), and let S(joules) be the total output energy of the pulse. Then

$$S = \int_0^\infty s(t)\ dt\ . \tag{16}$$

The true response of the receiver, v(T), at time T following the earliest possible round trip return is given by the convolution of s(t) over r(t), the impulse response function; i.e.,

$$v(T) = \int_0^T s(t)\ r(T-t)\ dt. \tag{17}$$

The total return energy is given by

$$V = \int_0^\infty v(T)\, dT \, . \tag{18}$$

Remembering that $r(t) = s(t) = 0$ for all t less than zero, it is easy to show by Eqs. (17) and (18) that

$$V = SR, \tag{19}$$

which simply states that the total return energy is the total input pulse energy multiplied by the return energy per unit input given by Eq. (15).

We now consider two limiting cases:

1. The case where the impulse response function is narrow compared to the laser pulse. This will apply for small depths and small values of αD. In this case the laser pulse power $s(t)$ changes very little over the values of t during which r is significant, and equation (17) becomes

$$v(T) = s(T) \int_0^T r(T-t)\, dt. \tag{20}$$

Since r(T-t) is non-zero only for small values of t, the upper limit of integration may be replaced by infinity giving

$$v(T) = R\, s(T). \tag{21}$$

The peak power of the return in this case is then

$$P_s = R\, s_{max}, \tag{22}$$

where s_{max} is the peak power of the source laser pulse.

2. The case where the impulse response function is broad compared to the laser pulse. This will apply for large depths and large values of αD. By an argument similar to the above, Eq. (17) in this case reduces to

$$v(T) = S\, r(T). \tag{23}$$

The peak power of the return in this case is

$$P_L = S \; r_{max}. \tag{24}$$

Using Eq. (14), we can rewrite Eq. (24) as

$$P_L = \frac{S \; P_r}{t_w \Delta} \; . \tag{25}$$

The results in Eqs. (22) and (25) must be multiplied by a factor to account for surface transmission, receiver altitude, and receiver characteristics, but the same factor is applicable in both cases. We can therefore compare the results in Eqs. (22) and (25) directly.

Since R is a function of αD but not of D alone, the peak power P_s for the short impulse response is independent of true depth. The peak power for the long impulse response function P_L, however, is inversely proportional to t_w, and therefore varies inversely with the true depth as well as with αD.

The ratio of the peak powers given in Eqs. (22) and (25) can be written as

$$\frac{P_s}{P_L} = t_w \Delta \left(\frac{P_r}{R}\right)^{-1} \left(\frac{s_{max}}{S}\right) , \tag{26}$$

which demonstrates that the durations and shapes of the impulse response and the incident laser pulse have a significant role in affecting the peak receiver power and will impact the transition from case (1) to case (2). Equation (26) gives a ratio for the peak powers in the limiting cases.

2.3.2 Bias Estimation

We can gain approximate estimates of the potential biases by applying a linear fractional-threshold detector to the impulse responses. In this method we compute the time, t_f, at which the impulse response rises through a given fraction, f, of the peak response. Since our simulation results are referenced to unit depth and unit velocity of light, we must convert to a specific depth in the real world by multiplying by t_w, the depth transit time. Thus we compute the time bias as

$$T_B = t_w \cdot t_f - T_R , \tag{27}$$

and, using Eq. (13), we have

$$T_B = t_w \{t_f - 2(\sec\phi - 1)\} . \tag{28}$$

In most of our presentations we have assumed a depth of 20 m, since this is the greatest depth at which the International Hydrographic Bureau (Special Publication No. 44, 1968) requires an accuracy of one foot (30cm). In this case, t_w is 88.7 ns.

Note that in the analysis of the impulse responses the fractional depth error is independent of the true depth. This is because the two-way transit time for unscattered light is $2t_w \sec\phi$ so that the fractional error is given by

$$F(f) \equiv \frac{T_B}{2t_w \sec\phi} , \quad (29)$$

which, by Eqs. (27) and (13), becomes

$$F(f) = (t_f/2+1)\cos\phi - 1. \quad (30)$$

It is not possible to relate the bias computed by these formulae in a simple way to that associated with an input pulse of finite duration. For very short laser pulses the bias corrector will be accurate. For long input pulses, the bias may be larger or smaller than the value given -- with a greater potential for error in the corrector as the input pulse duration increases. A formal estimate of the bias associated with the pulse stretching phenomenon requires the convolution of typical source pulse shapes over the impulse response functions scaled to various depths. In order to assess the impact of system electronics on the bias correction, we must then apply a simulation of the circuitry action to each convolution and generate bias results as a function of both αD and D. This work is the subject of an on-going effort.

2.4 Program Validation

The computation of the impulse response function for radiative transport to and from a reflecting surface based on Monte Carlo simulation is, to the best of our knowledge, unique. There exists no other method by which the impulse response function can be detailed as it has been here. Our present results are in qualitative agreement with those of Thomas and Guenther (1979), but the earlier calculations were not designed to be as quantitative as in the present effort. The validation of the program is therefore possible only on the basis of ancillary results.

The Monte Carlo simulation program is comprised of a number of large modules extracted from applications in atmospheric physics (see, for example, Holland, Thomas, and Pearce 1977). The individual modules were extensively tested and validated by comparison of the simulation results with those computed by other methods. There is reason to believe, therefore, that validation of the module integration is the most important requirement for the hydrographic laser simulation applications, and not validation of the individual modules.

While there exists no comparable estimate of the impulse response functions, it has been shown in experimental and theoretical studies (Timofeyeva 1972; Gordon, Brown, and Jacobs 1975) that the downwelling flux decays approximately in exponential fashion as the product, αD, is increased.

This behaviour has been observed in our simulations, and, further, the coefficients of the exponential decay agree quantitatively with the experimental results of Timofeyeva (1972). This will be discussed in greater detail in Section 4.2. Thus, we can be confident that the program correctly estimates the downwelling fluxes for the specified inherent properties. This lends confidence to the module integration that has been performed and all the other results generated by the program.

3.0 DISCUSSION OF RESULTS

The presentation of results has been divided into four sections. Firstly, we shall give a list of the inherent water parameters over which results have been computed and discuss the outputs that are available. Tabular listings, graphic presentations, and archived computer files have been generated, and we shall summarize the contents and formats of the results.

Secondly, we present a section on results relating to penetration. This provides information relevant to the extrapolation of experimental data to estimate the limiting operating conditions of the system. Both total received energy and peak power curves are given, and we discuss the parameterization requirement and applicable time domains for both cases.

Thirdly, we have organized a section on impulse responses and bias sensitivities to illustrate the effects of changing various water and system parameters. The parameters of interest are:

1. The phase function, $P(\theta)$,

2. The nadir angle in air, ψ,

3. The vertical optical depth, αD,

4. The albedo for single scattering, ω_0, and

5. The value of the fractional threshold, f, for pulse location. In addition to these sensitivities, we have also investigated variations in the parameter, KD, (with K and D varying) where K is the diffuse oceanographic attenuation coefficient.

Additionally, we discuss the behavior of the log-signal against log-time graphs for the leading edge of the return pulse.

The fourth results section deals with:

1. Nadir entry,

2. Detection based on the peak of the impulse response, and

3. A set of graphs likely to be valid for most practical cases.

3.1 The Cases Treated

Table 1 presents a list of the parameters employed as inputs to the simulations. We considered two phase functions designated "NAVY" or "clean" and "NOS" or "dirty". The volume scattering functions (VSFs) corresponding to these cases are plotted in Figs. 8 and 9 respectively. The associated phase functions can be computed by dividing the VSF by $\omega_0\alpha$. The values of ω_0 and α appropriate to the two cases are listed on the plots along with other key parameters. B is the probability of scattering in the backwards hemisphere, i.e., through an angle greater than 90°. The "slopes" given on the graphs are for a scattering angle of 0.1°. These slopes were used to estimate the VSF at 0.05°, and for smaller angles we assumed that each VSF was equal to the value at 0.05°. An assumption of this type is required to insure the integrability of the phase function for small angles. While this assumption may introduce some errors into the simulation due to the high value of the VSF at small angles, we believe that the phase functions we have used are reasonable representations of the experimentally available data. The mean cosine of the scattering angle is slightly higher for the NAVY phase function than for the NOS phase function, and, as a result, we would expect more forward scattering and less beam spreading for the NAVY case.

TABLE 1

List of parameters over which results were computed.

1. Scattering phase functions, $P(\theta)$
   a) "NAVY" or "clean" (See Figure 8)
   b) "NOS" or "dirty" (See Figure 9)

2. Nadir angle of entry in air, ψ (Degrees)
   0,15,25,35,45

3. αD = vertical optical depth of water column
   (Dimensionless)
   2,4,6,8,10,12,14,16

4. ω_0 = albedo of single scattering
   0.9, 0.8, 0.7, 0.6, 0.5, 0.4, 0.3, 0.2
   (Dimensionless)

At first sight the two phase functions appeared to be quite similar, but, on closer inspection, we found some significant quantitative differences. The cumulative scattering probabilities for the two cases are plotted in Fig. 10, and it can be seen that the NAVY phase function yields a higher scattering probability in the forward direction. There is a 38 percent probability for scattering through an angle less than one degree in the NAVY case while the corresponding figure for NOS is only 25 percent.

For each of the two phase functions we performed five simulation runs with nadir angles in air ranging from 0° to 45° for a total of ten runs.

In general, both αD and ω_0 are larger for the more "turbid" or "dirty" water. Nevertheless, to insure comprehensive results sets for the two phase functions, we performed simulations over full sets of αD and ω_0 values for the two cases. Eight values of both parameters were employed in each simulation run as listed in table 1 so that 64 sets of results were generated in each run.

The listed output includes the following for all cases:

1. The impulse response function for downwelling radiation reaching the bottom,

2. The impulse response function for upwelling radiation reflected from the bottom,

3. The convolution of functions (1) and (2) representing the response at the receiver, and

4. The spatial (radial and Cartesian) distribution of downwelling radiation at the bottom.

In addition to the listed output, a binary output file containing the receiver impulse response functions for all cases has been written onto disk storage. This file is organized according to the parameters in table 1 with the lower parameters being changed most frequently. Thus eight impulse response functions corresponding to the eight ω_0 values are written for each αD, and a total of 640 impulse response functions exist in the data base.

To facilitate transfer of this results "archive" to the Tektronix 4051 for plotting, the data was translated into two ASCII files (one for each phase function). The format associated with a single impulse response function is given in Appendix A. Most of the results presented in this report were graphed from this file or related files. Appendix B presents a complete set of all the computed bias errors as a percentage of the depth for a range of linear fractional thresholds; also reported are the risetimes in nanoseconds for 20-m water.

3.2 Energy and Peak Power Results

In this section we begin to present relationships for the impulse response of the system for exhaustive combinations and wide ranges of the basic input parameters: optical depth (αD), single-scattering albedo (ω_0), phase function, and nadir angle. First we will restrict ourselves to the nadir and investigate the energy reaching the bottom per unit input energy, the energy reaching a distant receiver, and the peak power reaching a distant receiver. The "energy" results that we derive also describe the power for a steady state or non-pulsed experiment since they represent the integration over all times of the impulse response functions. Thus the downwelling energy reaching the bottom maybe interpreted as the "flux" reaching the bottom for unit power input of a steady state system. It must be emphasized, however, that the "peak power" results we report are for an impulse input to the water. Attenuation coefficients are derived, and two alternate formal descriptions of the peak power at a distant receiver are formulated. Effects of these relationships on penetration predictions are noted. Next, off-nadir behavior is examined; and finally, the effect of the non-zero duration of the incident pulse is described.

The most elementary output from the simulation is the spatially integrated energy arriving at the bottom, i.e., the fractional number of incident photons reaching the bottom. Those not reaching the bottom are lost to either scattering or absorption. If one plots the log of the downwelling energy versus vertical optical depth (Figs. 11 and 12), it is seen that the results are effectively (but not perfectly) described by straight lines from the origin with slopes dependent on the single scattering albedo. (Note: the regions on the curves for joint high αD and low ω_0 are dashed because the extremely small "signals" resulting from these circumstances produced unacceptably large statistical variances in the results. These could have been removed by running the simulation longer, but it was not deemed necessary because such small values of ω_0 would never be found in coastal waters.)

If the slopes of the downwelling energy (E_B) curves are denoted as $m(\omega_0)$, then

$$E_B = e^{-m(\omega_0)\ \alpha D} . \tag{31}$$

Recalling that the downwelling energy can also be written as

$$E_B = e^{-KD} \tag{32}$$

(the defining relationship for K), it is clear that the slopes are

$$m(\omega_0) = \frac{K}{\alpha}(\omega_0) . \tag{33}$$

Because the curves extrapolate very closely to the origin, the average slope and the instantaneous slope are very nearly equal at all αD, and $\frac{K}{\alpha}(\omega_0)$ is thus very nearly independent of αD as seen in Fig. 13. This permits us to plot K/α versus ω_0 for the two phase functions as seen in Fig. 14. The phase function effect is seen to be not insignificant, but relatively small.

This is an extremely important relationship because it clearly demonstrates that the ratio of the two most commonly measured attenuation coefficients is determined solely by a third (not so well known and difficult to measure) parameter, the oft ignored single-scattering albedo. The relationship is also important because it provides the best opportunity for validation of the simulation. Timofeyeva (1972) derived $K/\alpha\ (\omega_0)$ experimentally for a number of scattering media. The curve plotted on Fig. 14 is for milk which is claimed to have scattering properties similar to those of seawater. The simulation results are seen to be in good quantitative agreement and demonstrate the correct trend with phase function (assuming that milk would have a somewhat "dirtier" phase function than our "NOS" water).

The pulse energy returned to a distant receiver (R from Eq. (15)) was calculated by temporally integrating the impulse responses (which were determined by convolving the downwelling response with a slightly perturbed version of itself). The effect of the perturbation turned out to be quite small as noted by the fact that the plots for R versus αD were nearly identical to the E_B versus αD plots with D replaced by 2D to account for the round-trip distance. If the small differences are ignored, the E_B versus αD curves can also be used for R versus αD (with the scale squared) as has been done on the "inside" axes in Figs. 11 and 12; i.e.,

$$R \cong E_B{}^2 . \qquad (34)$$

For this case, one could define a "system" attenuation coefficient for received pulse energy k_e, from the relationship

$$R = e^{-2\frac{k_e}{\alpha}\alpha D} = e^{-2k_e D} . \qquad (35)$$

It is clear, however, from Figs. 11 and 12 or from Eqs. (32), (34), and (35) that $k_e = K$, and thus we can write

$$R = e^{-2KD} . \qquad (36)$$

This familiar expression has often been used in signal equations for describing the return "strength" for airborne lidar systems. We shall see shortly how this must be modified to take pulse stretching and power (rather than energy) detectors into consideration.

First, however, it is instructive to look at the spatial distribution of the pulse energy at the bottom as shown in Fig. 15. It can be seen that the distributions are skewed toward the aircraft due to energy undercutting the (unscattered) reference path (recall Fig. 7). This skewness is more pronounced for higher αD and for the NOS phase function. It is also evident that the physical distance by which significant energy is displaced from the unscattered ray is a large fraction of the water depth. This highly scattered energy is reflected from the bottom at a location closer to the distant receiver and hence will arrive first and have a strong effect on the early shape of the impulse response. This is the chief reason for the predominantly "shallow" depth measurement biases which will be noted in the next section.

Energy-based pulse location algorithms such as correlators or centroids are not appropriate for timing underwater light propagation because pulse stretching strongly affects the shape and duration of the pulses. Much of the return energy is not "useful" because it occurs in the elongated tail of the return pulse. Typical leading edge power detectors such as a fractional threshold are also affected but to a much lesser degree. It is important, therefore, to investigate the behavior of the peak power of the return pulses as a function of optical depth, single-scattering albedo, and phase function.

It is clear that peak power and pulse energy are proportional, i.e., obey the same functionalities, as long as the pulse shape remains unchanged. Pulse stretching removes that proportionality; for example, although the pulse may contain the same total energy, the fact that it is distributed over a longer time interval causes its maximum amplitude (peak power) to be reduced. Furthermore, for a fixed αD, the absolute amount of stretching, i.e., the actual pulse length, is (from simple geometry) linearly proportional to the physical depth, D. For this reason, underwater propagation causes not only a loss of energy as a function of optical depth, but the associated pulse stretching causes a further loss of peak power with respect to the pulse energy which varies both as a function of the physical depth and the inherent optical parameters.

Relative peak power plots for the two phase functions at nadir entry are illustrated in Figs. 16 and 17 for constant physical depth, D. Several features are apparent if one compares these results with Figs. 11 and 12.

For high ω_0 the semi-log plots tend to be curved upwards; their slopes are initially steeper than for the corresponding received pulse energy curves, but at high αD the corresponding slopes became similar. The explanation for this behavior can be determined by studying the corresponding impulse response functions. At low αD the pulse begins to stretch significantly with increasing αD, but at higher αD the pulse shape "saturates" and does not continue to increase stretching. Conceptually one can understand this in terms of the more highly scattered paths (those which would have contributed to still more stretching) having a much higher probability of absorption at the higher optical depths. For lower ω_0 (some unrealistically low for coastal waters but included for sake of completeness) the peak power curves are relatively straight and do not differ greatly from the received energy curves because the relatively high probability of absorption for longer paths effectively curtails pulse stretching throughout the range of optical depths.

Because most of the semi-log plots of peak power vs optical depth for constant physical depth are relatively straight, one can again choose to describe the behavior as exponential and define an average system attenuation coefficient, k_p, for received power (P_r), from the slopes as follows:

$$P_r\Big|_{D=\text{const}} \propto e^{\frac{-2k_p\alpha D}{\alpha}} = e^{-2k_pD} . \tag{37}$$

Because of the previously mentioned added linear dependence on absolute depth, the peak power can then be written as

$$P_r \propto \frac{e^{-2k_pD}}{D} . \tag{38}$$

To the extent that several of the high ω_0 plots are slightly curved, the average power attenuation coefficient to a given optical depth will be a weak function of optical depth as seen in Fig. 18. It can be seen by comparing Figs. 16 and 17 that the sensitivity of the received power curves to phase function is somewhat stronger than was the case for received energy.

This is further illustrated in Fig. 18 where the derived k_p/α values are plotted as a function of αD and parameterized on ω_0 for both NAVY and NOS cases separately. Since the αD dependence is small, we can again select a representative value (say αD=10) and plot k_p/α vs ω_0 as in Fig. 19 where the earlier results for k_e/α are also shown for comparison.

It is clear from Fig. 19 that the system attenuation coefficient for power is significantly larger than that for energy -- particularly at high ω_0. This means simply that the "signal" predicted by Eq. (37) will drop off more quickly with increasing depth than one would predict from Eq. (36), and that this effect is worse for the "dirtier" water implied by high ω_0. The effect of phase function is seen to be small but not inconsequential.

Combining the information contained in Figs. 13 and 18 for K/α and k_p/α versus αD, we have produced the results for k_p/K versus αD for the impulse response as seen in Fig. 20. This ratio clearly demonstrates the extent to which the power attenuation coefficient can exceed the diffuse oceanographic attenuation coefficient. Note that, depending on the inherent water optical parameters, the ratio ranges between 1.0 and 3.0 (and could be even higher if ω_0 is permitted to range as high as 0.95 for very dirty "Chesapeake Bay-type" water).

Equation (38) can be rewritten as

$$P_r \propto \frac{e^{-2\frac{k_p}{K}KD}}{D} \qquad (39)$$

to emphasize that this ratio enters directly into the exponent and will have a very dramatic effect on penetration. The effect of ω_0 in the 0.7 to 0.9 range is very strong; and since its value is generally unknown in the field, a large variance in operational penetration depths for a given laser power can be expected for water masses with different scattering properties.

To emphasize the effect of the physical depth term in the denominator on increasing effective attenuation, one can invoke the identity $1/D \equiv e^{-\ell n\, D}$ and rewrite Eq. (39) as

$$P_r \propto e^{-2\frac{k_p}{K}KD + \ell n\, D} \qquad (40)$$

This highlights the fact that there are two loss mechanisms not included in Eq. (36). For a fixed loss term, it can be seen that the so-called extinction coefficient (KD_{max}) is not a constant at all, but will depend on the physical extinction depth due to the ℓnD term.

It is important to recognize that this result is for the impulse response alone and will require some modification when dealing with finite incident pulses (see section 2.3.1).

These impulse response results are to be considered as a bounding (worst) case; the other extreme is that of a very wide incident pulse for which the impulse response remains significantly smaller, effectively no pulse stretching occurs, and k_p/K thus remains near unity. This was the case for the NADC test flights with a wide (15ns) pulse width and explains why the effect was not discovered at that time.

A practical bathymetry system will experience a "transition" region between these two extremes. The exact location of the transition region in terms of optical depth depends both on the incident laser pulse width and on the physical depth. Pulse stretching and the associated loss of power compared to energy will not be evident until the duration of the impulse response becomes significant compared to the width of the incident pulse. This will begin to occur as both the physical depth and the optical depth increase. At large physical and/or optical depths, the impulse response will become broad, and the actual loss curve will tend toward the impulse response loss curves. The ratio of peak powers for long and short laser pulses is expressed in Eq. (26).

In conclusion, it is important to note that for a given system utilizing a power detection technique, "penetration" does not depend simply on some magic "extinction" coefficient (such as KD) but rather on αD, ω_0, D, and the incident pulse width.

It is generally helpful to describe the results derived from simulations in formal analytic terms. The k_p/K curves parameterized on ω_0 in Fig. 20 demonstrate basic linear behavior and fair independence on phase function. In order to determine expressions for them in the form

$$\frac{k_p}{K}(\omega_0) = m(\omega_0)\alpha D+b(\omega_0) \qquad (41)$$

we need only determine their slopes (m) and intercepts (b). These have been found to be quite linear with the scattering to absorption ratio (s/a) as seen in Fig. 21. (Note that $s/a \equiv \omega_0/(1-\omega_0)$.) By combining the descriptions for $m(\omega_0)$ and $b(\omega_0)$ from Fig. 21 with Eq. (41) we arrive at the expression

$$\frac{k_p}{K} = 10^{-3}\left[6.03-8.93\left(\frac{\omega_0}{1-\omega_0}\right)\right]\alpha D+0.23\left(\frac{\omega_0}{1-\omega_0}\right) + 1.02 \qquad (42)$$

for k_p/K at nadir entry. Perturbations due to off-nadir entry will be presented shortly.

The power loss equation derived by combining Eqs. (40) and (42) is fairly tedious. It is instructive to look for an alternate and perhaps simpler formulation.

An alternate presentation of the information included in Figs. 16 and 17 is seen in Fig. 22, where the log of return power is seen to vary linearly with ω_0 over the range from 0.2 to 0.9 in a manner which depends on αD. The effect of the phase function is significant but smaller than for αD and ω_0. Because none of the plots are curved as they are in the earlier representation, the formal description should be simpler. One can split the difference between phase functions and write

$$P_r \propto e^{m(\alpha D)\omega_0+b(\alpha D) - \ell n D} . \qquad (43)$$

Determining the slopes and intercepts (which in this case are not linear with αD) leads to the expression

$$P_r \propto \exp\left\{-2.21\alpha D+0.92\omega_0(\alpha D)^{1.22}+1.10-\ln D\right\}, \qquad (44)$$

which is good to within a factor of about 2. Equation (44) is an equivalent expression to Eqs. (40) and (42), and, given the numerical relationship between K/α and ω_0, will produce identical results.

The effect of an off-nadir entry angle on the bottom energy and on energy returned to a distant receiver are depicted in Fig. 23 for the "NOS" phase function. At low optical depths the loss per unit vertical optical depth is greater at a 45^o nadir angle due simply to the geometrical increase in the physical path length to a given vertical depth (sec ϕ where ϕ is the surface refracted water nadir angle). As the beam spreading increases with increasing depth, longer paths diverted from the central "core" are absorbed, and the radiation tends to a cone. The center of this cone tends toward the vertical with increasing depth because that is the shortest distance to the bottom and hence has less loss. (This effect is seen by scuba divers who note that regardless of the solar angle, the sunlight appears to come from directly overhead in all but the shallowest water.)

This behavior is illustrated in Fig. 24 where the mean secant of photon path angles from vertical is plotted as a function of αD. Note that for large optical depths, the distributions become quite similar.

Off-nadir power curves are shown in Figs. 25 and 26 for the two phase functions. Here again the initial loss is greater than at nadir, but then the incremental loss (slope) reduces to that for the nadir case as the vertical cone of energy is established.

The magnitudes of the off-nadir effects are less than the ω_0 effects, and no formal expression will be derived. Figures 25 and 26 can be used, if necessary, to supply corrections to the nadir results in Eqs. (42) or (44).

3.3 Impulse Response and Bias Sensitivity Studies

We have grouped sets of impulse response functions and composite bias plots for linear fractional thresholds to illustrate the effects of the input parameters over a wide range of possible operating conditions.

It must be emphasized that these results for the biases cannot be used directly to adjust experimental results for two reasons:

1. The finite duration of the source pulse is not considered, and

2. The impact of the receiver electronics is omitted.

Nevertheless, the impulse response functions derived form the basis for a formal correction estimate, and the bias estimates give an idea of the magnitude of the problem in the practical operating environment.

Figures 27 and 28 present a comparison of impulse responses for a vertical optical depth, αD, of 8 and a single-scattering albedo, ω_0, of 0.8. The time base is for a depth of

20 m; for other depths the time scales linearly with the depth. Results for four nadir angles are shown: namely, 0^{o}, 15^{o}, 25^{o} and 35^{o}. The time, zero, always corresponds to the earliest possible return from the bottom, i.e., to radiation that completes both its downward and upward transport in the water in the vertical direction. The "reference" time for the unscattered ray as defined by Eq. (13) is marked by the vertical line labeled 'REF', and the maximum or peak location if labeled 'P'.

The results for the NAVY phase function were compiled with 50,000 input photons while only 10,000 photons were simulated for the NOS phase function as a cost-saving measure. The errors in the impluse response functions can be gauged from the ripple in the plots. It is apparent that the noise is greater for the NOS phase function, and this, of course, relates to the smaller number of input photons. It was felt, however, that manual smoothing could be accomplished readily for these cases, and, even without any smoothing, acceptable accuracy in the bias estimates is obtained. In general, the variances in the results increase with increasing αD and decreasing ω_0. Since the NOS phase function is attributed to "dirty" water, the associated value of ω_0 will be larger in practice, and this reduces interest in the worst case of large αD and small ω_0. Thus the more limited simulated was considered acceptable for the NOS case.

The leading edges of the impulse responses are not very sensitive to the phase function over any of the conditions considered. Some variation in the location of the peak signal is observed, with a tendency towards a greater delay for the NOS case. The trailing edges or tails of the impulse responses tend to be somewhat broader for the NOS phase function.

The insensitivity of the leading edge to the phase function leads to similar bias curves for the two cases as illustrated in Fig. 29. The results given are the biases in centimeters, at a depth of 20 m, for linear fractional thresholds of 50 and 10 percent and four nadir angles. Negative biases imply an underestimate of depth. The upper graphs were all obtained for an ω_0 value of 0.8, and it can be seen that the separation of the curves for the two phase functions are reasonably small except at large optical depths where they grow as large as 15 cm in certain cases. For the 10% threshold the shallow bias magnitudes tend to saturate when αD reaches about 6. The biases for the NAVY case continue to increase slightly, while for the NOS phase function they reach a maximum at an αD of about 10 and then decrease slightly with increasing optical depth. For the 50% threshold, the results are qualitatively similar for nadir angles of 25° and above, but below 25° there is a pronounced phase function effect with the NOS function producing a deep bias for αD greater than 10 or 12.

The lower graphs in Fig. 29 compare biases for values of ω_0 that may be more likely in practice, namely 0.6 for NAVY and 0.8 for NOS. The curves numbered 5 thru 8 are identical in the upper and lower plots. The separations of the NAVY and NOS cases are more pronounced in the lower graphs and exhibit differences as large as 20 cm.

For nadir angles of 0° and 15°, the magnitudes of the biases are less than 30 cm for practical operating conditions, but there would be some advantage in applying a small correction. For nadir angles of 25° and more, the biases exceed 30 cm, and in this case, correction would be mandatory. In general, however, for any given values of αD we see that the error in the prediction arising from uncertainty in the phase function and single-scattering albedo is no greater than 20 cm.

Figures 30 and 31 illustrate the effect of the vertical optical depth, αD, on the impulse response function. The results shown are for αD values of 4, 8, 12, and 16, a value of ω_0 of 0.8, and a nadir angle in air of 25^o. Figure 30 is for the NAVY phase function while Fig. 31 is for NOS. It is clear that while for $\alpha D = 4$ the impulse response is quite narrow and reasonably symmetric in its central portion, the width increases with increasing αD together with an increasingly pronounced tail. There is a tendency for the peak of the impulse response to be delayed beyond the reference time for large values of αD, particularly in the case of the NOS phase function.

Figures 32, 33, and 34 are designed to show the effect of changing the nadir angle. Figures 32 and 33 display impulse response functions for the five nadir angles considered and for values of αD of 8 and ω_0 of 0.8. The peak of the response tracked the reference time quite well, but the widths of the response increased as the nadir angle increased. (Note the scale change on the abscissa when going from 25^o to 35^o nadir angle.) Figure 34 shows the computed biases for linear fractional thresholds of 1, 10, 50, and 100 percent of the peak as a function of αD with ω_0 fixed at 0.8. In all cases the <u>underestimate</u> in depth <u>increases</u> with increasing nadir angle and <u>decreases</u> with an increasing fractional threshold. As before, the biases shown are not very sensitive to the phase function.

An important observation is that, for small fractional thresholds, there is a tendency for the curves to reach a saturation value when the optical depth reaches 6 or 8. Variations in biases for larger values of αD are very small. This fact may be a good basis for depth corrections in turbid waters since a precise estimate of the narrow-beam attenuation coefficient would not be required. Nevertheless, a critical review of the impact of the characteristics of the laser pulse and the system electronics is necessary before a correction algorithm can be finalized.

Figures 35 and 36 indicate the importance of the single-scattering albedo, ω_0, in affecting the impulse response function. Results are shown for both phase functions at a nadir angle of 25^o, an αD value of 8, and for ranges of values of ω_0 appropriate to the two phase functions. In general, the tails of the response functions were much more strongly influenced than the leading edges, but in both cases the width of the response function increased with increasing ω_0.

Figures 37, 38, and 39 present more detailed information on the variability of the leading edge of the impulse response as ω_0 changes. Computed biases at depths of 20 m are plotted as a function of αD for practical ranges of ω_0 for both phase functions. For a linear fractional threshold of 10% of the peak, the range of the corrections for a given value of αD was generally less than 30 cm. Depths estimated from the <u>peak</u> of the impulse response were much more variable, however, and, for all nadir angles, the range of biases for αD values greater than about 10 was greater than 30 cm.

The impact of the selected value of the linear fractional threshold, f, is detailed in Figs. 40 and 41 where bias errors for a depth of 20 m are plotted as functions of αD for a value of ω_0 of 0.8. When f is 10% or less, the biases reach a constant value, independent of phase function, at an αD of 6 or less. For larger values of f, however, there is a tendency for the underestimate in depth to become smaller for large values of αD (or for the overestimate to increase). Here the bias errors for the two phase functions differ; the NOS phase function generally causes a greater overestimate in depth for large values of αD.

The bias errors at a 20 m depth for a full range of nadir angles are plotted in Fig. 42 as a function of threshold fraction for an αD of 10 and an ω_0 of 0.8. It is apparent that if one considers only the magnitude of the bias, peak detection provides the optimum pulse location algorithm. It will be seen in section 3.4, however, that the low bias benefits of peak detection are counteracted by an insurmountable random noise problem caused by detection at a low slope region. The next best choices are middle or high fractions such as 50% or 80%. Low thresholds lead to increasingly large biases, particularly below 10% where the errors grow very rapidly.

We had considered the potential use of the product, KD, (where K is the diffuse oceanographic attenuation coefficient) as a predictor for two purposes:

1. to estimate receiver energy and perhaps power; and

2. to parameterize the appropriate bias correction.

Interest in this parameter is driven by our belief that K can be estimated by an appropriate analysis of the volume backscattering return, i.e., of radiation not reflected at the bottom, but rather by the scatterers in the water. We have seen in the preceding section that the KD product alone does not adequately describe the loss of peak power with depth. That it is also inadequate for bias prediction will now be demonstrated.

We are able to compute the ratio, $\frac{K}{\alpha}$, from our simulation results. This ratio is unity when ω_0 is 0 and always decreases when ω_0 increases. This behavior leads to a prediction that the parameter, KD, is not adequate, on its own, for computing the bias. Suppose, for example, that we have a bias result for a specified value of KD, and wish to investigate the bias change as KD is increased. The value of KD can be increased by increasing αD -- in which case the width of the impulse response generally <u>increases</u> -- or, alternately, we can increase KD by reducing the value of ω_0 -- in which case the width of the impulse response <u>decreases</u>. It follows that the width of the impulse response cannot be predicted unambiguously from a knowledge of K or KD alone. This conclusion is borne out by the following simulation results.

Figures 43 and 44 present impulse response functions for four different combinations of αD and ω_0 for which KD=3, and Fig. 45 presents computed biases with these differing conditions corresponding to KD=3 represented as black dots. It is apparent that a wide range of impulse response widths and hence biases can result from the condition cited. It is of particular importance that the results for single scattering albedos of 0.8 and 0.9 should be so different from each other since these are conditions that may well be appropriate for coastal waters loaded with suspended particulates.

Further analysis of the impulse response functions and their implications could be aided by the development of a suitable functional description of the leading edge characteristics. In Figs. 46 thru 49 we have plotted the impulse responses on log-signals vs. long-time scales. In Figs. 46 and 47 we compare plots at a nadir angle of 15°, an albedo of single scattering of 0.8, and αD values of 4, 8, 12, and 16. Figure 46 is for the NAVY phase function while Fig. 47 is for the NOS case. The curves all exhibit nearly linear sections with gradients between 3 and 4, which rise to substantial fractions of the total peak height. Thus, a power-law behavior for the leading edge of the form t^p is indicated (where t is the time since the earliest possible return and p is a constant in the range from 3 and 4). Figures 48 and 49 are for an αD value of 10 and an ω_0 value of 0.8 with four different nadir angles. In general, the linear sections appear with the slope normally in the range from 3 to 5.

The plots presented here are all for off-nadir operation. When operating at the nadir and small values of αD, the peak of the impulse response occurs very early, often in the first sampling bin. In this case the rise to the peak cannot be meaningfully characterized from our results. For large values of both αD and ω_0, a significant delay in the peak is observed, but it appears that the power law appropriate to this case is different from that for the other cases. Sometimes a linear behavior seems to apply, but it may be that the power law description is not the best.

From the impulse response functions, "full" risetimes (from 1% to 100% of peak height) have been calculated for the two phase functions and are presented in Fig. 50 as a function of nadir angle for D=20 m, αD=10, and ω_0=0.8.

These risetimes, which scale linearly with physical depth, can be seen to increase sharply for nadir angles beyond about 20^o. This is detrimental to performance because larger risetimes cause larger random pulse location error (loss of precision). If the impulse response functions are convolved with an incident laser pulse of fixed duration, the resultant system response "full" risetime will be nearly equal to the sum of the two risetimes. Thus, as seen in Fig. 50, the system response risetime for a 7 ns incident pulse will be 7 ns greater than for the impulse response. For small nadir angles it can be seen that the phase function plays a relatively significant role in the duration of the risetime, while for large nadir angles the effect is quite small.

3.4 Special Cases

We have organized some graphs to treat certain conditions of particular interest:

1. Operations at the nadir,

2. The use of the signal peak for detection, and

3. Parameters most likely to be valid for reasonable operational conditions.

Figures 51 and 52 present impulse response functions for nadir operations. For values of αD up to and including 8, the peak of the impulse response function normally occurs in the first sampling bin. The tail of the impulse response is initially steep but tends to an exponential form at large times. At values of αD larger than 8, the peak in the impulse response function is delayed, particularly for large values of ω_0. The portion of the tail that can be discerned from the generated data in these cases appears to be approximately linear.

Figure 53 presents the computed depth bias at nadir for 20-m water. As pointed out previously, only overestimates in depth are possible. Significant biases occur only for large values of the linear fractional threshold, with no large error being observed for thresholds of 10% or less or a value of αD of 8 or less.

Bias errors scaled to 20-m water for detections based on the peak of the impulse response function are presented in Fig. 54. The bias generally reaches 30 cm or more for αD values greater than about 8. For large values of αD, the bias magnitude generally increases with αD, with the overestimate in depth becoming smaller as the nadir angle increases, and with the depth being underestimated when the nadir angle reaches 45°. The most serious errors occur for the NOS phase function and an ω_0 value of 0.9 -- conditions that might be appropriate for waters with substantial loading of suspended inorganic solids. The estimates of bias for peak detectors are seen to have a large variance in the simulations, particularly for larger value of αD, ω_0, and nadir angle. These arise from the flatness of the peak of the impulse response and will also occur in the analysis of field data. Thus, even if peak detectors have a small associated bias, their use cannot be recommended because of the generation of large random errors. This effect is discussed in detail in a report on a Monte Carlo "Pulse Location Estimation" simulation (Guenther and Thomas, 1981).

Figures 55 through 57 present results that might well be appropriate for "typical" operating conditions: namely, ω_0 values from 0.5 to 0.8 for the NAVY phase function and from 0.8 to 0.9 for the NOS phase function. We have concentrated on nadir angles of 0°, 15°, and 25° because biases for larger angles appear to be unacceptably large even after "correction". Figure 55 presents impulse response functions for the NAVY phase function at an αD of 8 and for the NOS phase function at an αD of 12. The results for the NOS case show a significant delay in the peak and a very prolonged tail. The impulse responses for the NAVY phase function are generally more peaked and exhibit shorter tails.

Figures 56 and 57 present biases computed using 10 and 50 percent linear fractional threshold detectors. For αD values below 10, the NAVY and NOS phase functions yield very similar results. For greater αD, the 10% threshold results are fairly similar, but at a 50% threshold the NOS results turn up more sharply -- particularly for high ω_0. At high αD, shallow biases caused by undercutting for the NAVY case tend to saturate, while for NOS water they tend to reach a maximum at an αD of about 8 and then increase (toward the "deep" direction) -- sometimes rapidly. For small nadir angles ($\lesssim 15^{o}$) the high αD biases become deep very quickly due to dominance of multiple scattering over geometric "undercutting".

The magnitudes of the errors are seen to depend strongly on the nadir angle and threshold fraction. The goal is to prevent the bias errors from becoming large enough that correctors requiring knowledge of the water optical properties would have to be invoked. In order to minimize the absolute magnitude of the bias errors, one should seriously consider selecting threshold fractions as a function of the nadir angle (including roll/pitch). For example, at a 15^{o} nadir angle a 10% threshold produces smaller biases while at 25^{o} the 50% threshold is superior. This procedure could easily be accomplished in a digital system with a simple algorithm during post-flight data processing.

Perhaps the most important results which can be displayed are in Fig. 58 which indicates that prevention is more effective than cure. For a 15^{o} nadir angle the maximum error is -18 cm at a 20-m depth using a 10% threshold. One can simply apply an ad hoc fractional bias corrector of -0.45% (9 cm per 20 m) and never err by more than ±9 cm for αD's from 0 to beyond 16. For a 25^{o} nadir angle the maximum error is 35 cm at an αD of 16. The bias error at high αD's is strongly dependent on the water optical properties. Several approaches are possible depending on the maximum error magnitude permitted. If a ±17 cm bias error is acceptable, an ad hoc fractional bias of -0.85% could be arbitrarily imposed for all measurements. If greater accuracy is desired, some rough estimates of the optical properties could be made. The simplest solution would be to estimate K from the slope of the volume backscatter and, using the depth estimate, compute KD. Using an ad hoc value of 0.8

for ω_0 then leads to $\alpha D \simeq 3.3$ KD, and this estimate of αD could then be used with Fig. 58 to provide a bias estimate which should be good to less than ±0.50% (±10cm/20m depth). Section 4.0 contains further discussion on determination of the input parameters for the bias model.

It must be remembered that the results presented here have been for the impulse responses. They will have to be verified for the full system responses (i.e., after convolution with a finite input pulse), but they are certainly encouraging and indicate that careful selection of design, operational, and data processing parameters can probably limit propagation-induced bias errors to an acceptable level within the error budget without requiring a sophisticated analysis of backscatter or pulse shapes.

4.0 PRACTICAL REQUIREMENTS FOR BIAS CORRECTION

It has been emphasized that the results discussed in the previous section are only the first step in the process of computing the bias correction for operational practice. The results for the impulse response functions have been computed for specified inherent water parameters, αD and ω_0, and the first part of this section describes a general correction procedure for circumstances where these parameters are known. The second part of the section discusses the most promising approaches to actually calculating these inherent parameters from airborne field data, and the third section considers additional possible lines of attack should these methods not prove usable. This information is presented for the sake of completeness and for operations not constrained as described in the previous section.

4.1 Computation of The Bias For Known Inherent Parameters

The specific steps required to estimate the relevant bias from the parameters, αD and ω_0, given the phase function, the nadir angle, and the temporal profile of the source pulse are as follow:

1. Select the appropriate impulse response function from the existing archive by interpolating between the relevant tables.

2. Scale the impulse response function to the depth, D, using the uncorrected depth measurement as a first guess.

3. Perform a convolution of the scaled impulse response function over the source pulse profile to obtain an estimate of the profile of the received signal; and

4. Apply an algorithm that duplicates the impact of the system electronics to determine the depth estimated by the system. The bias is then the difference between this estimate and the assumed depth, D.

If the depth correction is large, steps (2), (3) and (4) might have to be repeated iteratively, with increasingly accurate estimates of the depth being inserted in step (2). The fractional depth error without corrective iteration will be of the order of the square of the fractional bias and is generally small.

The procedure outlined above is too laborious for real-time application. Therefore, a set of tables is currently under construction for use by direct access in look-up fashion. The tables are specific to D, αD, ω_0, the phase function, the assumed source pulse profile, and the system electronics. A change in any one parameter will affect the bias to be applied, and separate tables must be generated for any significant change in the source profile or system electronics.

4.2 Estimation of the Inherent Parameters

We have reviewed the data of Petzold (1972) to determine relationships which may be helpful in quantifying the parameters, αD and ω_0, of the water column. There is no easy method by which these can be computed directly from the return signal, and we have been forced to review indirect methods. The parameter that appears likely to be obtained from the log-slope of the volume backscattering is K, the diffuse oceanographic attenuation coefficient. Additionally, the absolute magnitude of the volume backscattering signal is proportional to $\sigma(\pi)$, the volume scattering function at 180°, and there is a chance that in a radiometrically calibrated system, $\sigma(\pi)$ can be independently estimated. Our investigation has therefore concentrated on the use of K and $\sigma(\pi)$ as inputs for predictions of the inherent properties.

From K we can easily obtain KD, but, as we have seen, this alone is not adequate for bias estimation. The single-scatter albedo, ω_0, is the key to the problem. In addition to being one of the two required parameters, it provides the link whereby α (hence αD) can be obtained from K (or KD) through the known K/α versus ω_0 relationship (Fig. 14).

Based on the Petzold results, it appears that while there is no simple, single-valued relationship between $\sigma(\pi)$ and ω_0, there is a strong one with low variance between $\sigma(\pi)/K$ and ω_0 as seen in Fig. 59. Thus, the value of ω_0 can be estimated if $\sigma(\pi)/K$ is known. Because of the slope of the function, the estimate of ω_0 will be more accurate for larger values of ω_0.

The behavior of $\sigma(\pi)/K$ as function of ω_0 is the only relationship we have found that allows a unique estimate of ω_0 to be made. If we are able to predict ω_0 in this way from airborne field data, then the K/α vs ω_0 relationship can be used to convert K to α. This will then lead to an estimate of αD by using the uncorrected depth for D; and both required inherent parameters will have been determined.

The chief worry is that ω_0 may not be able to be determined with sufficient accuracy in this way due to uncertainties in the experimentally derived values of K and $\sigma(\pi)$. Furthermore, the reported $\sigma(\pi)/K$ vs ω_0 relationship is based on a limited data set, and it may not be valid for all water types. An alternative or corroborating procedure would be helpful. Some possibilities are discussed in the next section.

4.3 Alternative Correction Stategies

The return signal can be periodically sampled and compared with the source laser pulse. A direct comparison of the two pulses yields an immediate indication of pulse stretching. The use of suitable statistical parameters, possibly the moments of the return pulse, could then yield an estimation of the bias appropriate to the processing electronics, without any need to perform the intermediate step of calculating the inherent water parameters. This possibility can be reviewed while constructing depth corrections for specified inherent properties by identifying those measures of the return pulse that correlate well with the computed correction independent of αD, the phase function, and ω_0.

In the absence of good estimates of αD and ω_0 or a correlation with pulse widths we would be forced to make some assumptions. We have observed that, for small linear fractional thresholds, the bias saturates for large values of αD (greater than about 6) and that the limiting bias is only a weak function of the phase function and ω_0. It follows that, for these conditions, we can make a reasonable estimate of the bias from the nadir angle alone -- independent of αD or ω_0.

For values of αD less than 6 the true depth is often small (much less than 20 m) so that the absolute error in depth may be small even though the fractional error is not. Hence, for conditions where αD is believed to be small, it may be possible to ignore the correction. The greatest danger of a significant bias that is hard to correct is in the region of low αD but large depth, namely, in relatively clear but deep water.

For low nadir angles of 15° or less the bias is always small and negative for small fractional thresholds. When the fractional threshold is increased, the underestimate in depths is reduced; and for some intermediate threshold the bias can become quite small. For large fractional thresholds there are significant overestimates of depth when αD is large. It follows that the neglect of the bias may provide acceptable accuracy for operations at small nadir angles and small or intermediate linear fractional thresholds, or that cursory correctors requiring little or no knowledge of optical properties may prove to be sufficient if the threshold is adapted to the nadir angle as discussed in section 3.4.

5.0 CONCLUSIONS

We have succeeded in developing a technique for investigating the impact of underwater light propagation mechanisms on laser bathymetry measurements. A Monte Carlo simulation program has been suitably adapted to yield the impulse response function (i.e., the shape and size of the return pulse for a very brief input pulse) at an airborne receiver. This calculation has been performed for a range of conditions valid for coastal waters.

The actual lidar bottom return pulses will vary considerably in shape and arrival time depending on the water depth, the scanner nadir angle, the incident laser pulse width, the optical properties of the water, the airborne system signal processing electronics, and the depth determining algorithm or procedure. These perturbations of the return signals will cause depth measurement biases which can be considerably larger than the International Hydrographic Bureau shallow water accuracy requirements.

In general, bias error predictions can be used as bias error correctors which, when applied to the raw depth measurements during post-flight data processing, will significantly reduce the magnitude of the errors. The first step in the estimation of these errors is the determination of the impulse response functions of the medium for various permutations of the relevant optical parameters. An output data set consisting of 640 impulse response functions has been generated which provides the basic results of this phase of the investigation.

We have determined that the shapes of the impulse response functions are sensitive to the nadir angle and that the width of the response (particularly the tail, or trailing edge) always increases with increasing nadir angle. The dependence on the phase function, which describes the redistribution of energy at scatterings, is not very significant, provided we specify phase functions within a reasonable range. The width of the impulse response functions increases both with increasing αD, the vertical optical depth of the water column, and increasing ω_0, the albedo for single scattering.

The characteristics of the impulse response function cannot be directly estimated from the parameter, KD, the product of the diffuse oceanographic attenuation coefficient and the depth. This fact is explained in terms of the behavior of the ratio of K to the narrow-beam attenuation coefficient, α, as the single-scattering albedo, ω_0, changes.

For non-zero nadir angles, the leading edge of the impulse response function behaves approximately as a power law with an exponent of 3 to 4; i.e., the receiver power varies as t^3 or t^4, where t is the time since the earliest return.

We have found that the biases are not very sensitive to the phase function. For non-zero nadir angles and small fractional thresholds an underestimate in depth is caused which increases towards a limit as αD reaches 6 or 8. This limit increases with increasing nadir angle. The biases for nadir angles of 35^o and 45^o are large and cannot be predicted to acceptable accuracy because of the uncertanties in ω_0 and αD. Hence, unless reliable predictions of the inherent optical properties can be found, operations at nadir angles above 25^o should not be undertaken. The bias is not very sensitive to ω_0 over most of the conditions considered. With larger fractional thresholds the biases are small for αD values of

8 or less, but the use of peak detection is not recommended because of the impact of statistical noise. The computed biases scale linearly with the true depth, and, for moderate depths, the results show that a correction may be unnecessary.

Example bias predictor/correctors have been calculated from the impulse responses alone. These predictors are reported and discussed for a wide range of nadir angle, optical depth, single-scatter albedo, and the depth algorithm threshold fraction. They are presently considered valid only for the case where the impulse response temporal width is very long compared to the incident laser pulse width (i.e., deep water) and where the signals are processed linearly with a fractional amplitude threshold for the depth determining algorithm. Bias results for realistic system responses will be available in the near future; it is felt, however, that they will probably not differ greatly from the results presented here.

In order to calculate bias predictors (and hence correctors) generally valid in all cases for a specific lidar system, one must first convolve a selected impulse response with the intrinsic laser pulse shape to obtain a prediction for the actual bottom return pulse. This signal must be "processed" in a manner consistent with the signal processing which takes place in the electronic hardware and, finally, operated upon by the depth determining algorithm to be used with actual field data.

The bias predictors are necessarily parameterized on their driving, inherent optical properties (i.e., beam attenuation coefficient and single-scatter albedo). Neither of these optical properties will be directly measured in the water as part of a typical airborne survey. It is thus necessary to provide continuous estimates of their values based solely on specially processed, ancillary flight data. A preliminary discussion of the required data and how one might make these determinations has been given. We have also considered alternative and/or supporting bias estimation procedures that do not require knowledge of the inherent properties. This subject is being studied further as part of an on-going effort.

REFERENCES

Chandrasekhar, S., 1960: Radiative Transer. Dover Publications, New York, N.Y., 385pp.

Gordon, H.R., 1974: Mie theory models of light scattering by ocean particulates. Suspended Solids in Water. Plenum Press, Ed. Ronald J. Gibbs, 73-86.

Gordon, H.R., Brown, O.B., Jacobs, M.M., 1975: Computed relationships between the inherent and apparent optical properties of a flat homogeneous ocean, Appl. Opt., 14, 417-427.

Guenther, G.C., and Thomas, R.W.L., 1981: Error analysis of pulse location estimates for simulated bathymetric lidar returns. Proceedings of the Laser Hydrography Symposium, Salisbury, South Australia, 30 Sept. - 3 Oct. 1980.

Hammersley, J.M., and Handscomb, D.C., 1965: Monte Carlo Methods. Metheun Monographs, London, 149 pp.

Holland, A.C., Thomas, R.W.L., and Pearce, W.A., 1977: Information content of sky polarization measurements at right angles to the solar direction. Appl. Opt., 17, 2153-2161.

Petzold, T.J., 1972: Volume scattering functions for selected ocean waters. SIO Ref. 72-78, Scripps Institution of Oceanography, San Diego, Ca., 79 pp.

Thomas, R.W.L., and Guenther, G.C., 1979: Theoretical calulations of bottom returns for bathymetric lidar. Proceedings of the International Conference on Lasers '78, Orlando, Fla., 48-59.

Timofeyeva, V.A., 1972: Relations between certain optical properties in turbid media with different scattering patterns. Isv., Atmospheric and Oceanic Physics (Acad. of Sci., USSR), 8, 895-896.

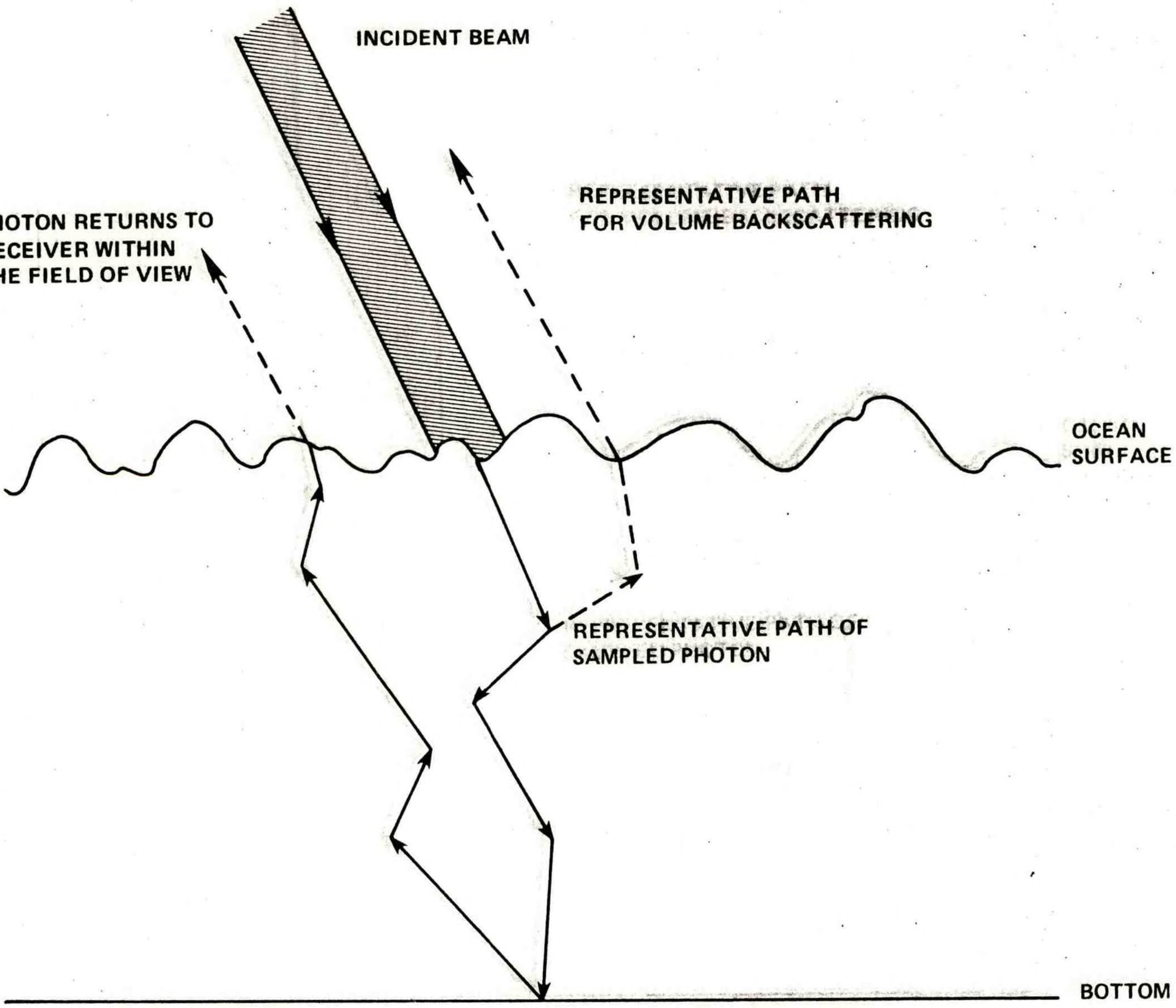

FIGURE 1. SCHEMATIC ILLUSTRATION OF RADIATION TRANSPORT

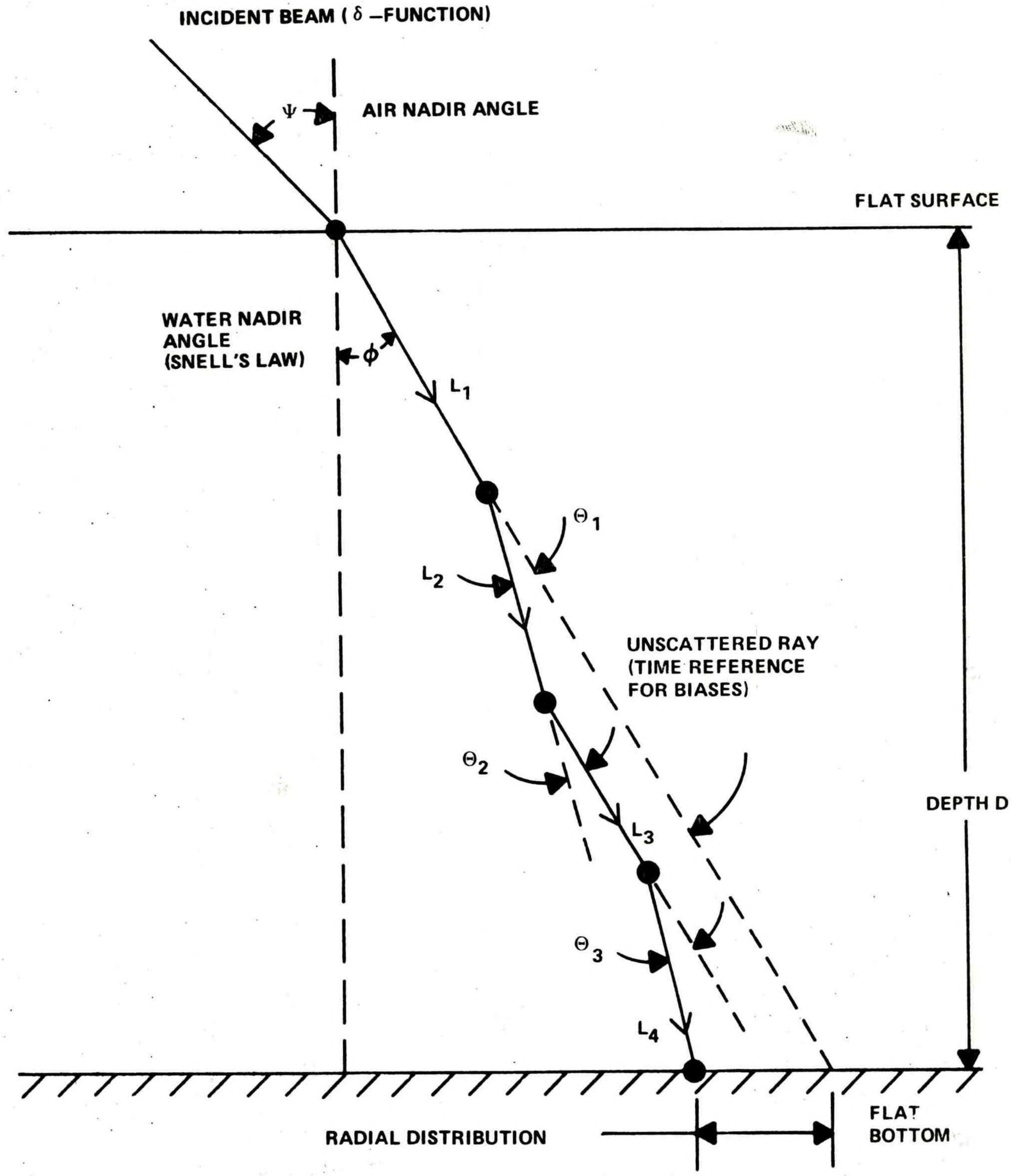

$$\text{DELAY TIME } T = \frac{1}{C_W}\left[\sum_i L_i - D\right]$$

FIGURE 2. PROPAGATION SIMULATION GEOMETRY

FIGURE 3. DEFINITION OF NARROW BEAM ATTENUATION COEFFICIENT

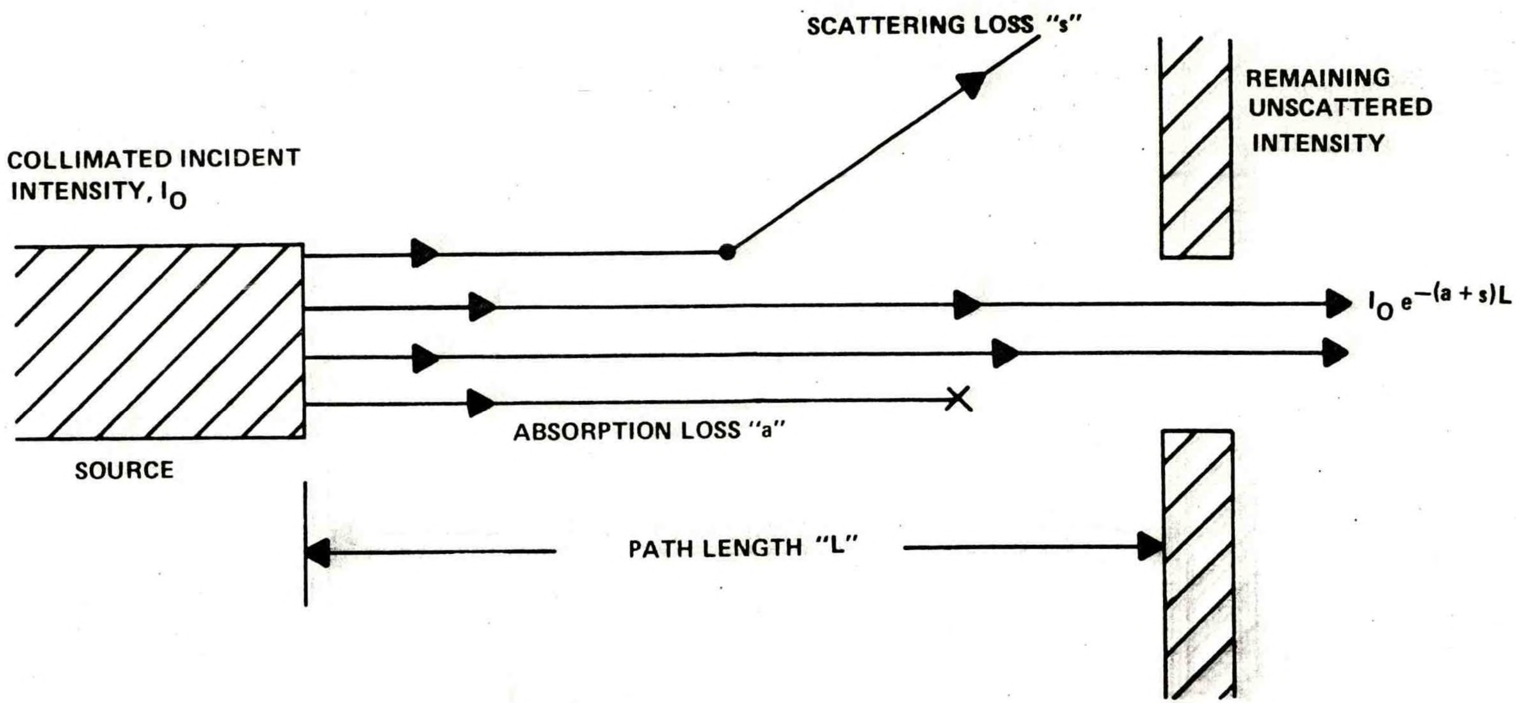

α = a + s = NARROW BEAM ATTENUATION COEFFICIENT

α L = "OPTICAL DEPTH"

FIGURE 4. DESCRIPTION OF SCATTERING EVENT

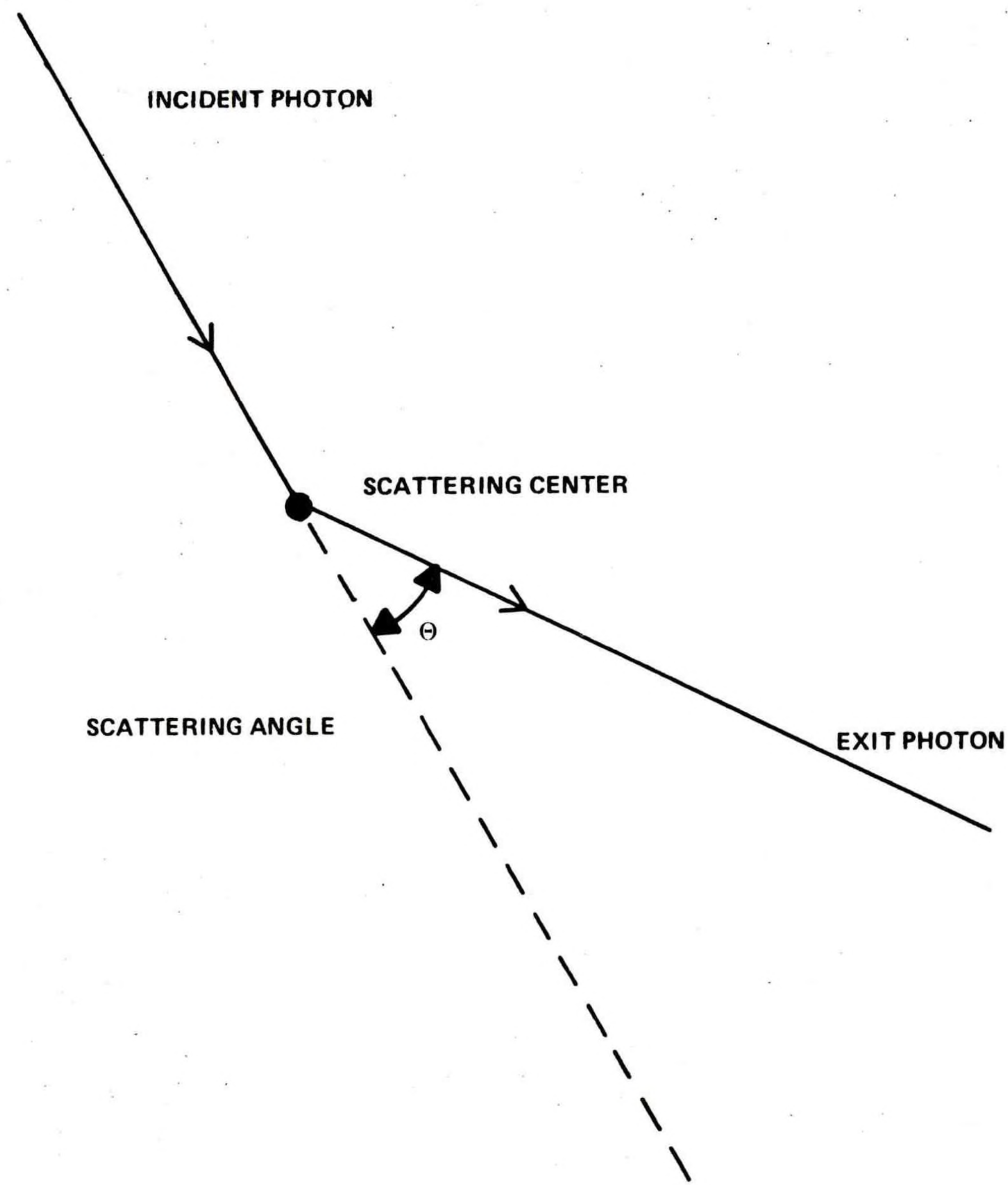

FIGURE 5. ILLUSTRATION OF SCALING RULE FOR ESTIMATIONS APPROPRIATE TO DIFFERENT DEPTHS

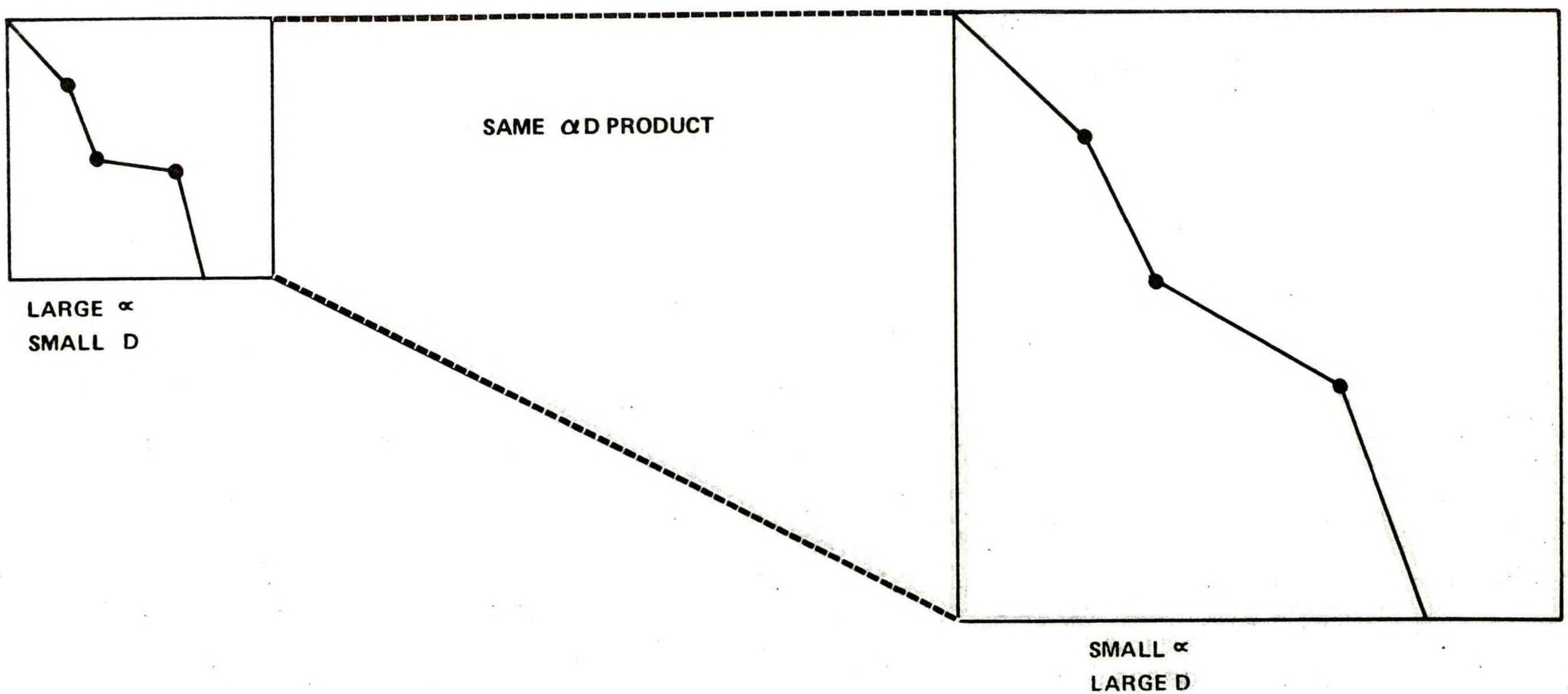

FIGURE 6. SCHEMATIC ILLUSTRATION OF VIRTUAL PHOTON SAMPLING

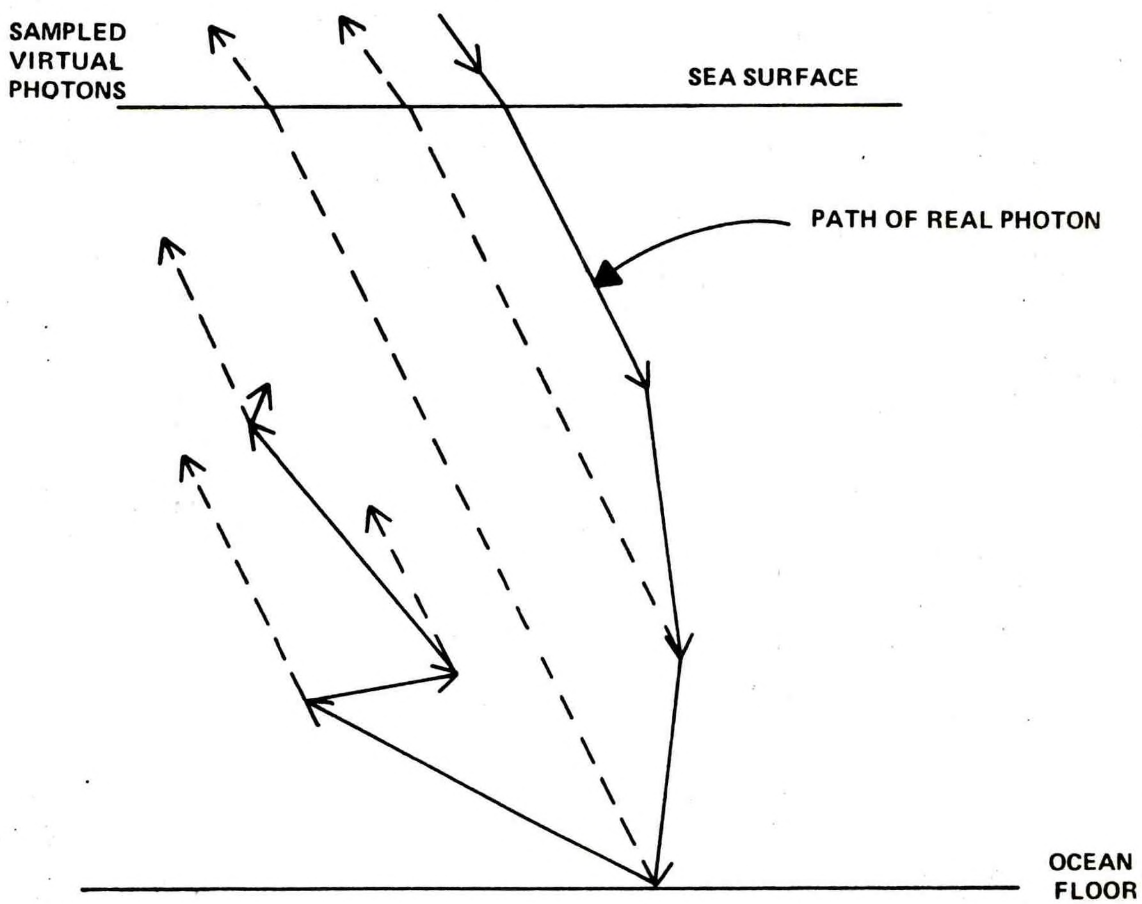

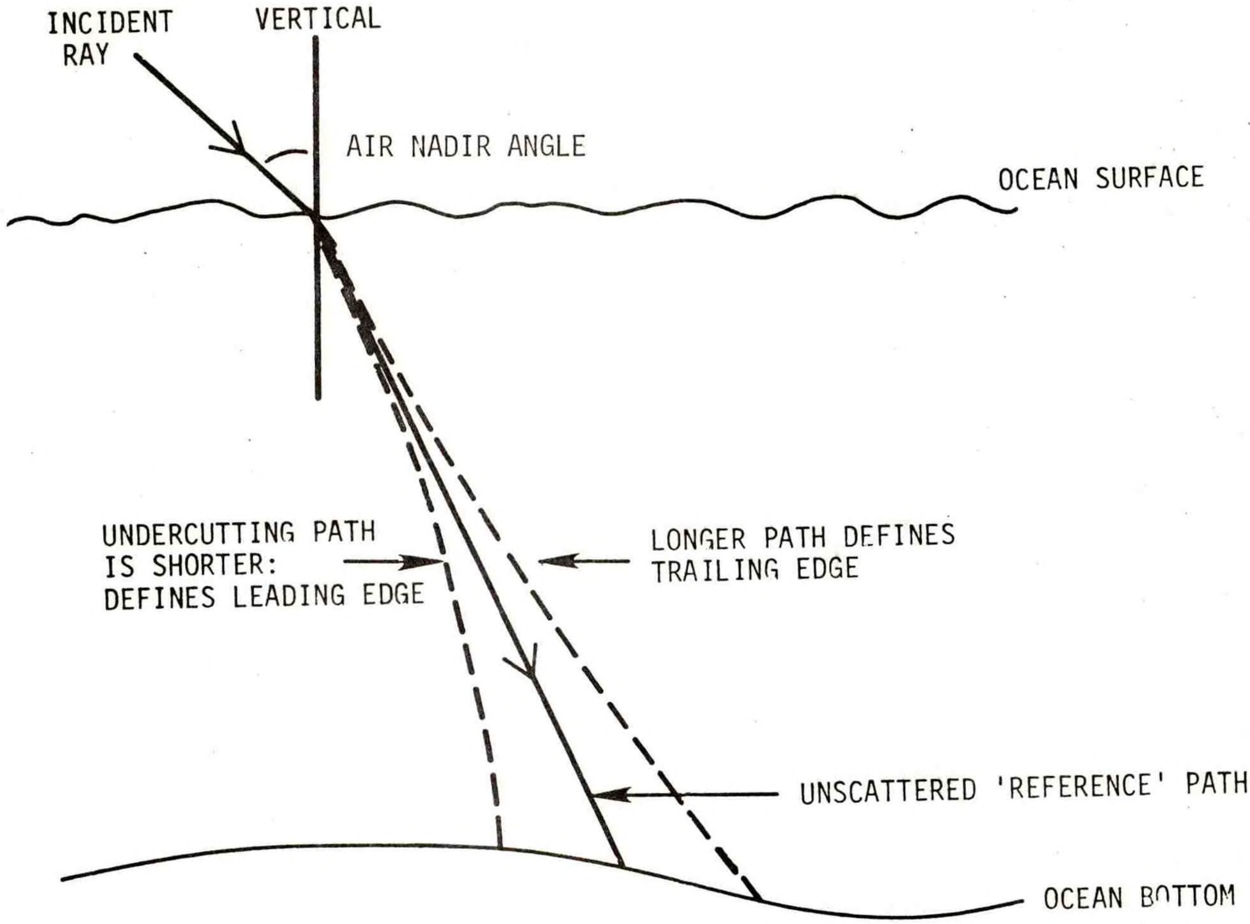

FIGURE 7. GEOMETRICAL RELATIONSHIPS AFFECTING IMPULSE RESPONSE FUNCTION

"NAVY WATER"

α	= 0.47 m^{-1}	SLOPE	= −1.546 @ 0.1°
ω_0	= 0.585	VSF (0.05°)	= 5700
B	= 0.014	$\overline{\cos\,\theta}$	= 0.9466

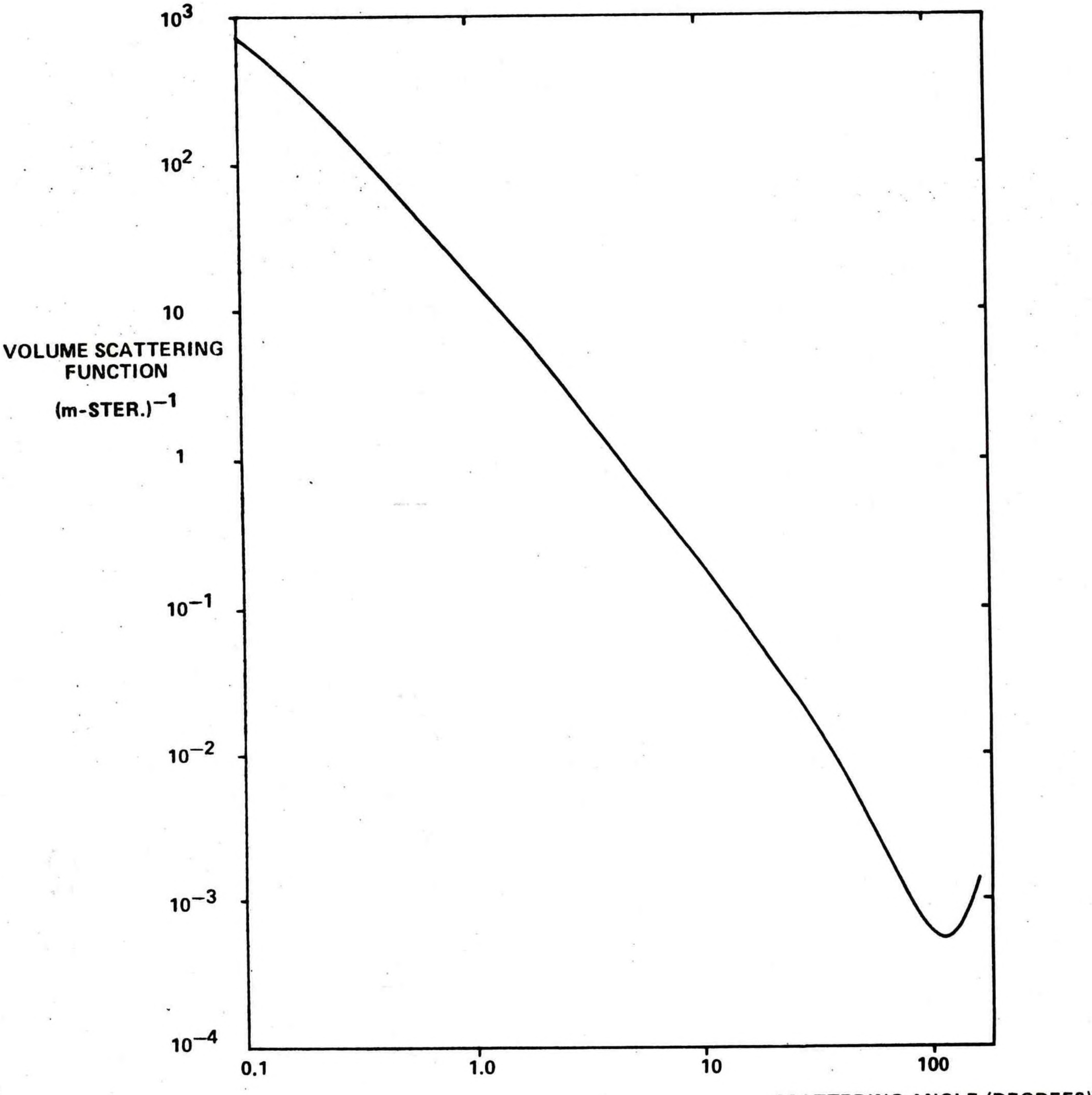

FIGURE 8. VOLUME SCATTERING FUNCTION FOR 'CLEAN' OR 'NAVY' WATER

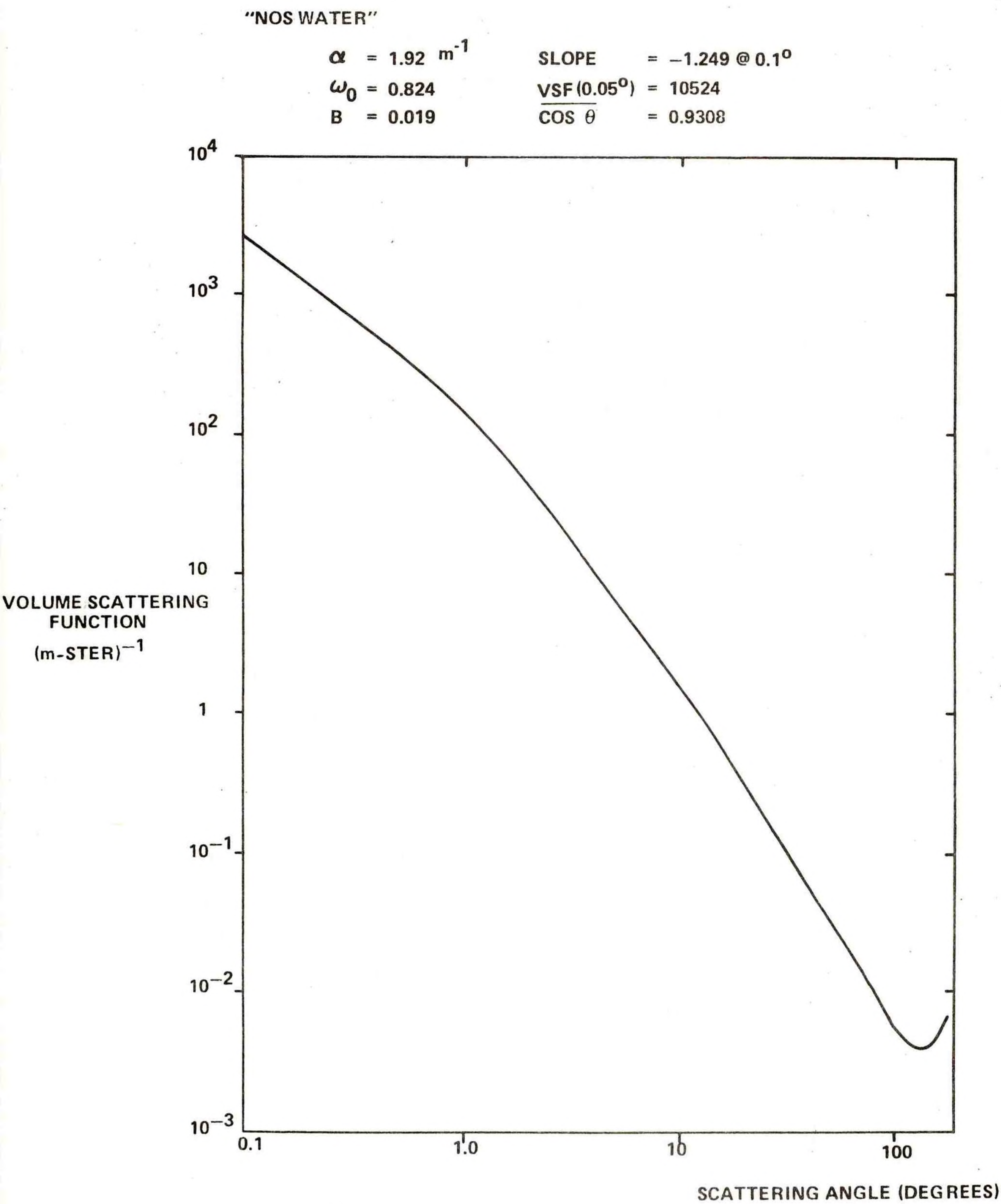

FIGURE 9. VOLUME SCATTERING FUNCTION FOR 'DIRTY' OR 'NOS' WATER

FIGURE 10. PROBABILITY OF SCATTERING THROUGH LESS THAN GIVEN ANGLE

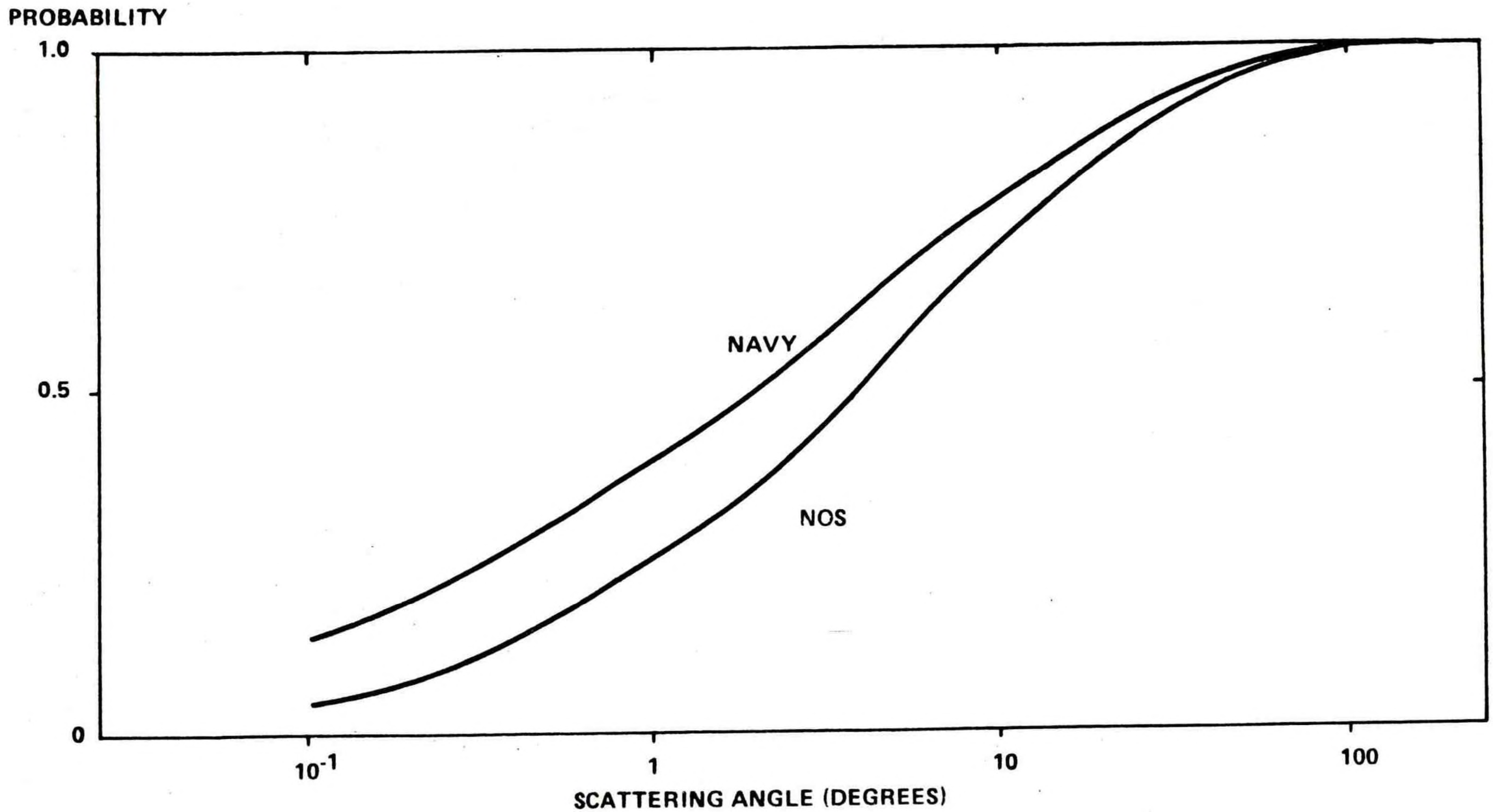

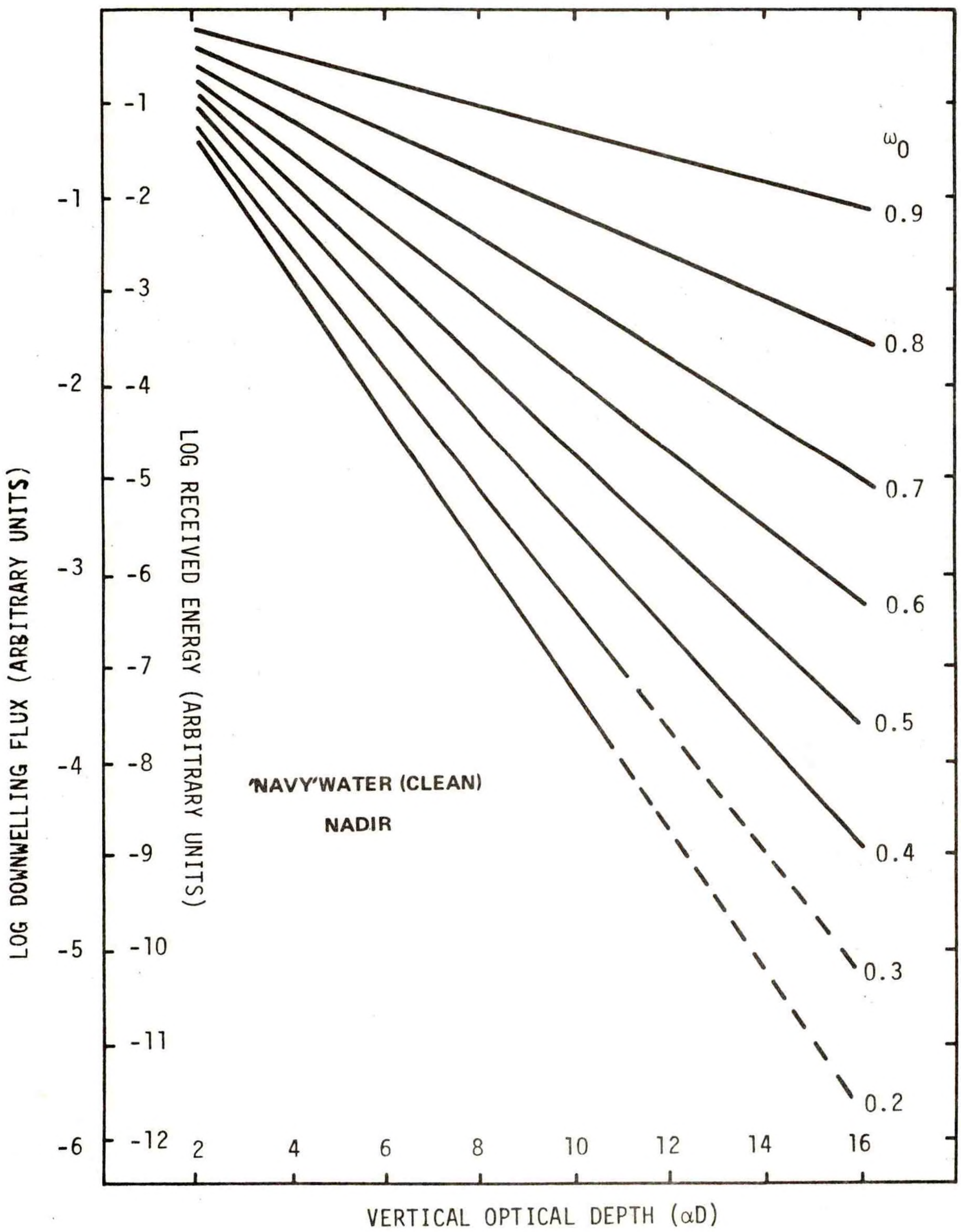

FIGURE 11. DOWNWELLING ENERGY AND TOTAL RECEIVED ENERGY AS FUNCTION OF VERTICAL OPTICAL DEPTH

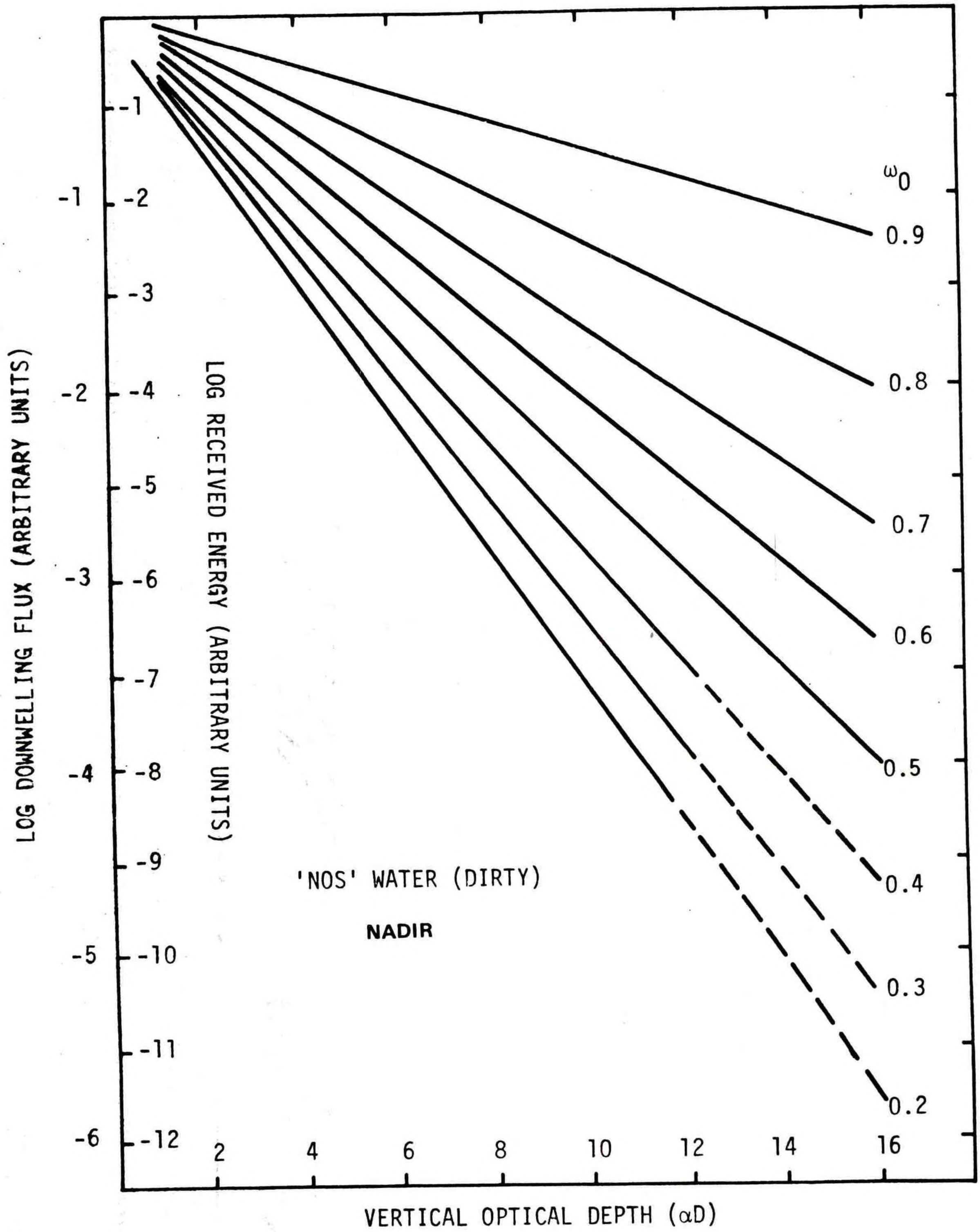

FIGURE 12. DOWNWELLING ENERGY AND TOTAL RECEIVED ENERGY AS FUNCTION OF VERTICAL OPTICAL DEPTH

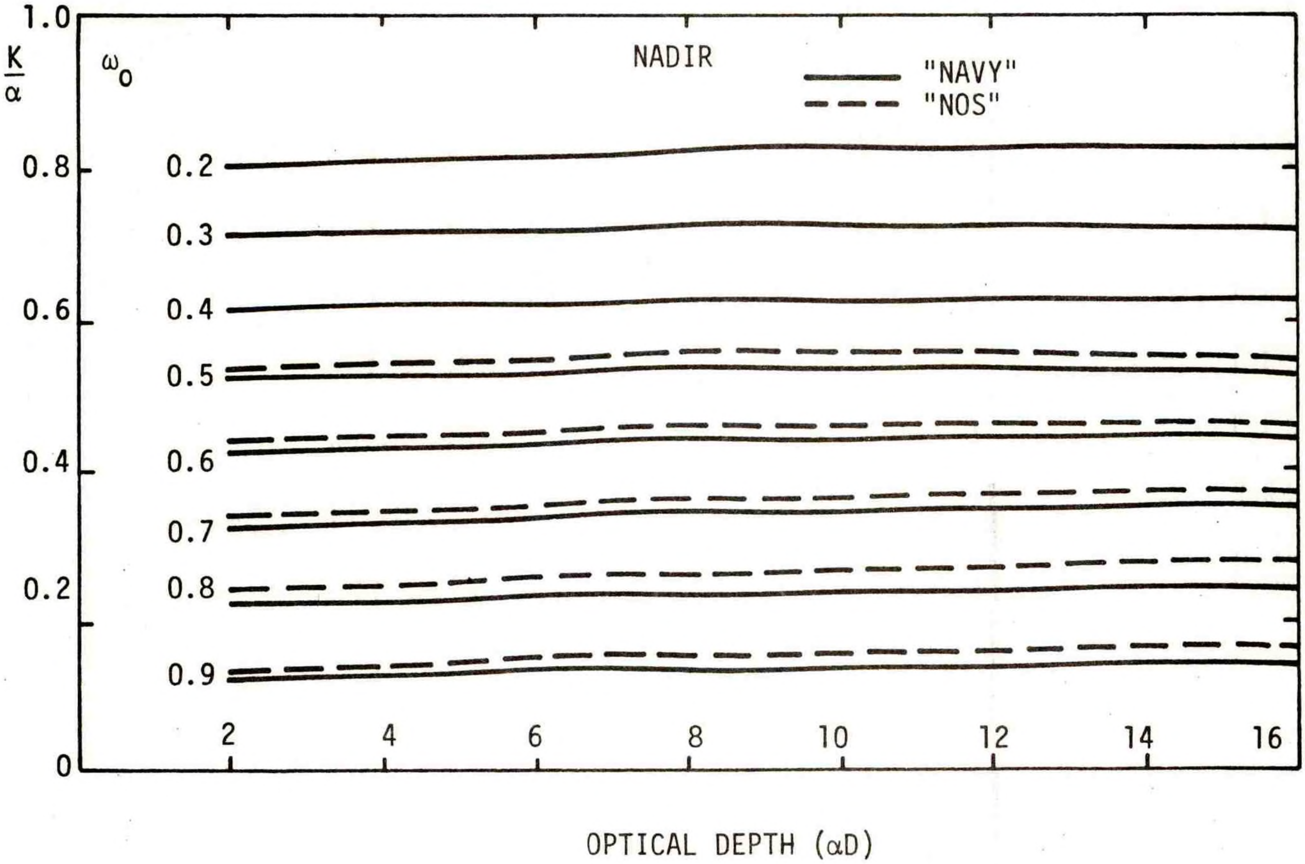

FIGURE 13. AVERAGE VALUES OF RATIO OF DIFFUSE TO NARROW BEAM ATTENUATION COEFFICIENTS AS FUNCTION OF VERTICAL OPTICAL DEPTH

FIGURE 14.

NORMALIZED ATTENUATION COEFFICIENTS AS FUNCTION OF ALBEDO OF SINGLE SCATTERING

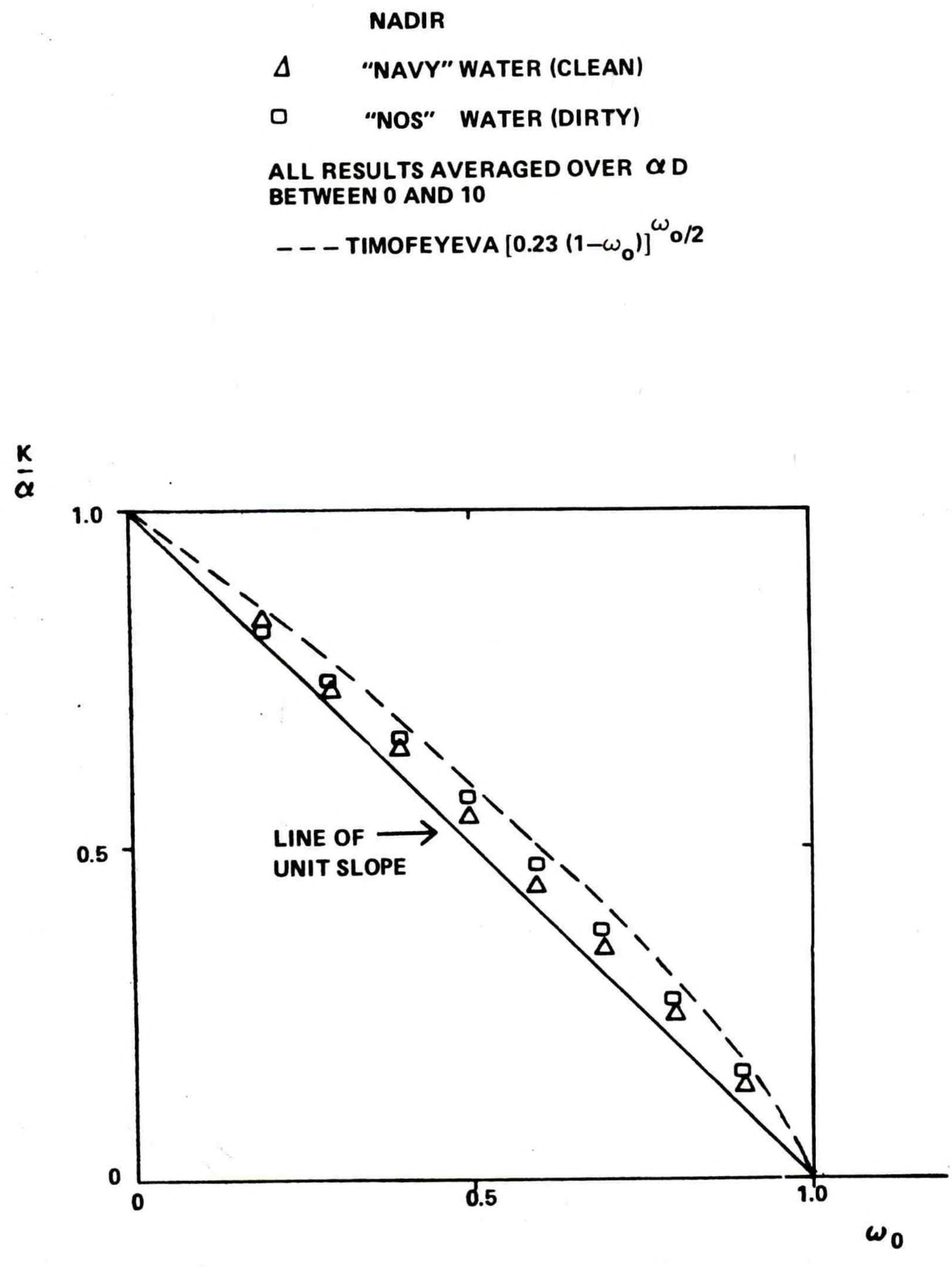

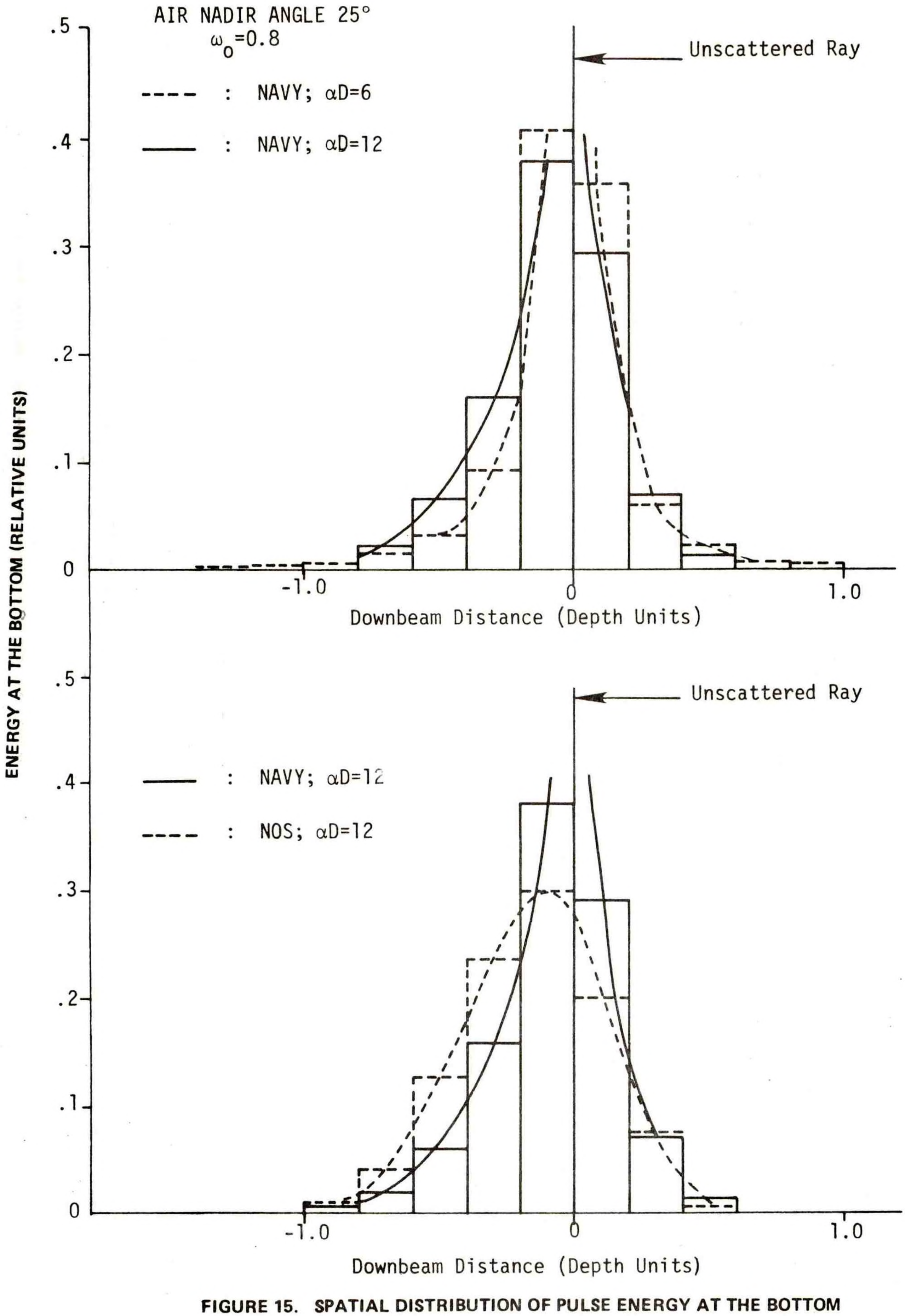

FIGURE 15. SPATIAL DISTRIBUTION OF PULSE ENERGY AT THE BOTTOM

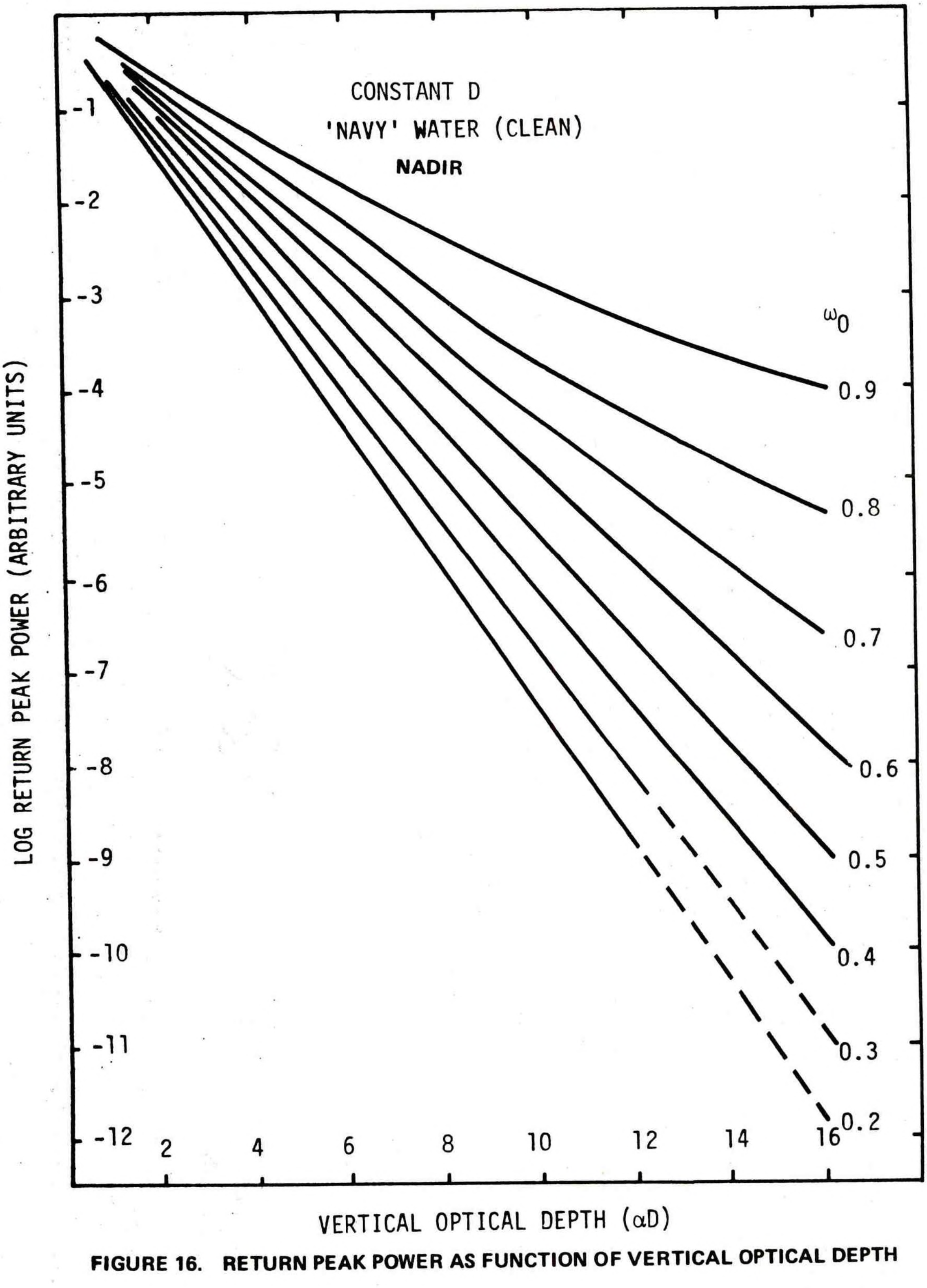

FIGURE 16. RETURN PEAK POWER AS FUNCTION OF VERTICAL OPTICAL DEPTH

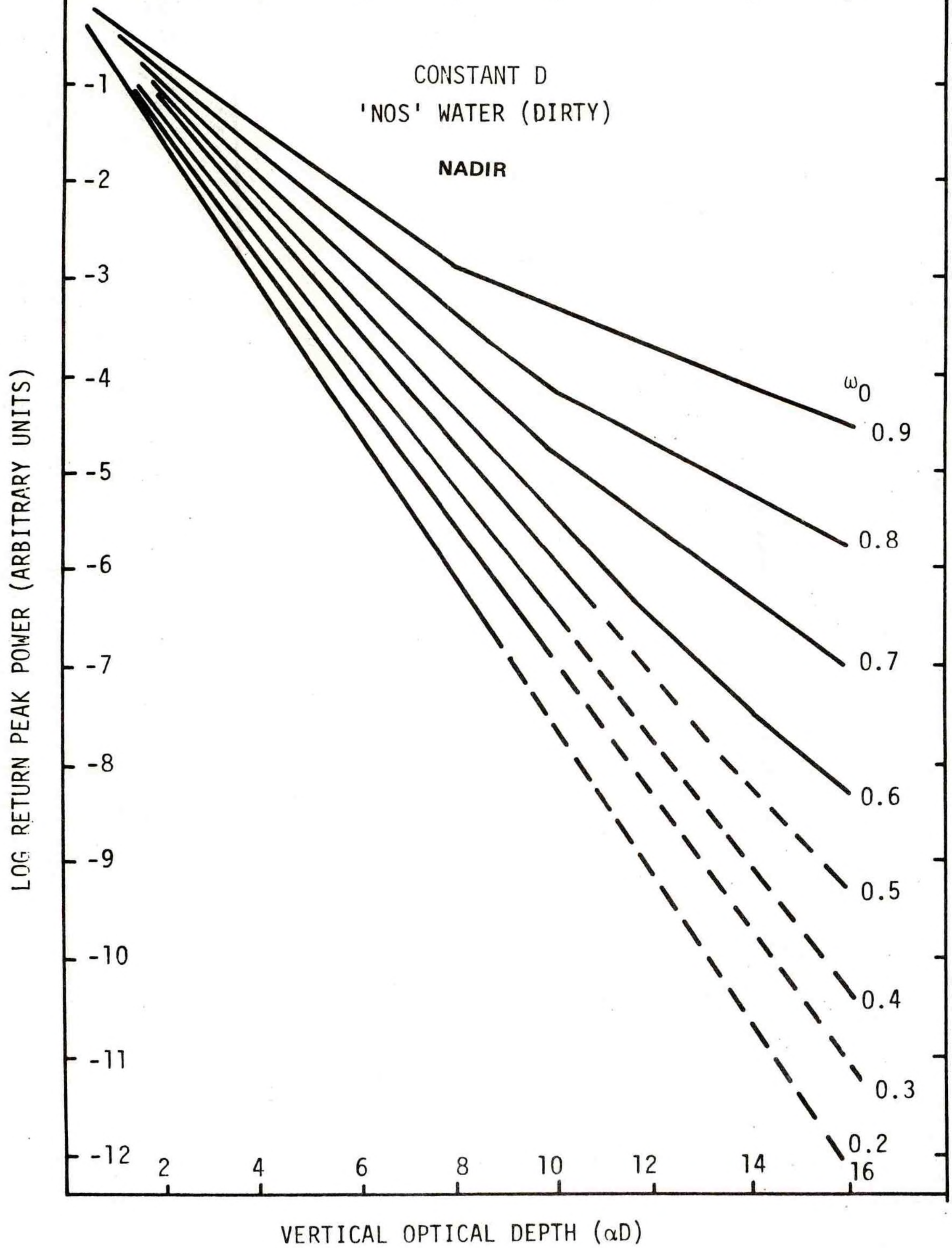

FIGURE 17. RETURN PEAK POWER AS FUNCTION OF VERTICAL OPTICAL DEPTH

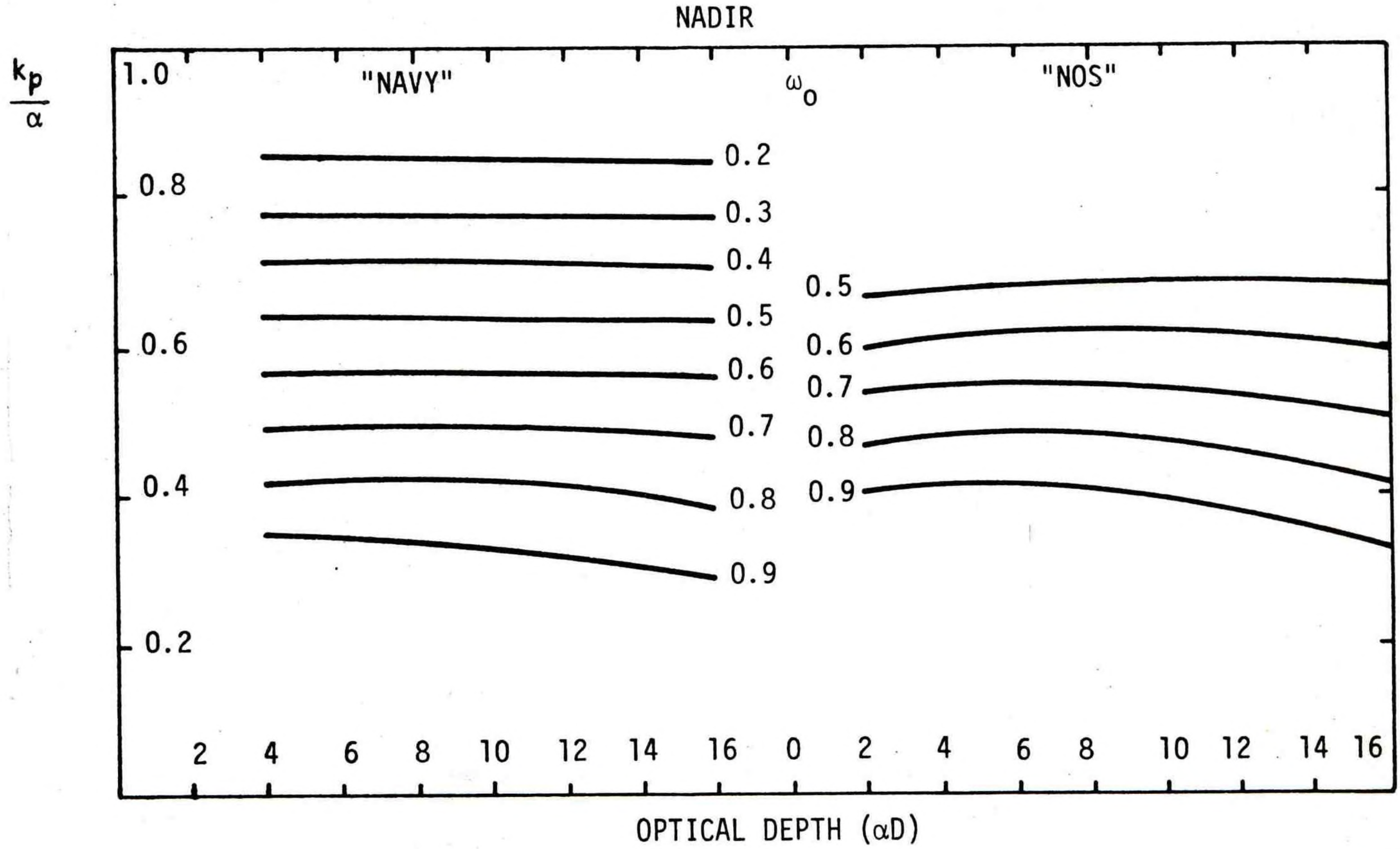

FIGURE 18. AVERAGE VALUE OF THE RATIO OF THE SYSTEM POWER ATTENUATION COEFFICIENT TO NARROW-BEAM ATTENUATION COEFFICIENT AS FUNCTION OF VERTICAL OPTICAL DEPTH

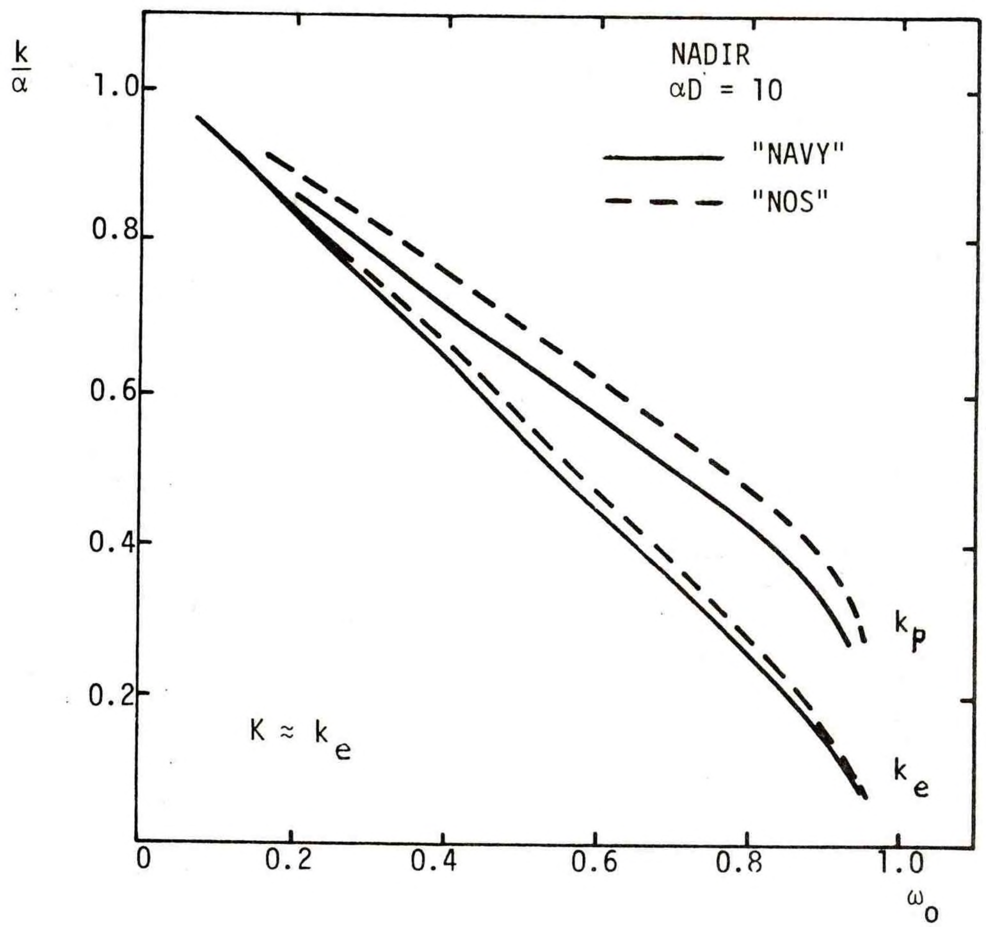

FIGURE 19. AVERAGE VALUES OF RATIOS OF SYSTEM POWER AND ENERGY ATTENUATION COEFFICIENTS TO NARROW-BEAM ATTENUATION COEFFICIENT AS FUNCTION OF SINGLE-SCATTERING ALBEDO

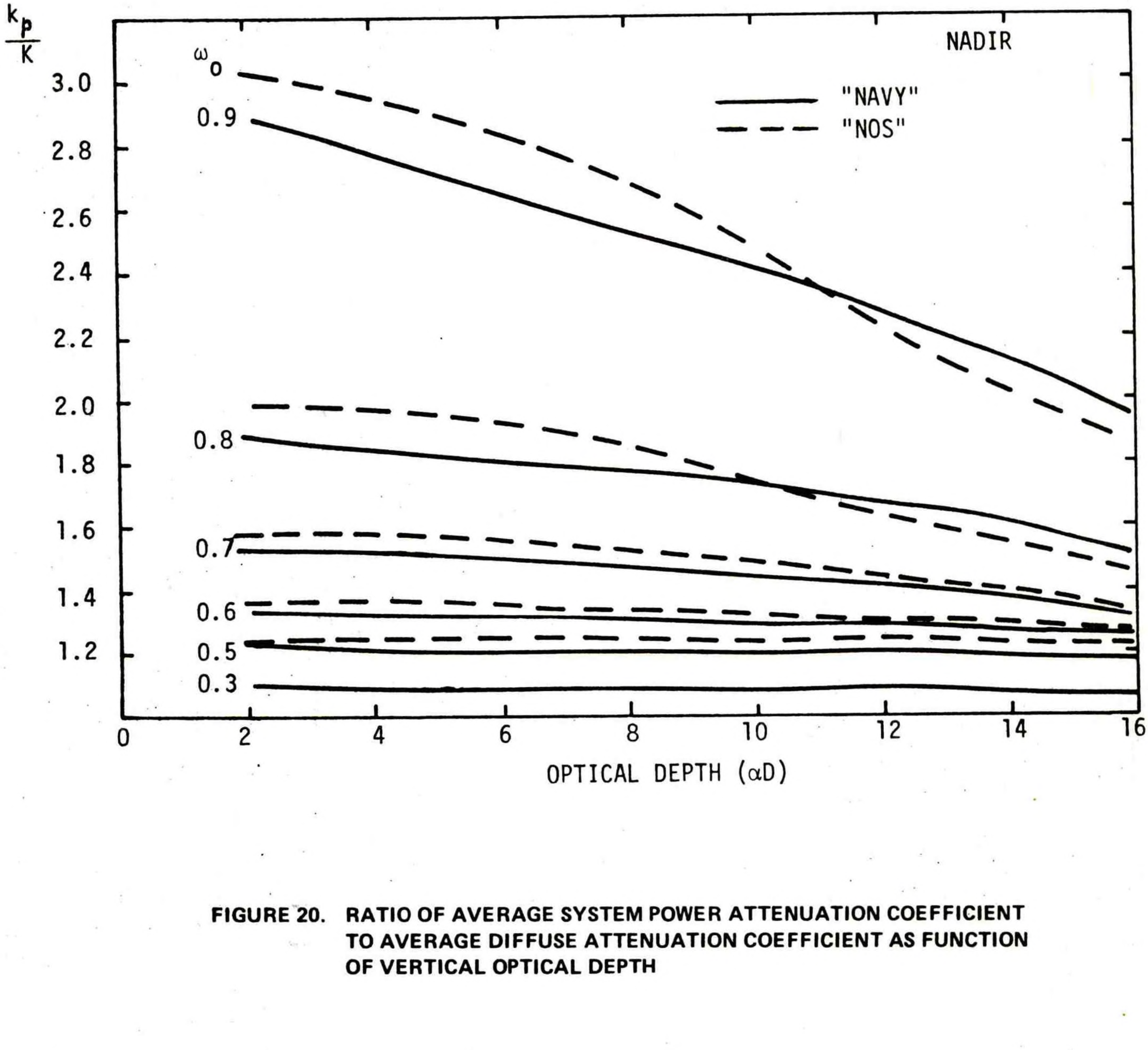

FIGURE 20. RATIO OF AVERAGE SYSTEM POWER ATTENUATION COEFFICIENT TO AVERAGE DIFFUSE ATTENUATION COEFFICIENT AS FUNCTION OF VERTICAL OPTICAL DEPTH

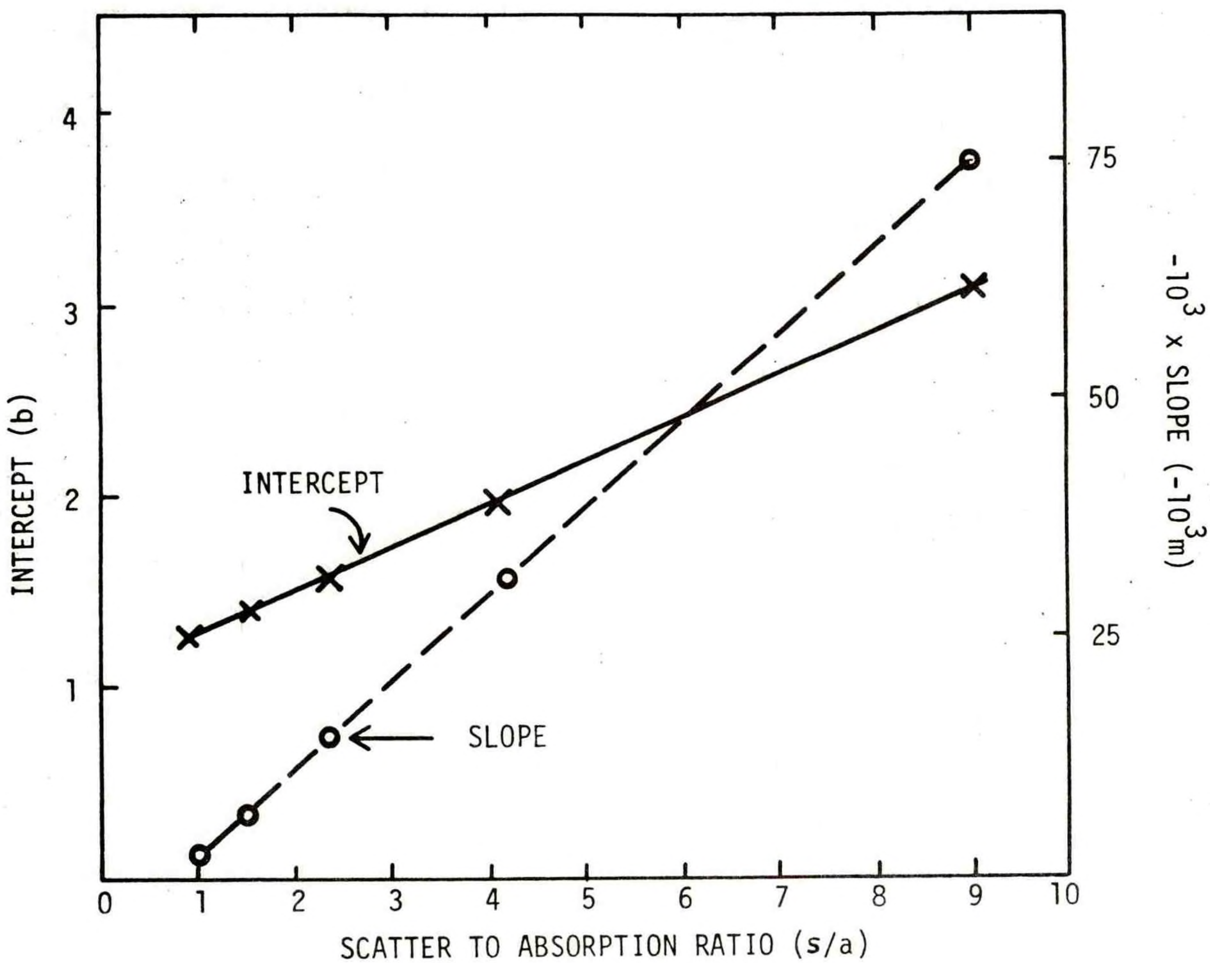

FIGURE 21. SLOPE AND INTERCEPT PARAMETERS OF $k_p/K = m\alpha D + b$ AS FUNCTION OF SCATTER TO ABSORPTION RATIO

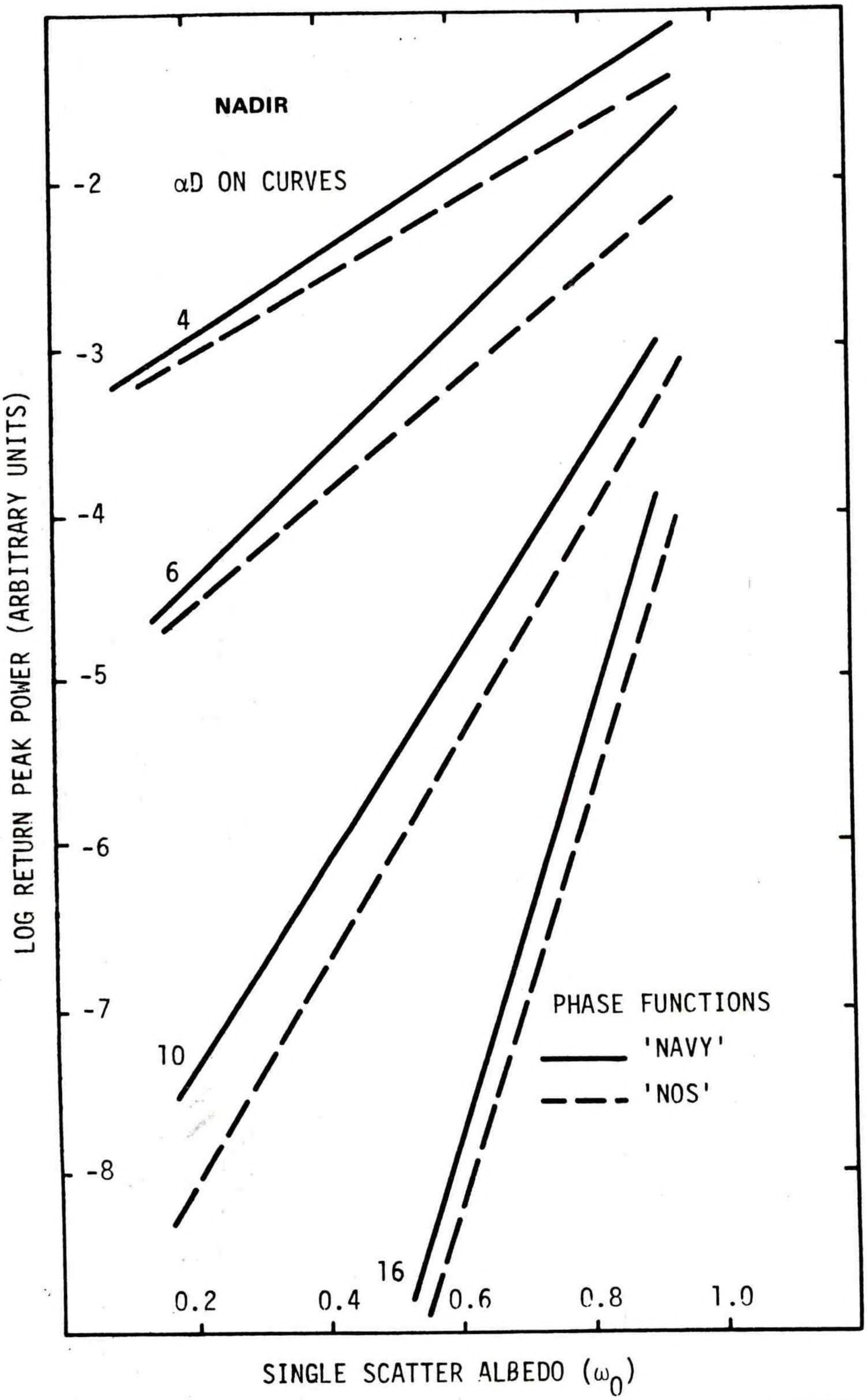

FIGURE 22. RETURN PEAK POWER AS FUNCTION OF SINGLE-SCATTER ALBEDO

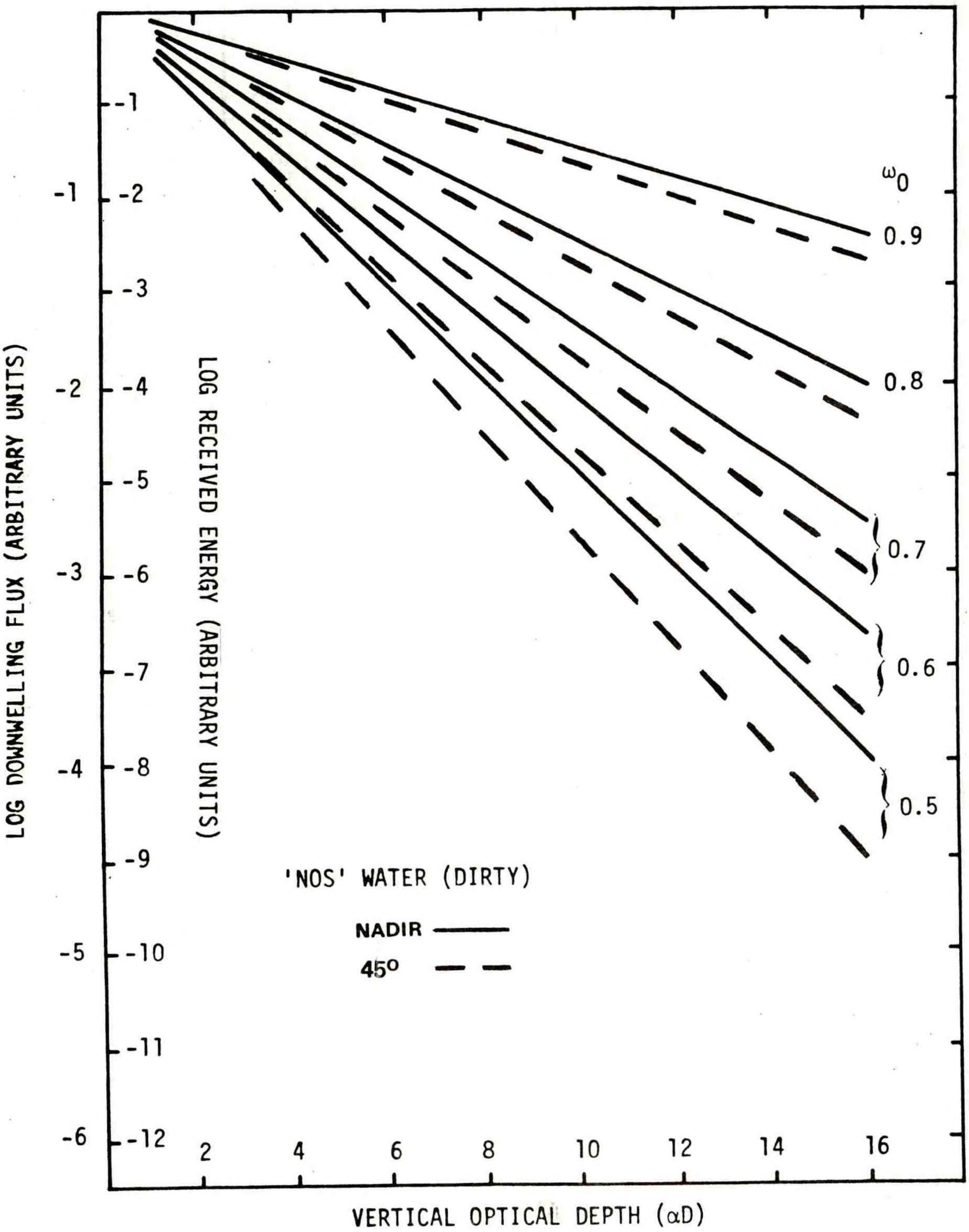

FIGURE 23. DOWNWELLING ENERGY AND TOTAL RECEIVED ENERGY AS FUNCTION OF VERTICAL OPTICAL DEPTH

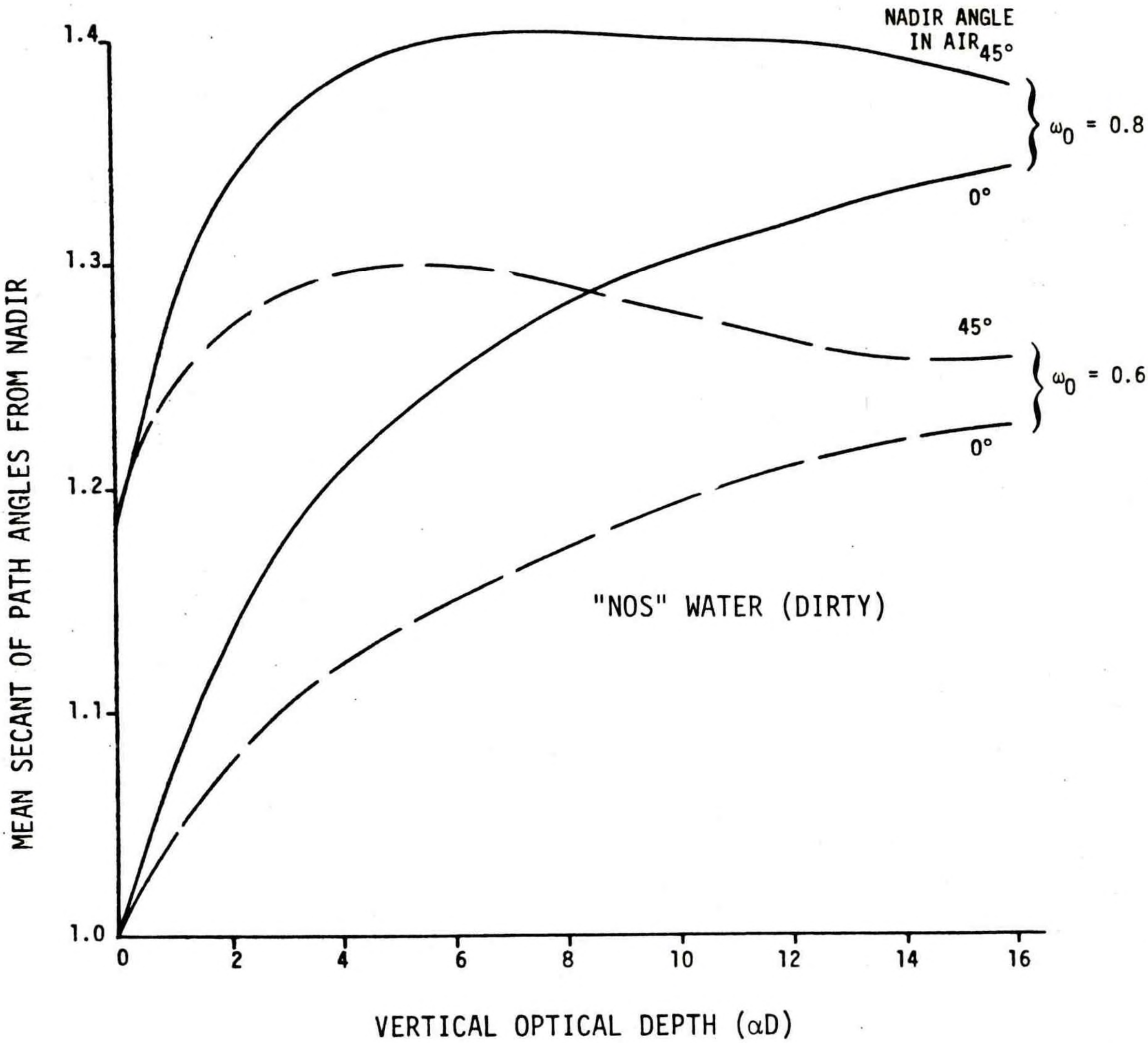

FIGURE 24. MEAN SECANT OF PHOTON PATH ANGLES FROM NADIR AS FUNCTION OF VERTICAL OPTICAL DEPTH

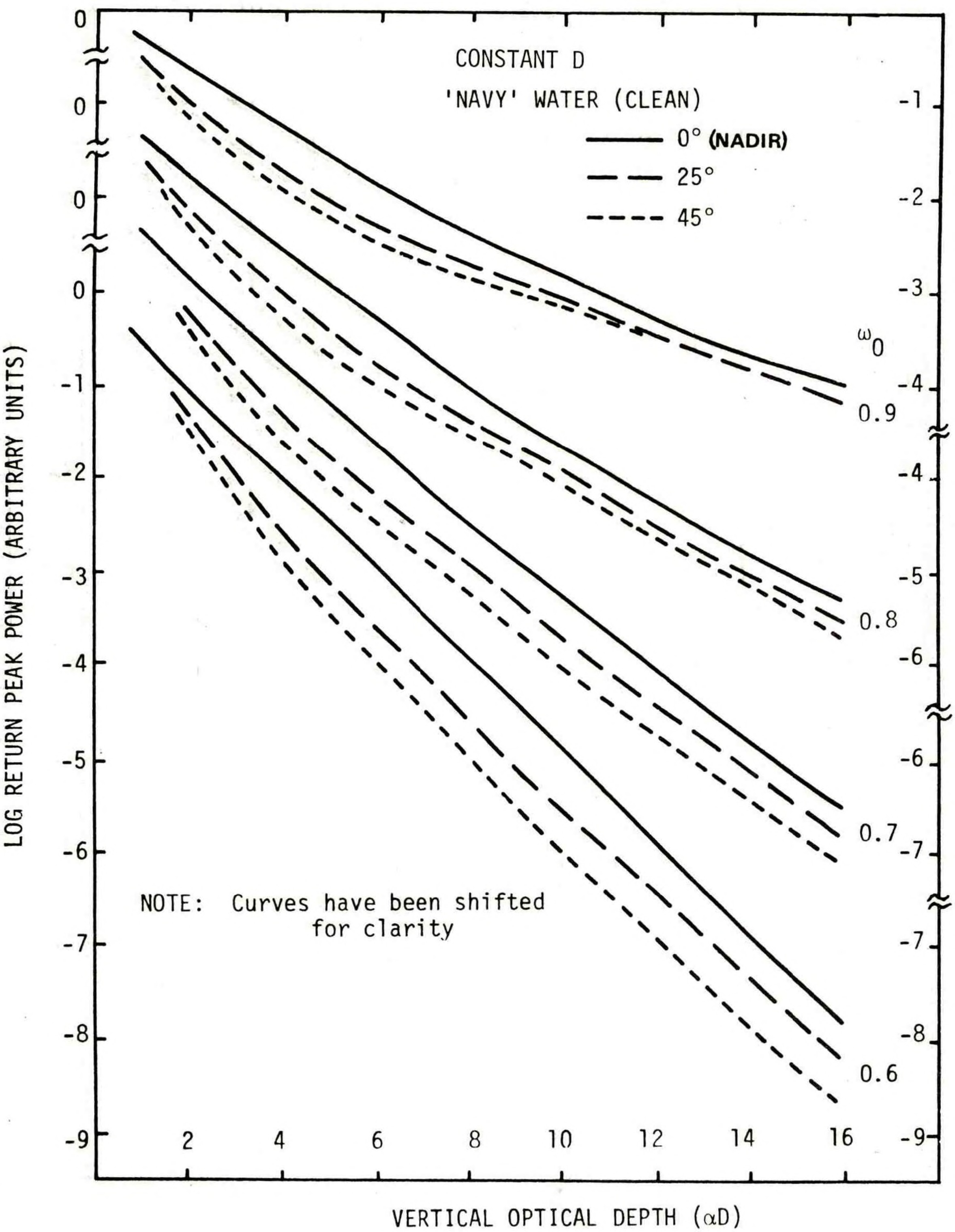

FIGURE 25. RETURN PEAK POWER AS FUNCTION OF VERTICAL OPTICAL DEPTH AT THREE NADIR ANGLES

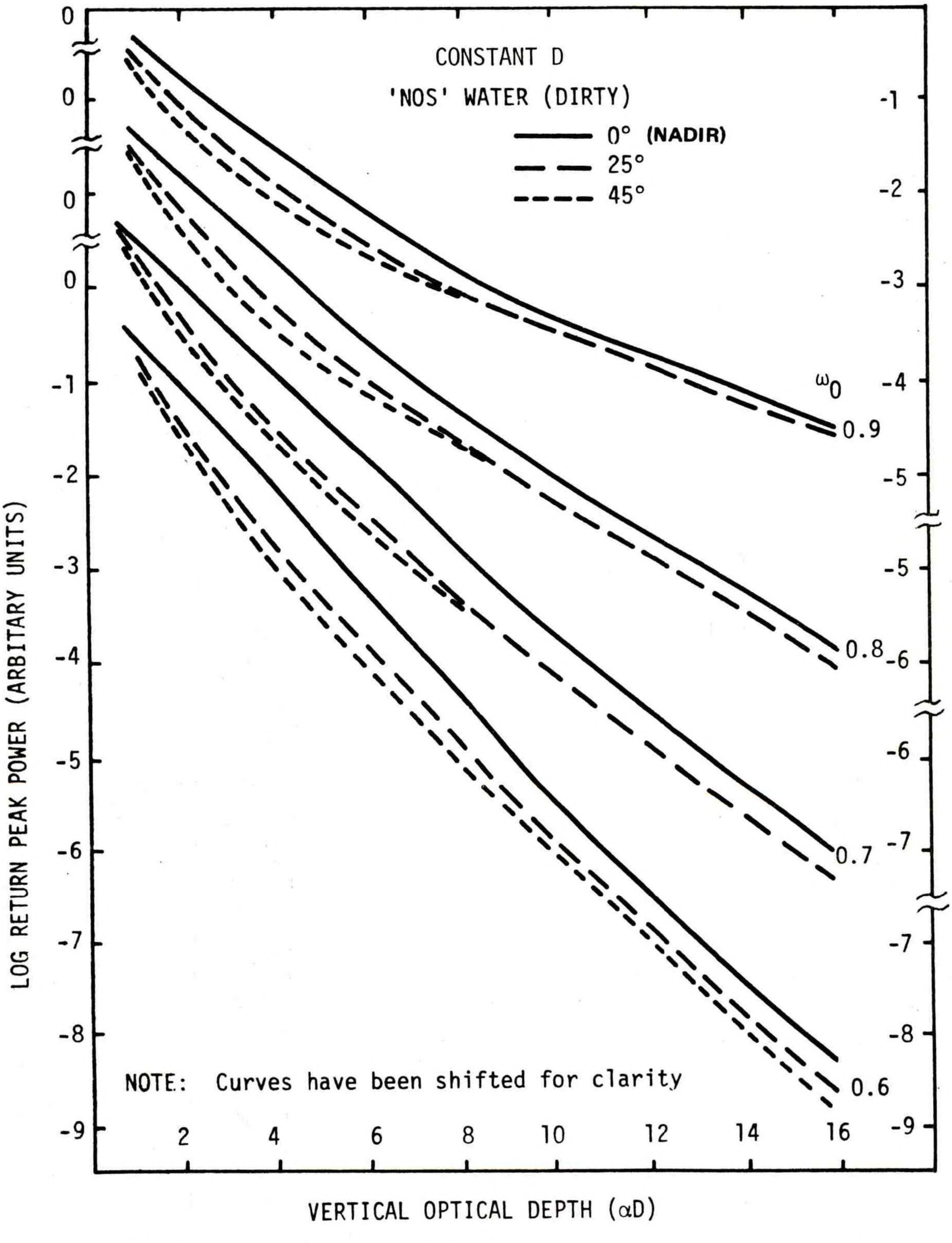

FIGURE 26. RETURN PEAK POWER AS FUNCTION OF VERTICAL OPTICAL DEPTH AT THREE NADIR ANGLES

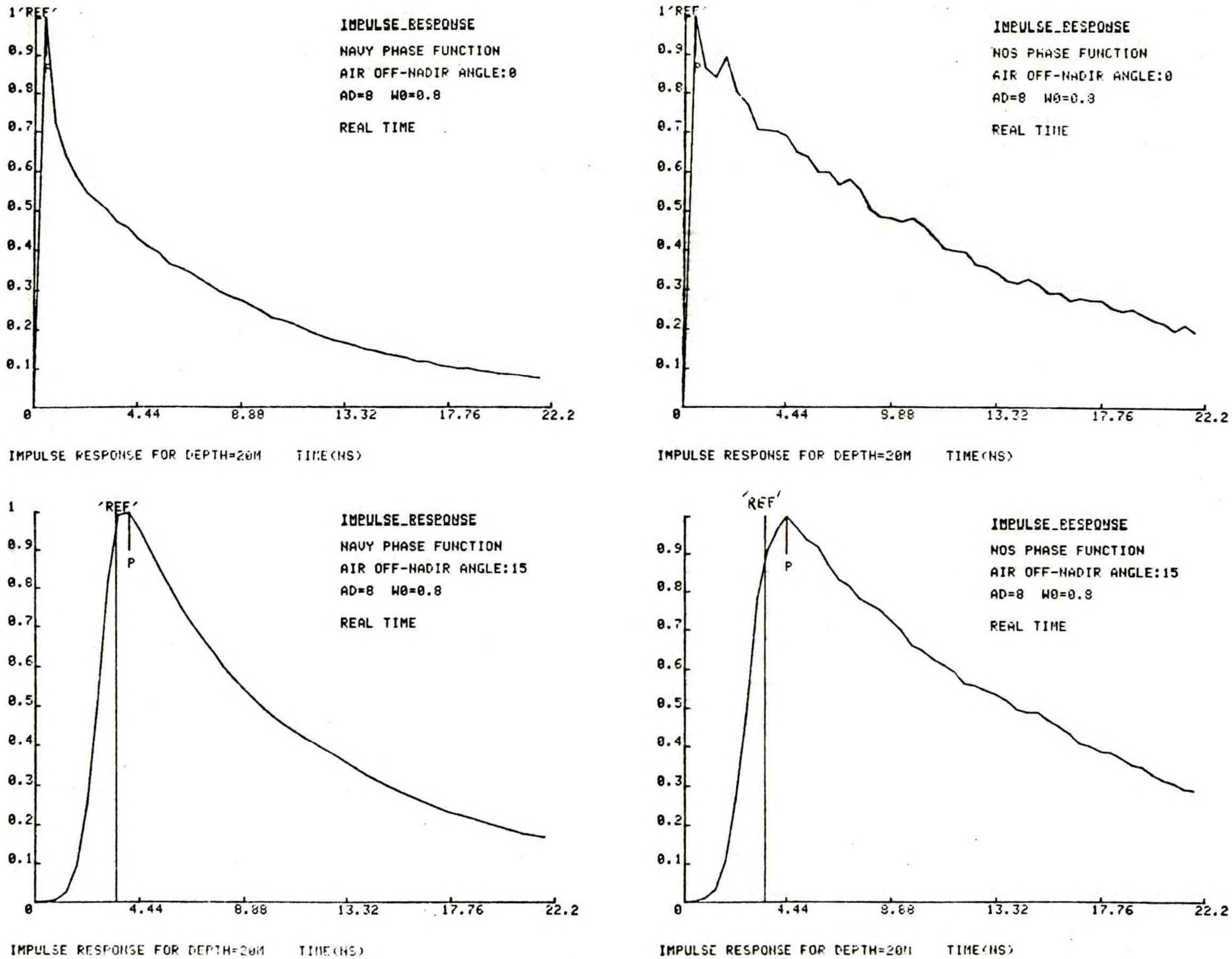

FIGURE 27. SENSITIVITY TO PHASE FUNCTION

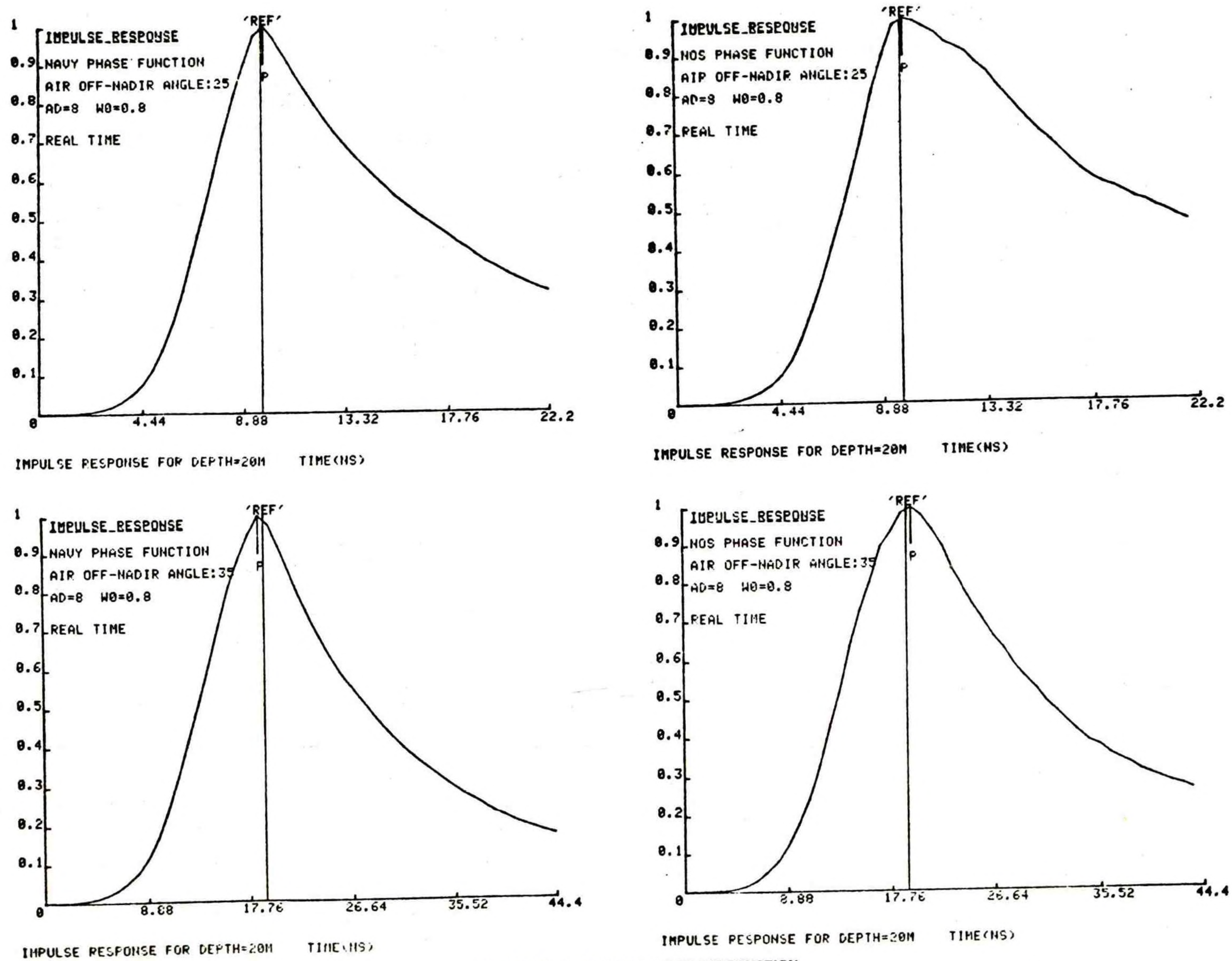

FIGURE 28. SENSITIVITY TO PHASE FUNCTION

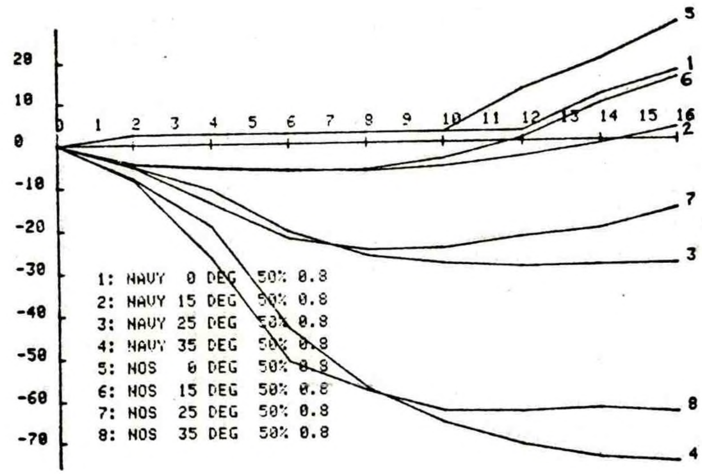

DEPTH MEASUREMENT BIAS (CM) VS OPTICAL
DEPTH AT A DEPTH OF 20 M

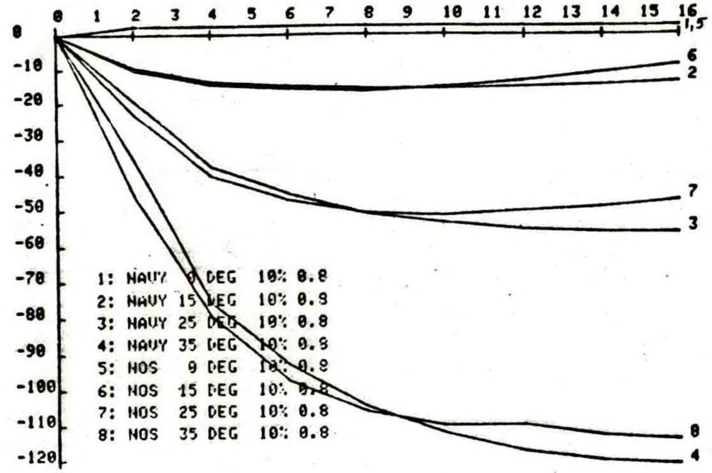

DEPTH MEASUREMENT BIAS (CM) VS OPTICAL
DEPTH AT A DEPTH OF 20 M

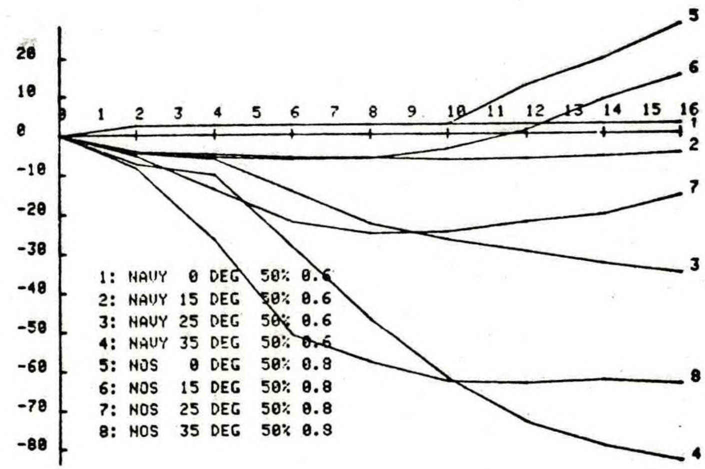

DEPTH MEASUREMENT BIAS (CM) VS OPTICAL
DEPTH AT A DEPTH OF 20 M

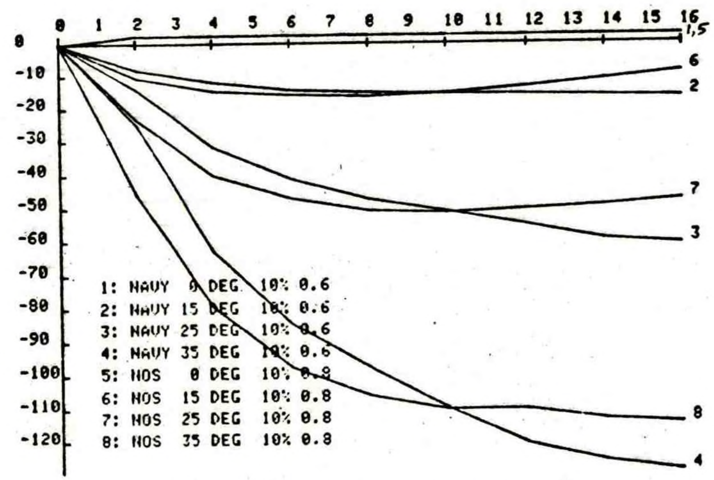

DEPTH MEASUREMENT BIAS (CM) VS OPTICAL
DEPTH AT A DEPTH OF 20 M

FIGURE 29. SENSITIVITY TO PHASE FUNCTION

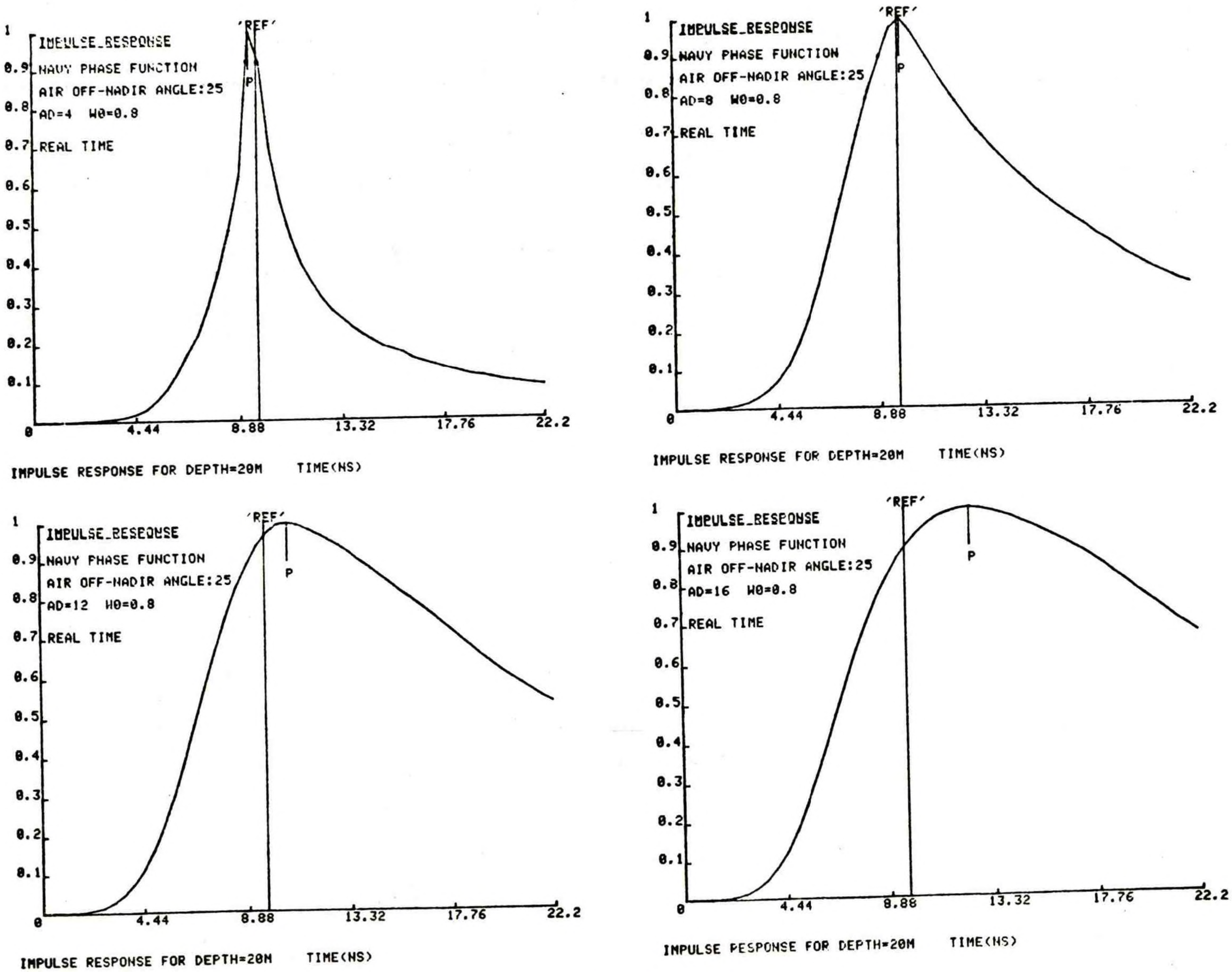

FIGURE 30. SENSITIVITY TO αD

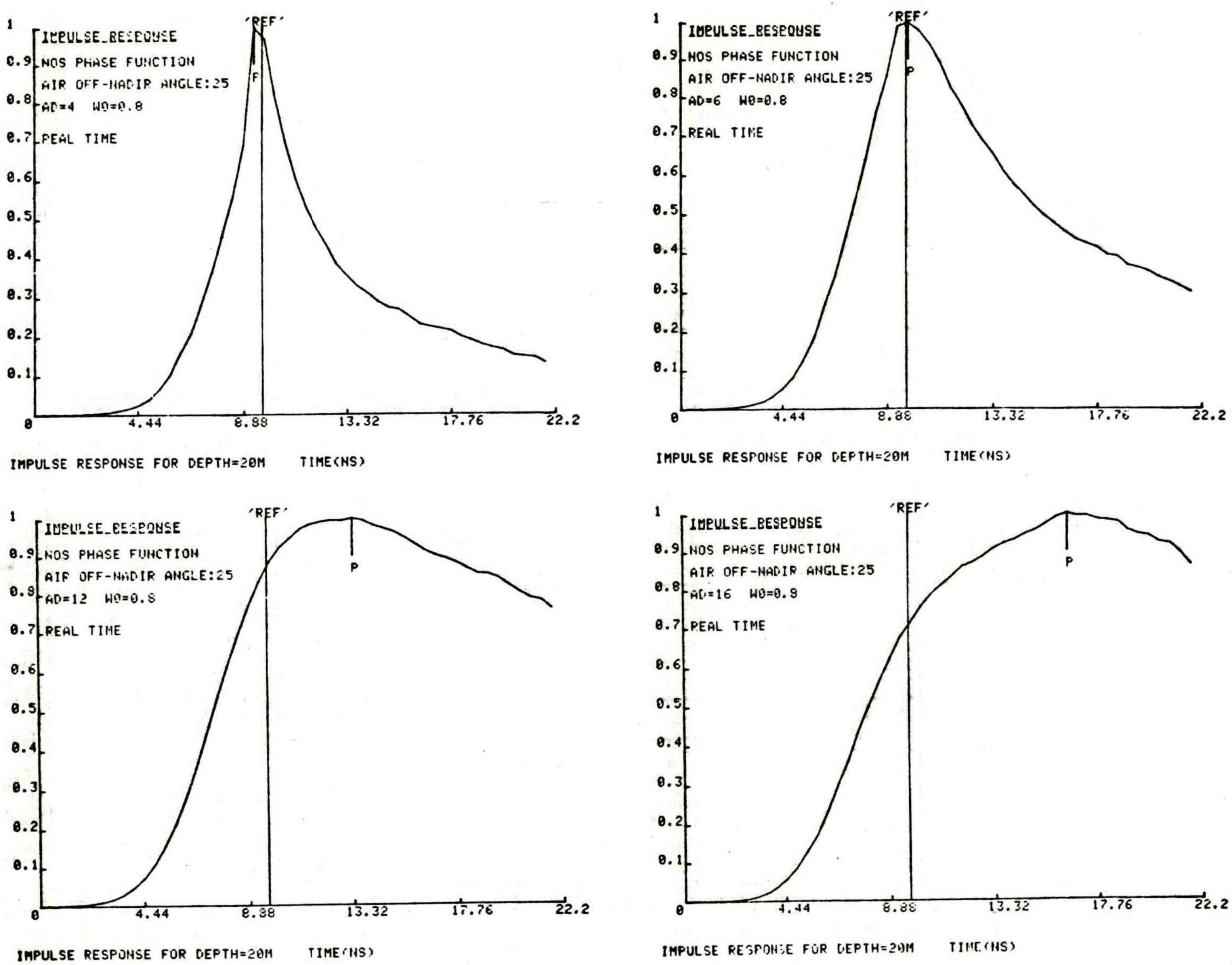

FIGURE 31. SENSITIVITY TO αD

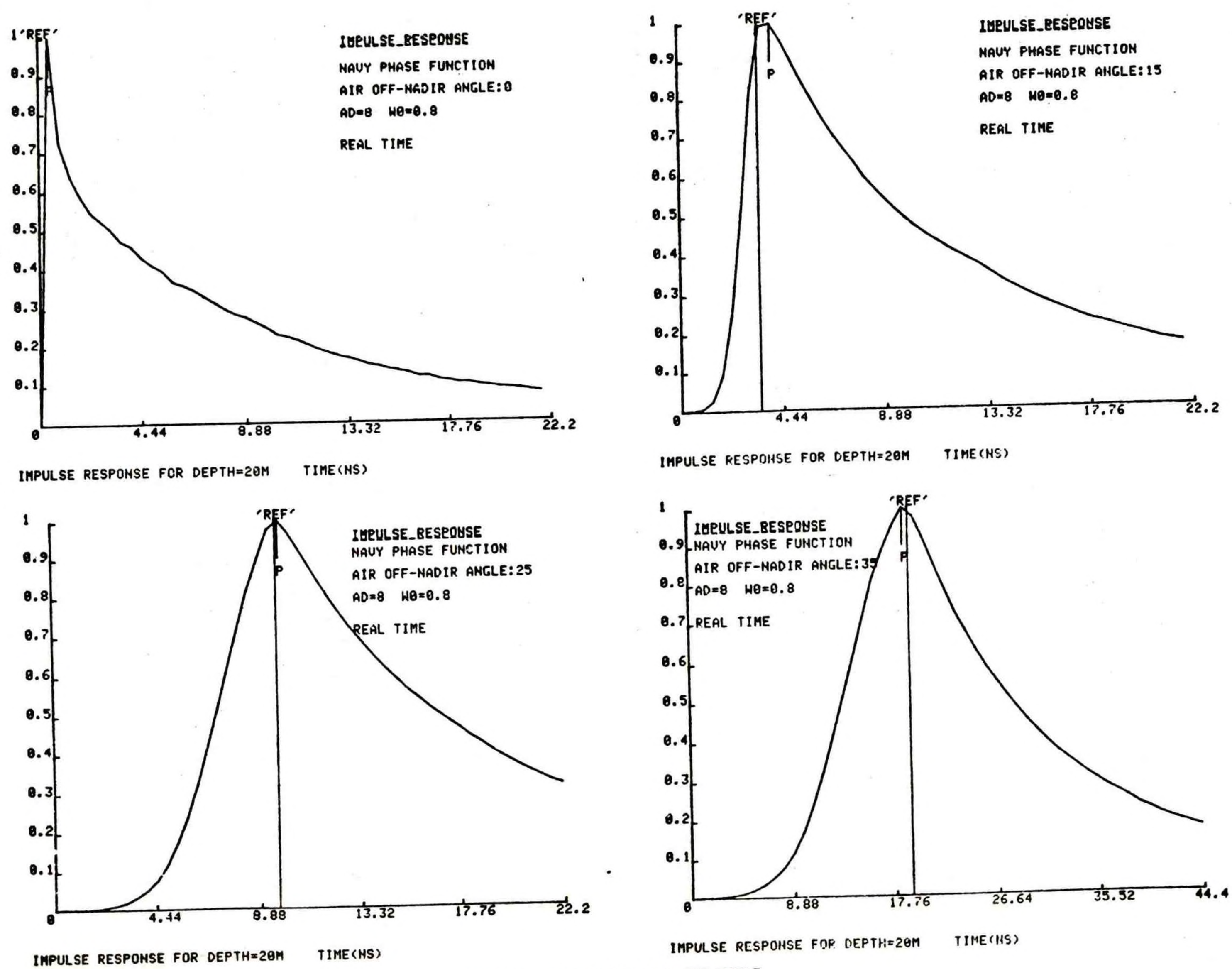

FIGURE 32. SENSITIVITY TO NADIR ANGLE

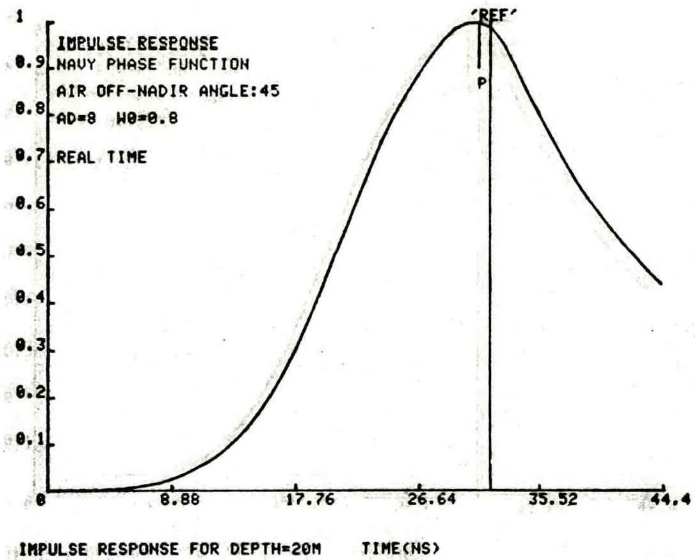

FIGURE 32A. SENSITIVITY TO NADIR ANGLE

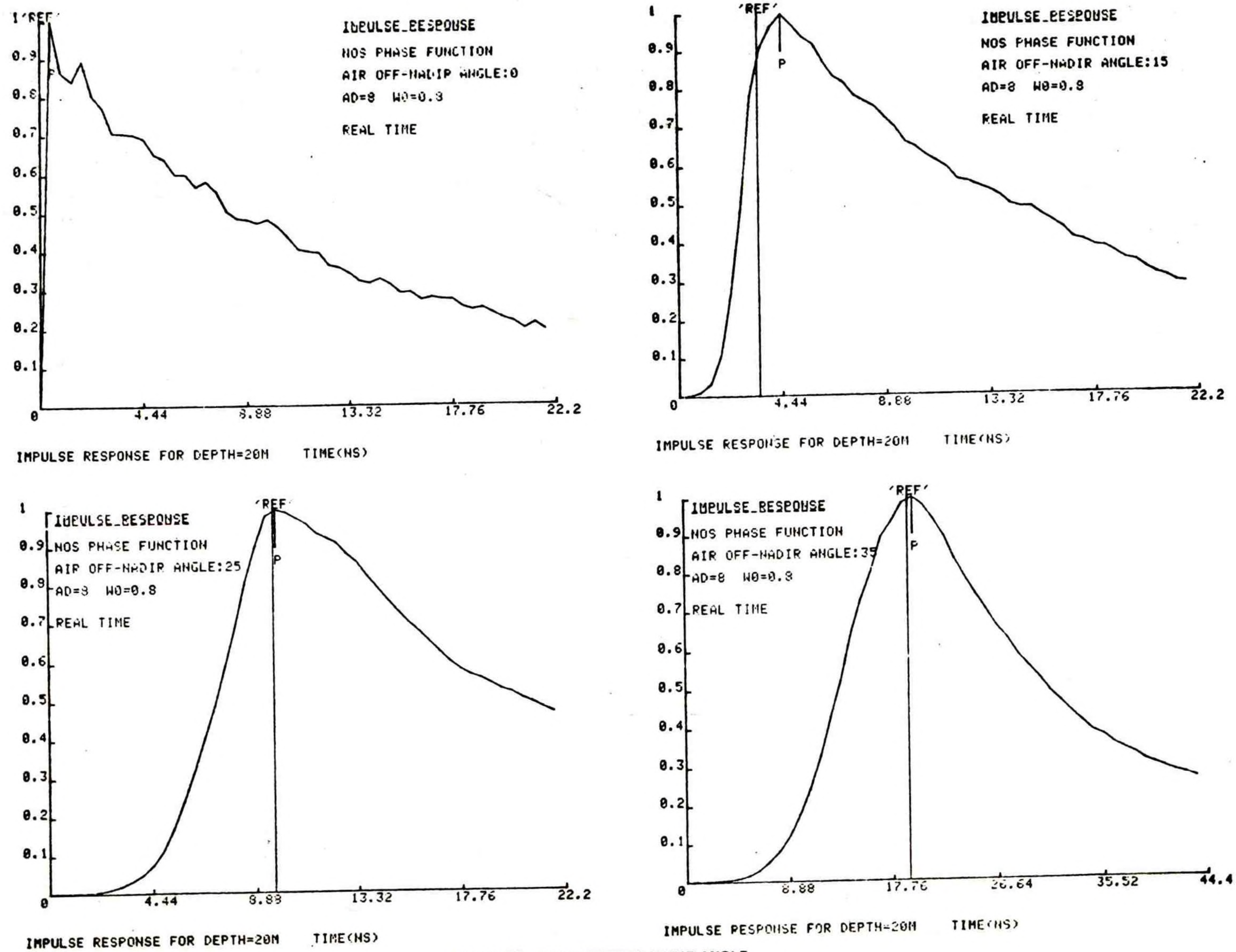

FIGURE 33. SENSITIVITY TO NADIR ANGLE

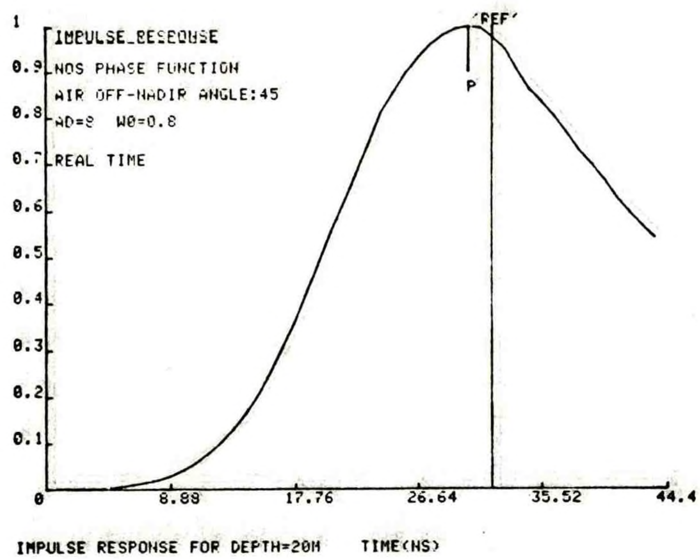

FIGURE 33A. SENSITIVITY TO NADIR ANGLE

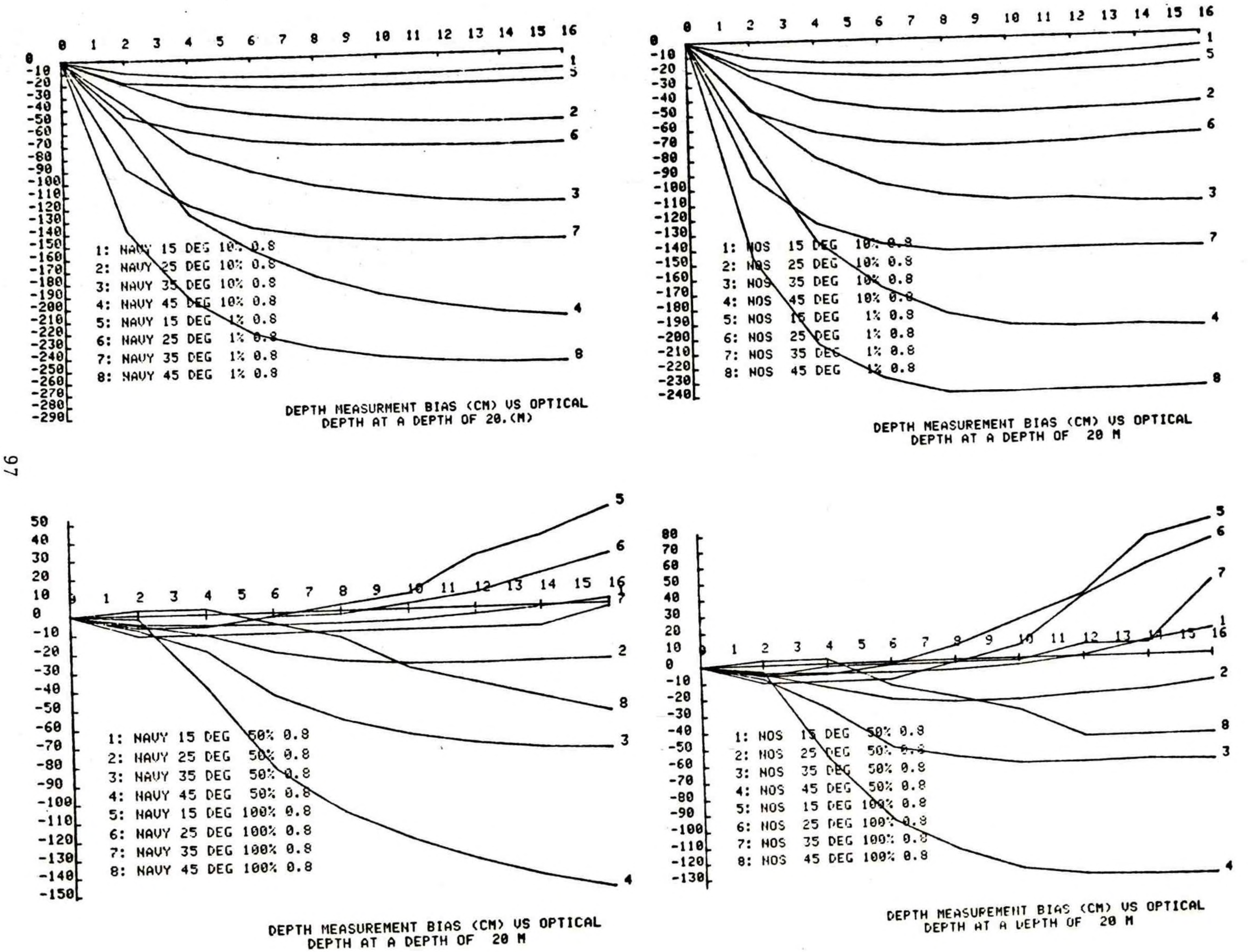

FIGURE 34. SENSITIVITY TO NADIR ANGLE

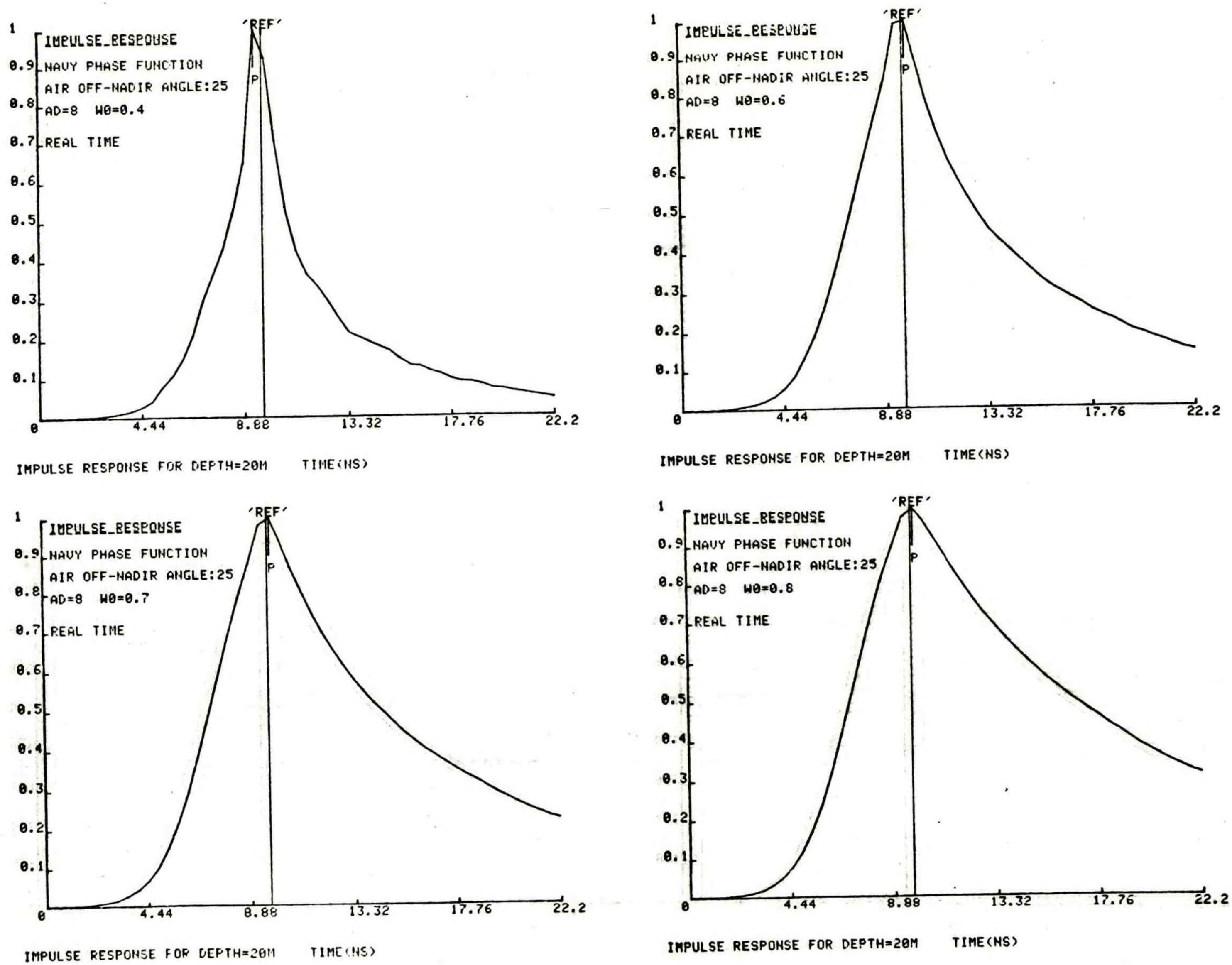

FIGURE 35. SENSITIVITY TO ALBEDO FOR SINGLE SCATTERING

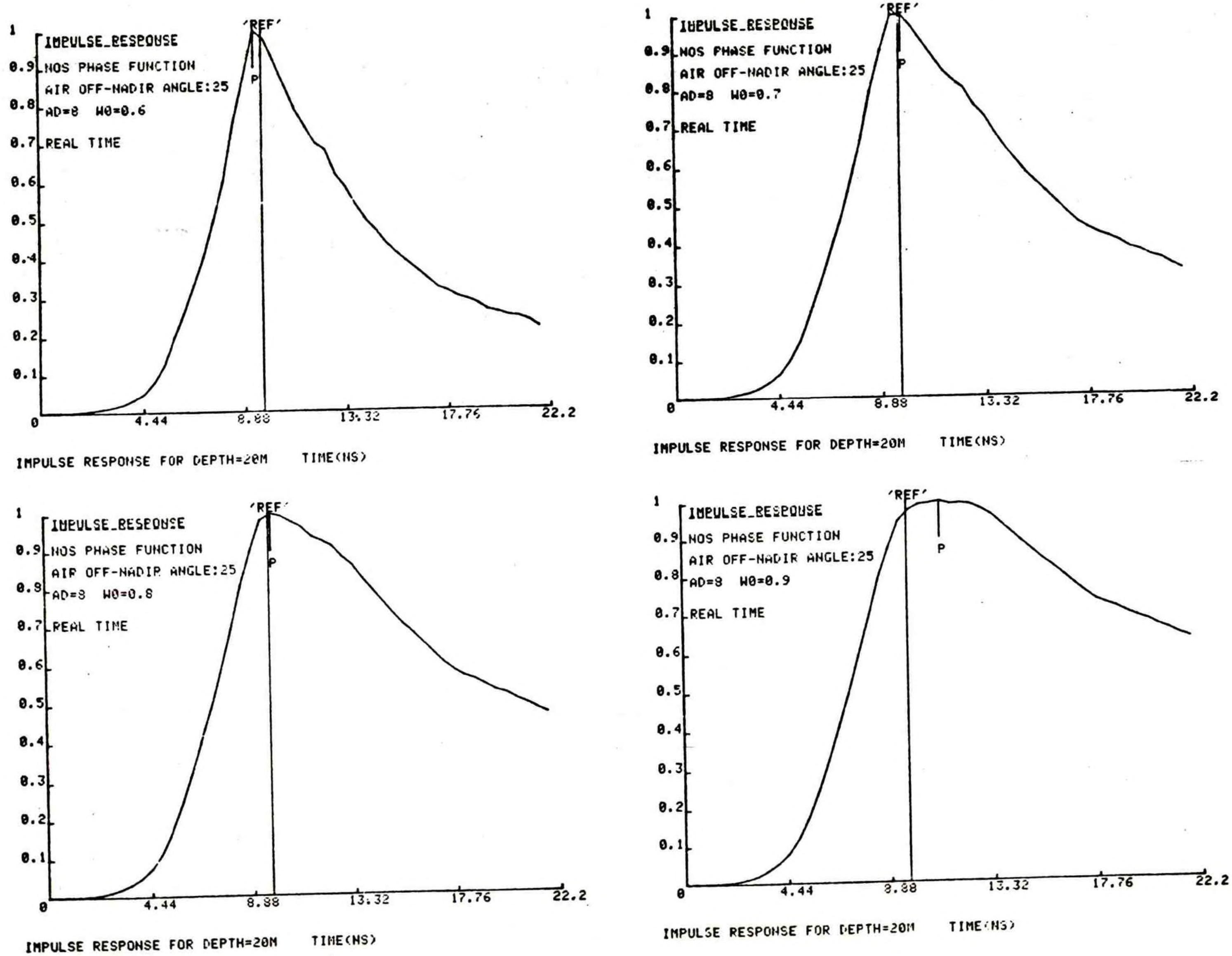

FIGURE 36. SENSITIVITY TO ALBEDO FOR SINGLE SCATTERING

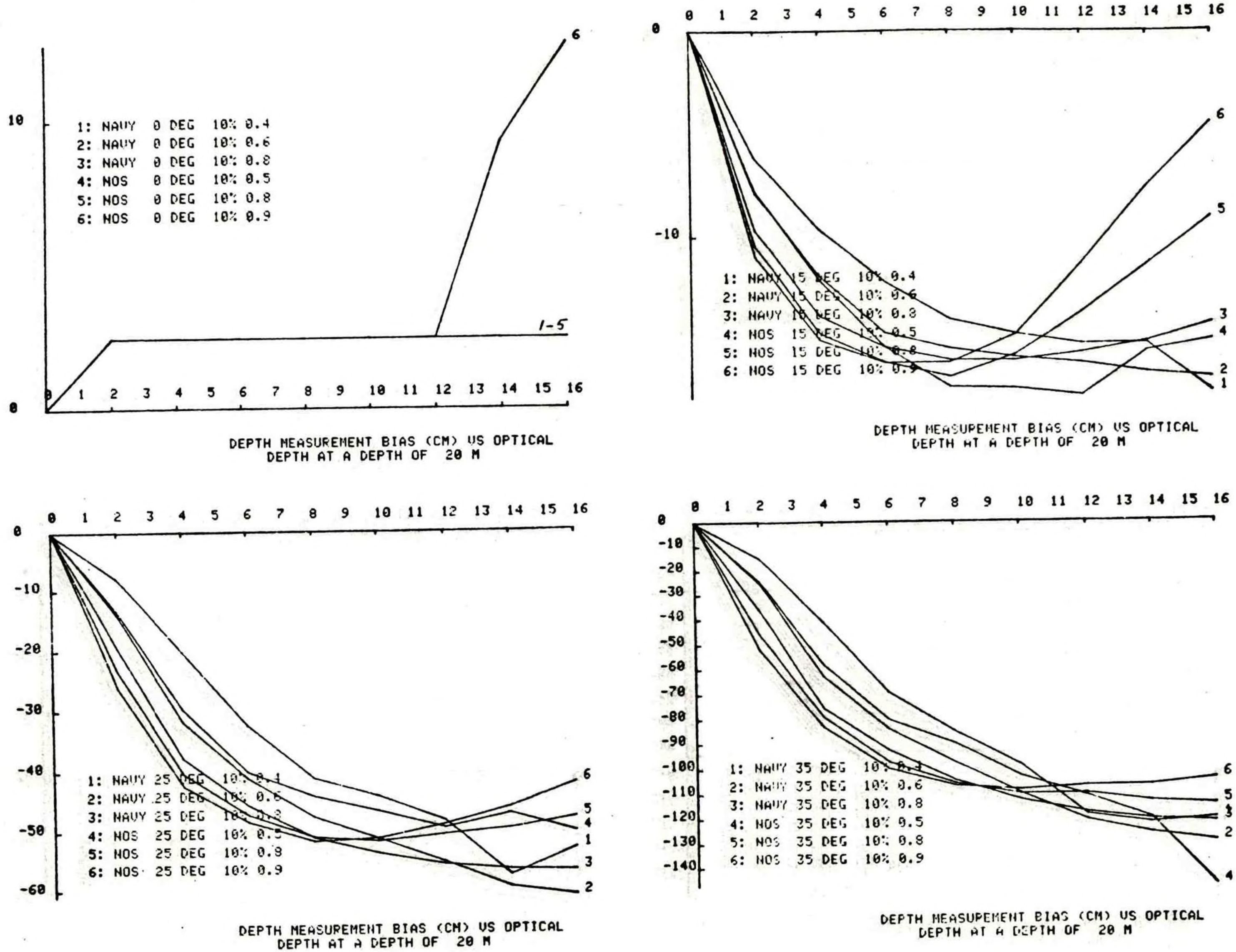

FIGURE 37. SENSITIVITY TO ALBEDO FOR SINGLE SCATTERING

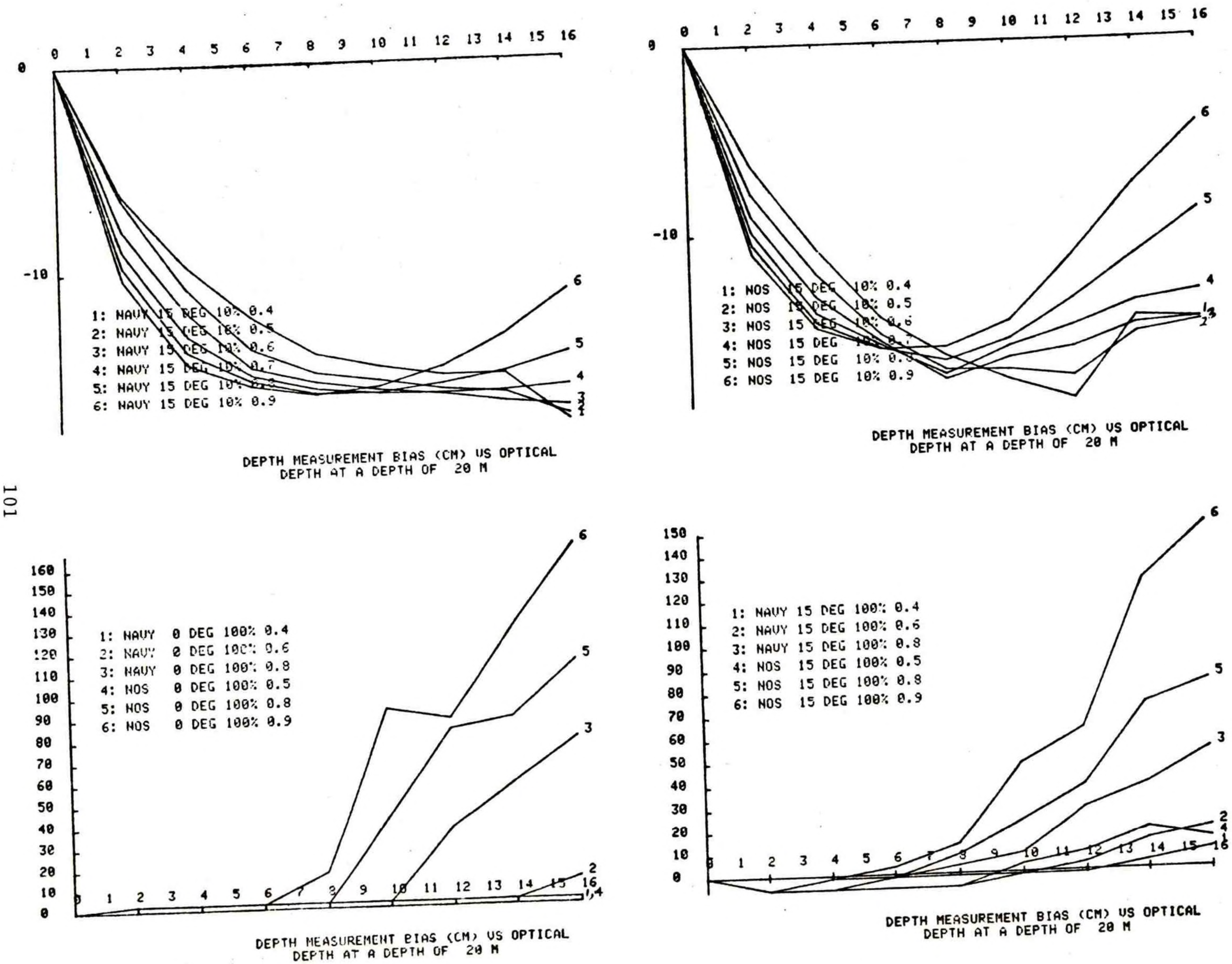

FIGURE 38. SENSITIVITY TO ALBEDO FOR SINGLE SCATTERING

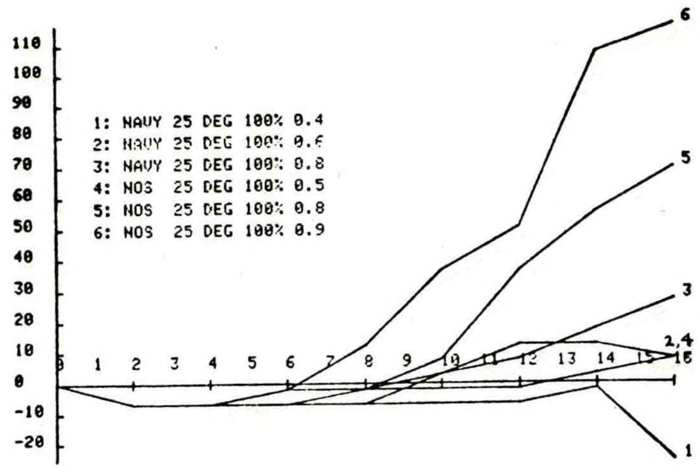

DEPTH MEASUREMENT BIAS (CM) VS OPTICAL
DEPTH AT A DEPTH OF 20 M

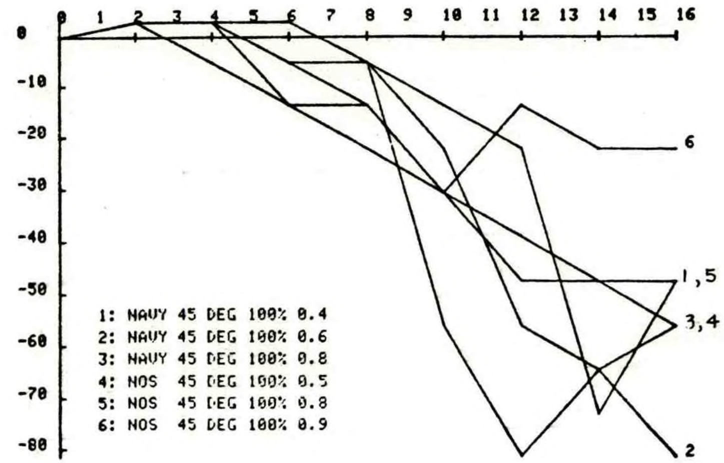

DEPTH MEASUREMENT BIAS (CM) VS OPTICAL
DEPTH AT A DEPTH OF 20 M

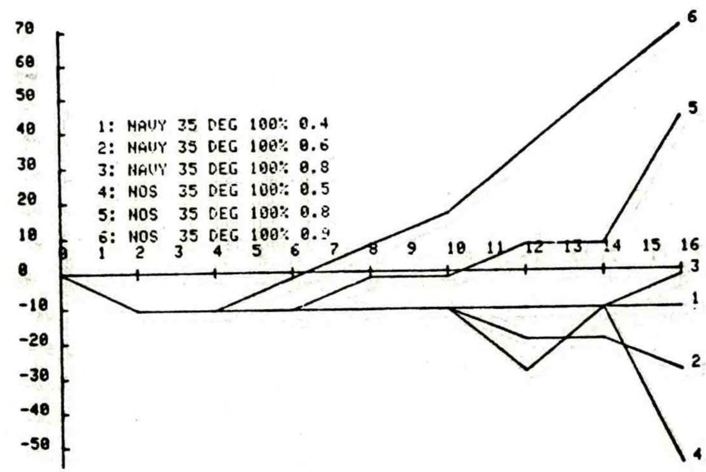

DEPTH MEASUREMENT BIAS (CM) VS OPTICAL
DEPTH AT A DEPTH OF 20 M

FIGURE 39. SENSITIVITY TO ALBEDO FOR SINGLE SCATTERING

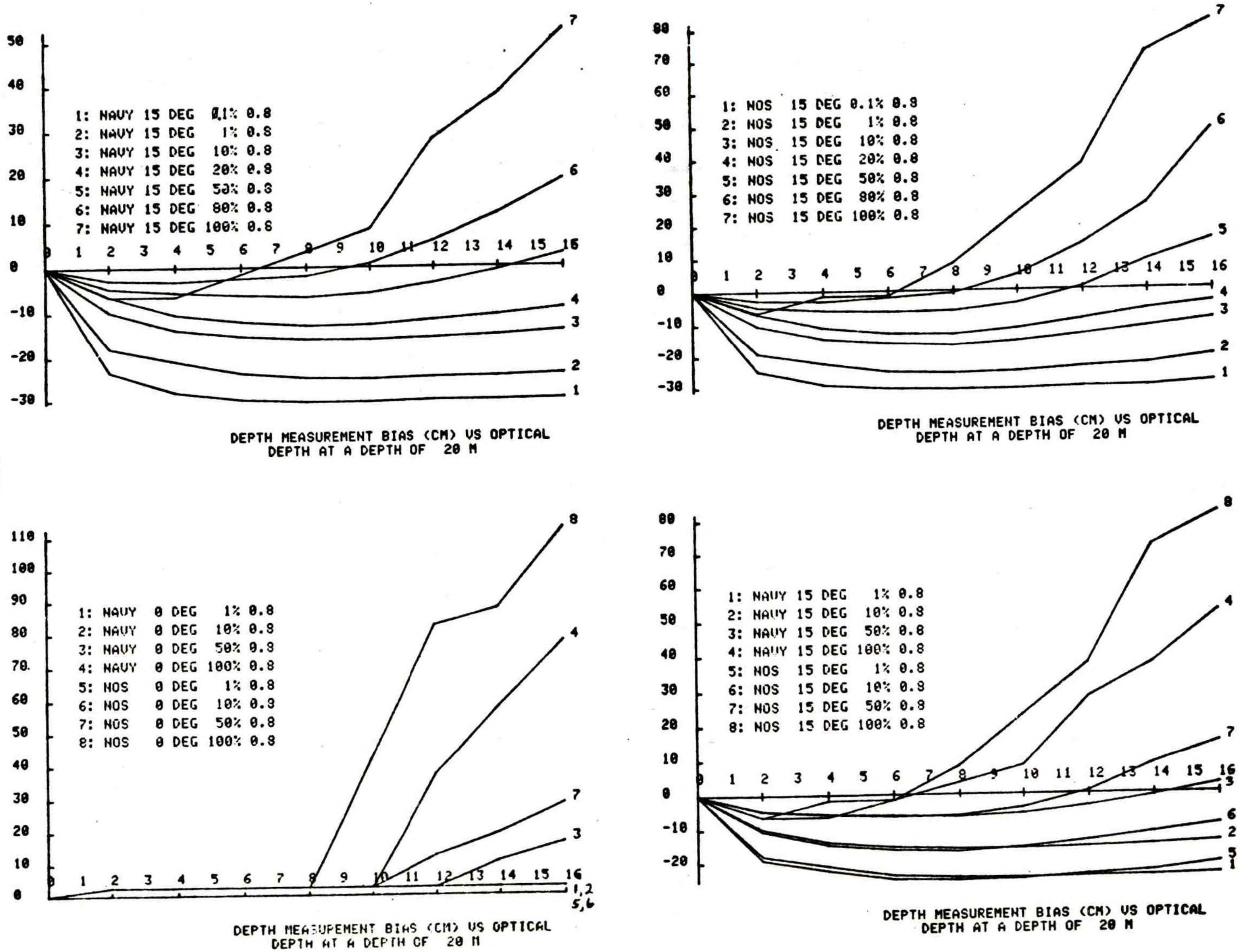

FIGURE 40. SENSITIVITY TO LINEAR FRACTIONAL THRESHOLD

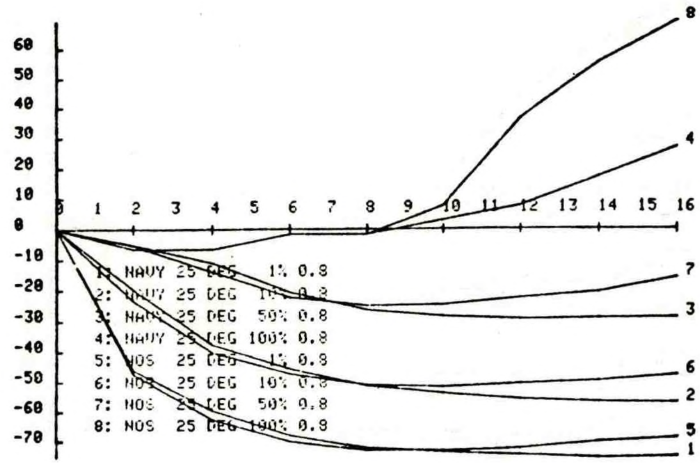

DEPTH MEASUREMENT BIAS (CM) VS OPTICAL
DEPTH AT A DEPTH OF 20 M

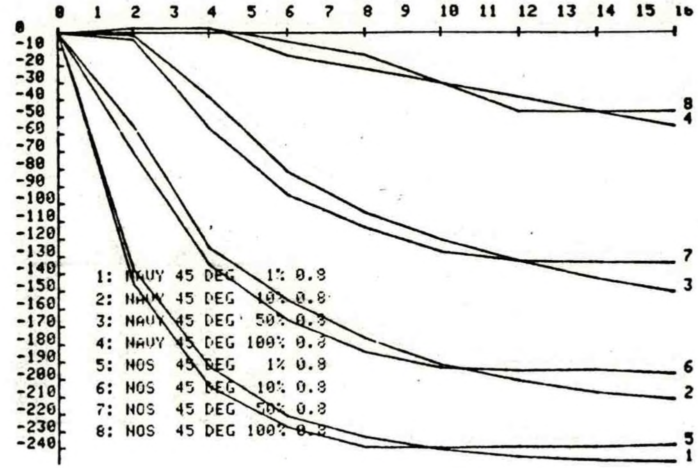

DEPTH MEASUREMENT BIAS (CM) VS OPTICAL
DEPTH AT A DEPTH OF 20 M

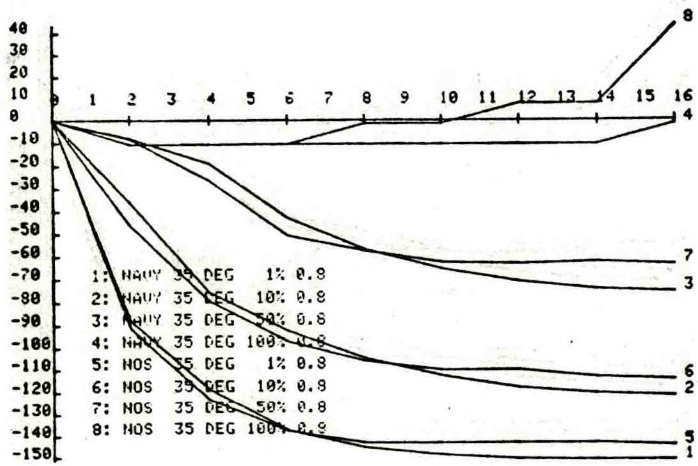

DEPTH MEASUREMENT BIAS (CM) VS OPTICAL
DEPTH AT A DEPTH OF 20 M

FIGURE 41. SENSITIVITY TO LINEAR FUNCTIONAL THRESHOLD

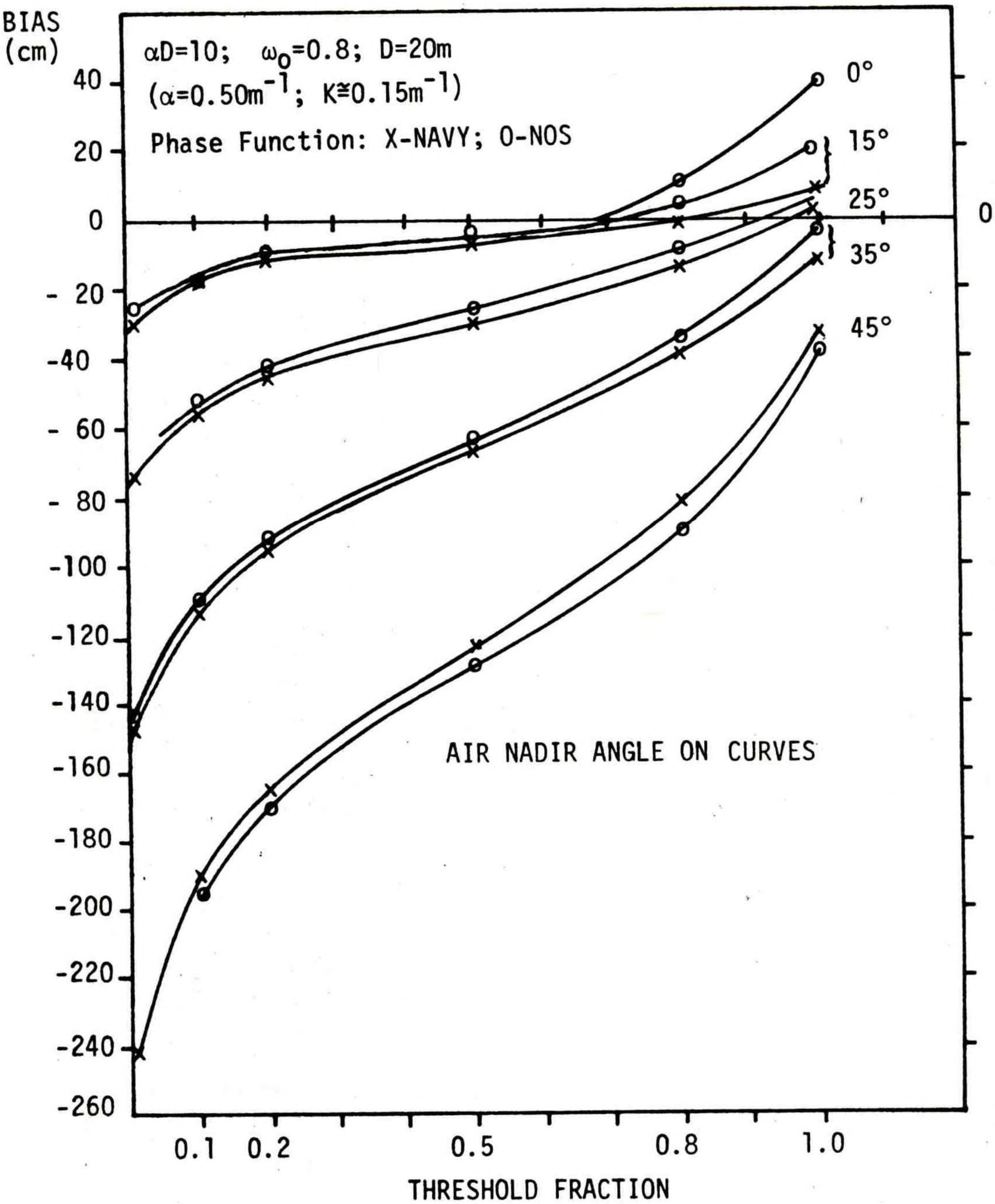

FIGURE 42. DEPTH MEASUREMENT BIAS VS. PULSE LOCATION THRESHOLD FRACTION

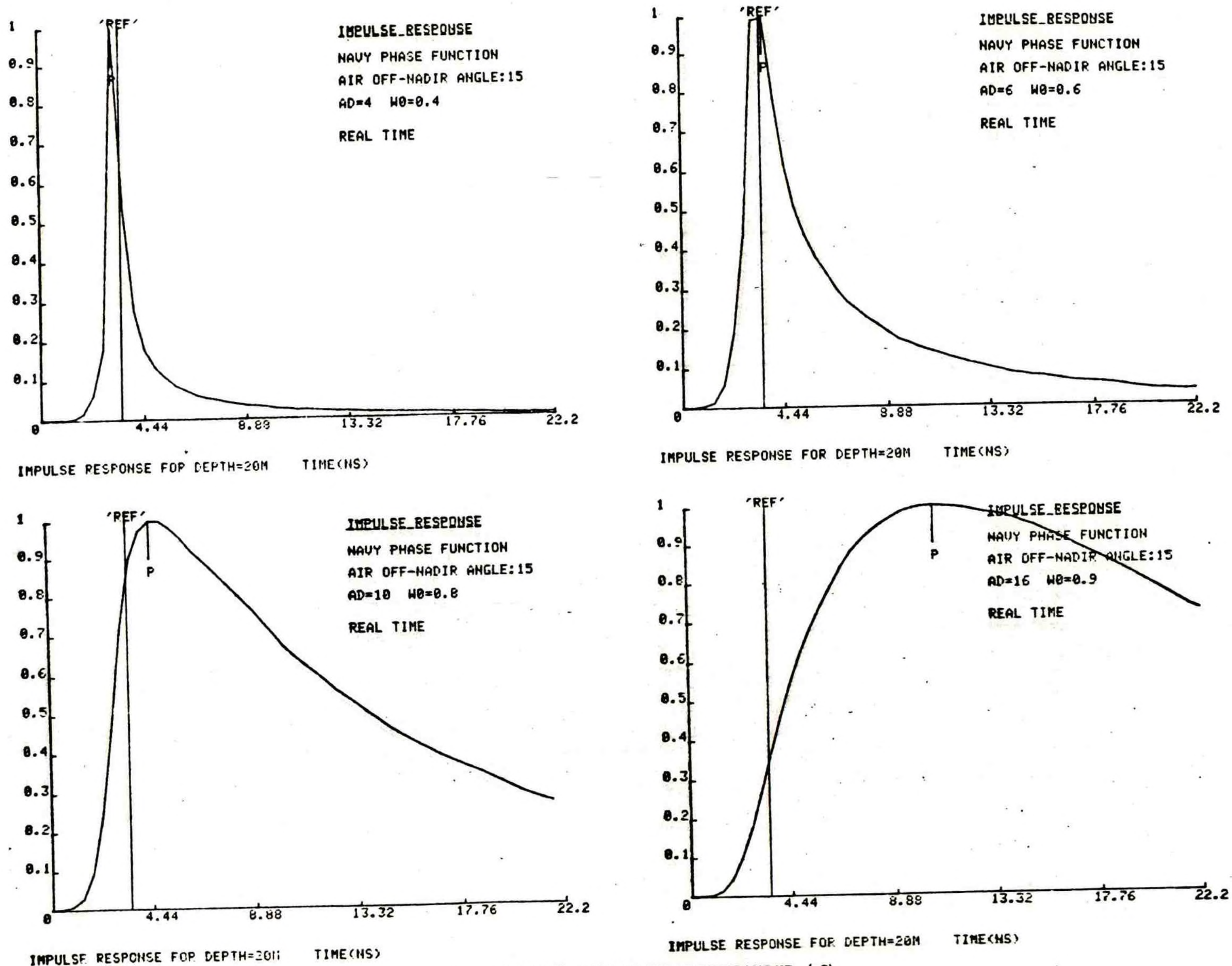

FIGURE 43. VARIABILITY AT CONSTANT KD (=3)

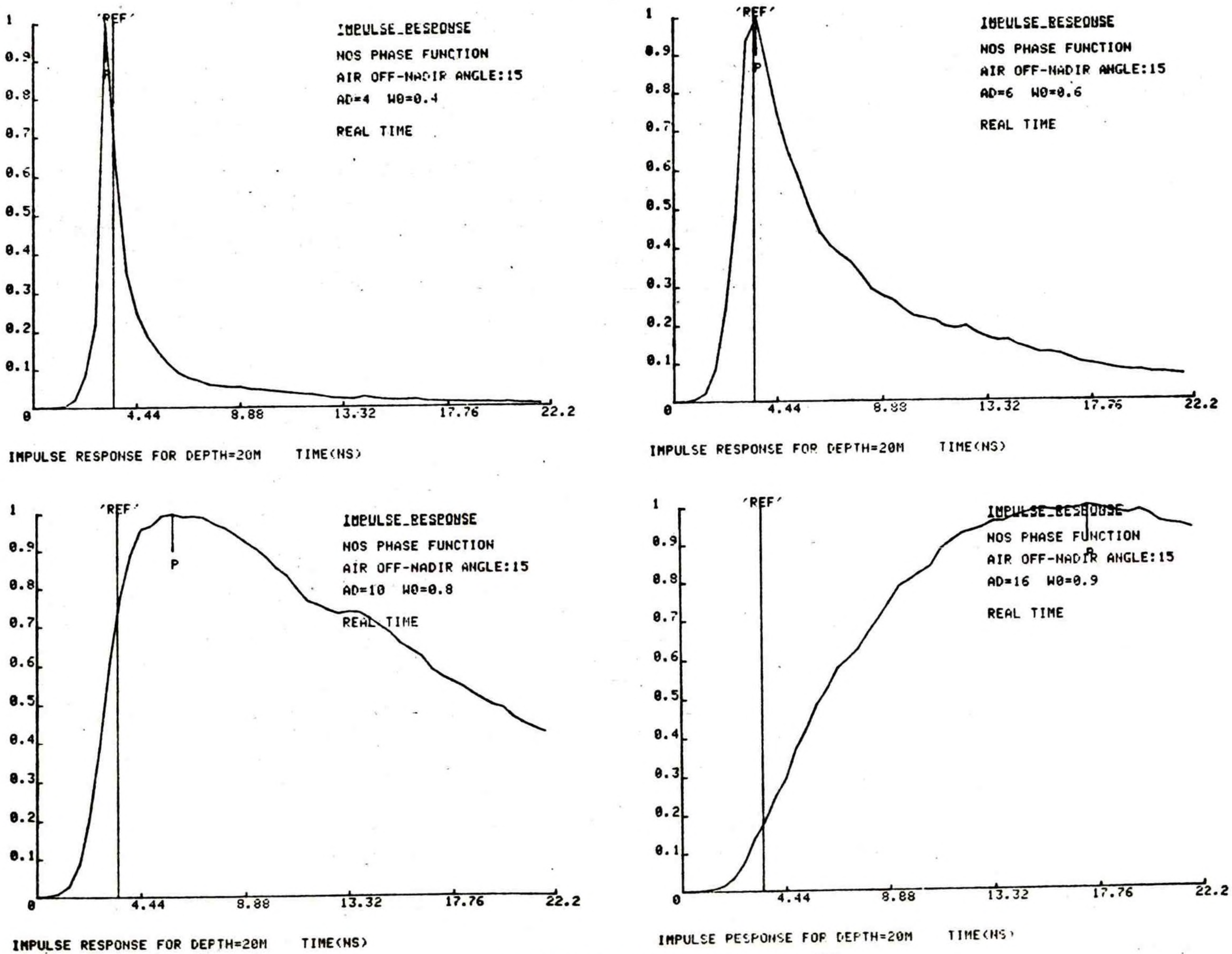

FIGURE 44. VARIABILITY AT CONSTANT KD (=3)

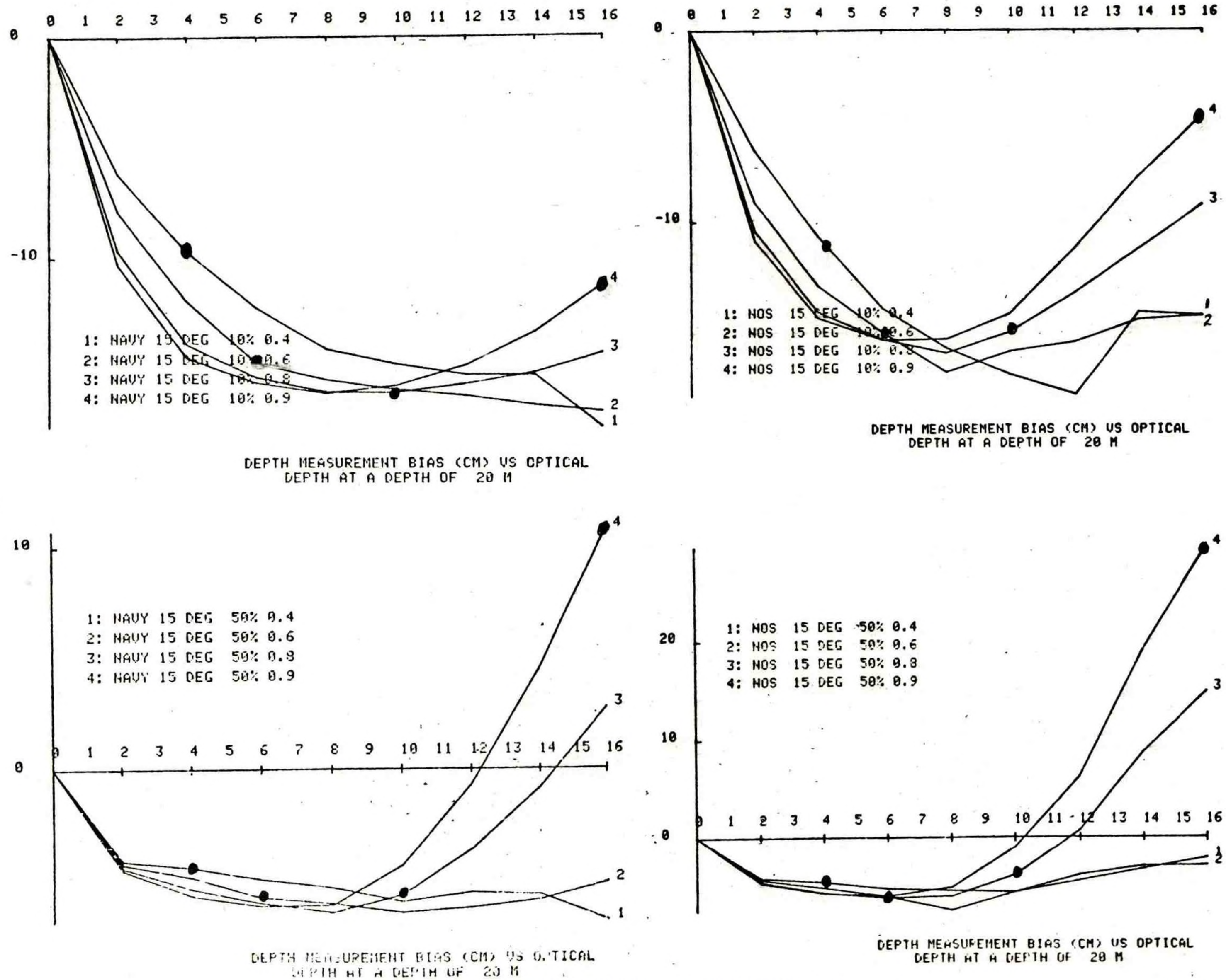

FIGURE 45. VARIABILITY AT CONSTANT KD (=3)

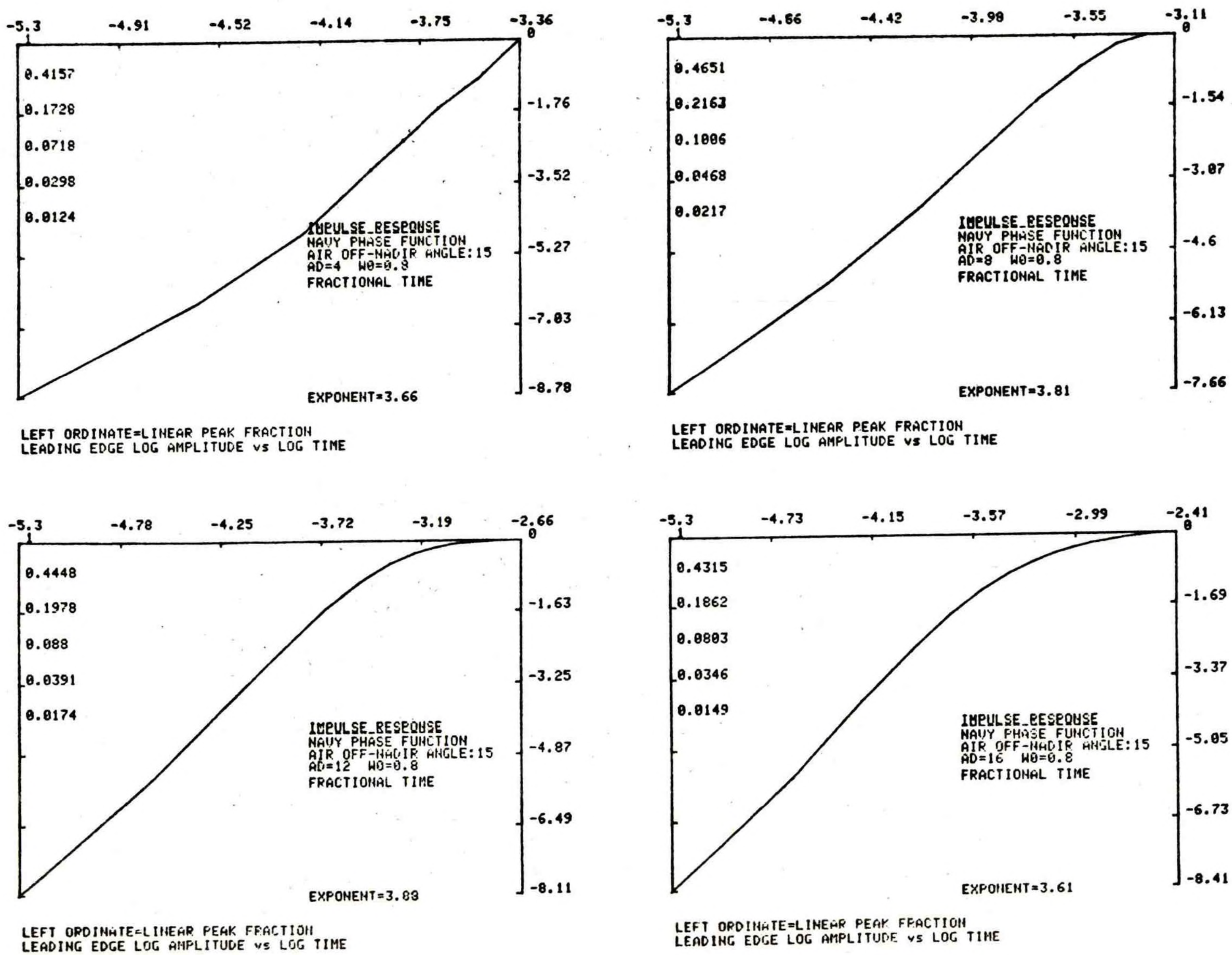

FIGURE 46. LOG–LOG PLOTS OF LEADING EDGE OF IMPULSE RESPONSE FUNCTION

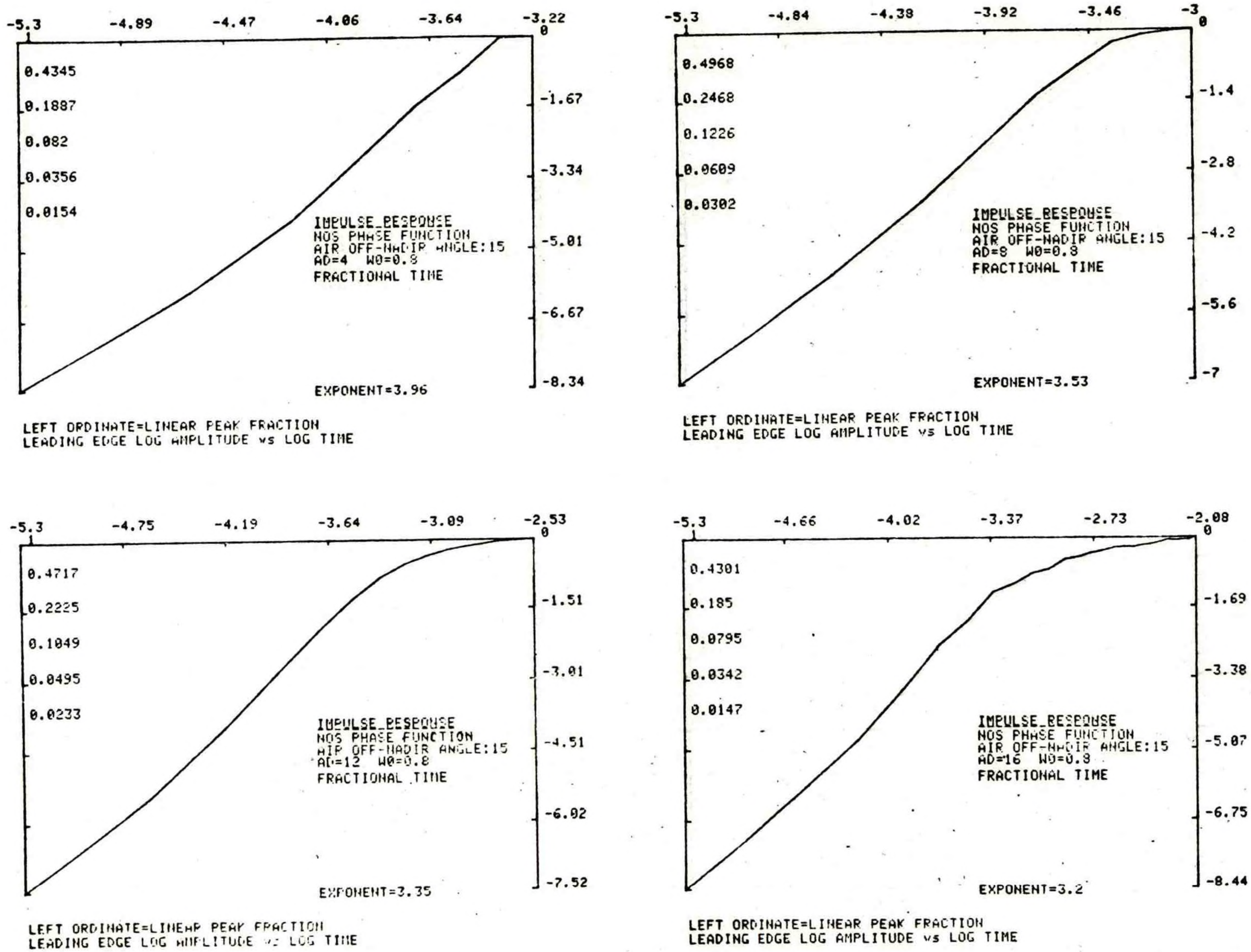

FIGURE 47. LOG–LOG PLOTS OF LEADING EDGE OF IMPULSE RESPONSE FUNCTION

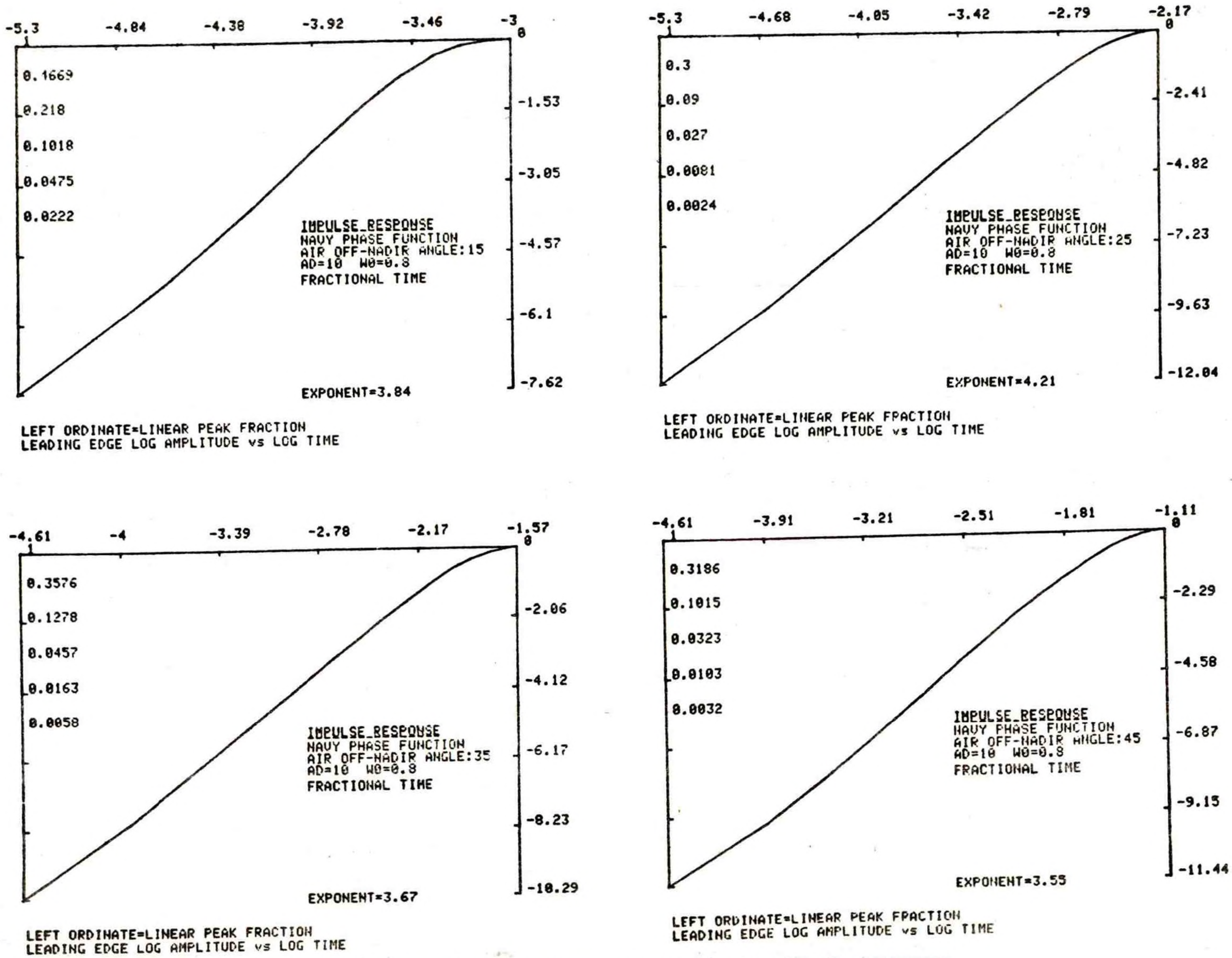

FIGURE 48. LOG–LOG PLOTS OF LEADING EDGE OF IMPULSE RESPONSE FUNCTION

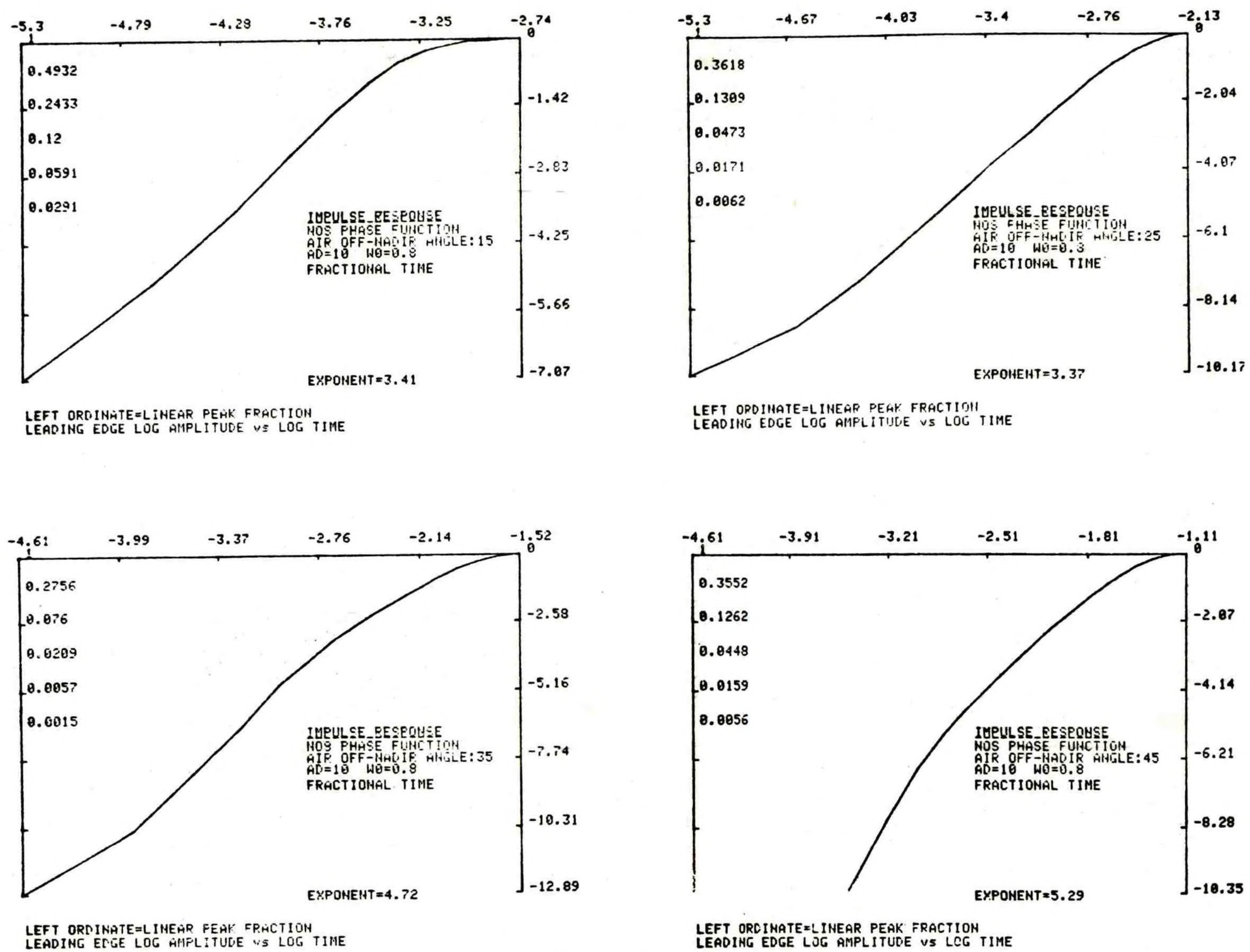

FIGURE 49. LOG—LOG PLOTS OF LEADING EDGE OF IMPULSE RESPONSE FUNCTION

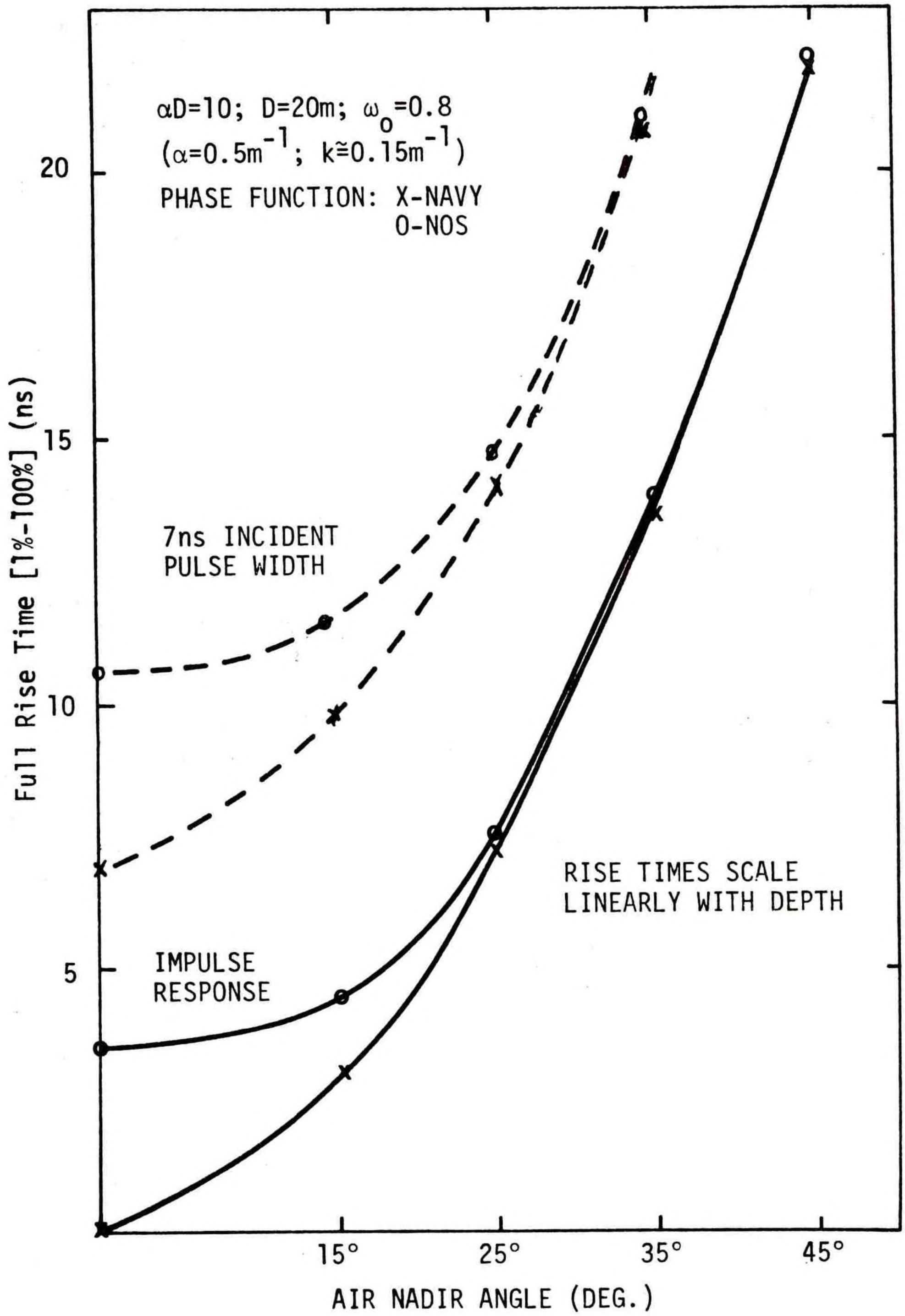

FIGURE 50. IMPULSE RESPONSE FULL RISE TIMES AS FUNCTION OF NADIR ANGLE

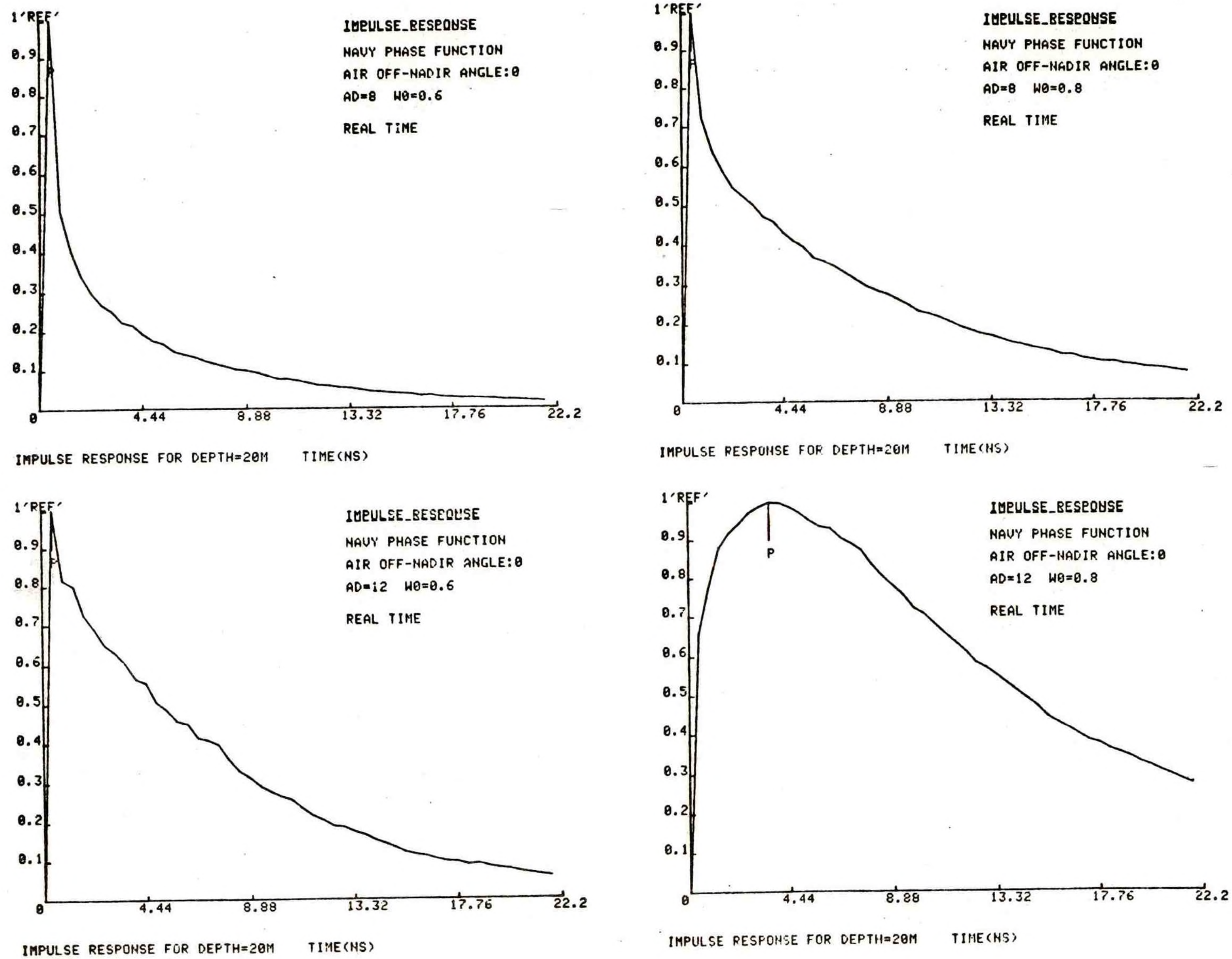

FIGURE 51. RESULTS FOR OPERATIONS AT THE NADIR

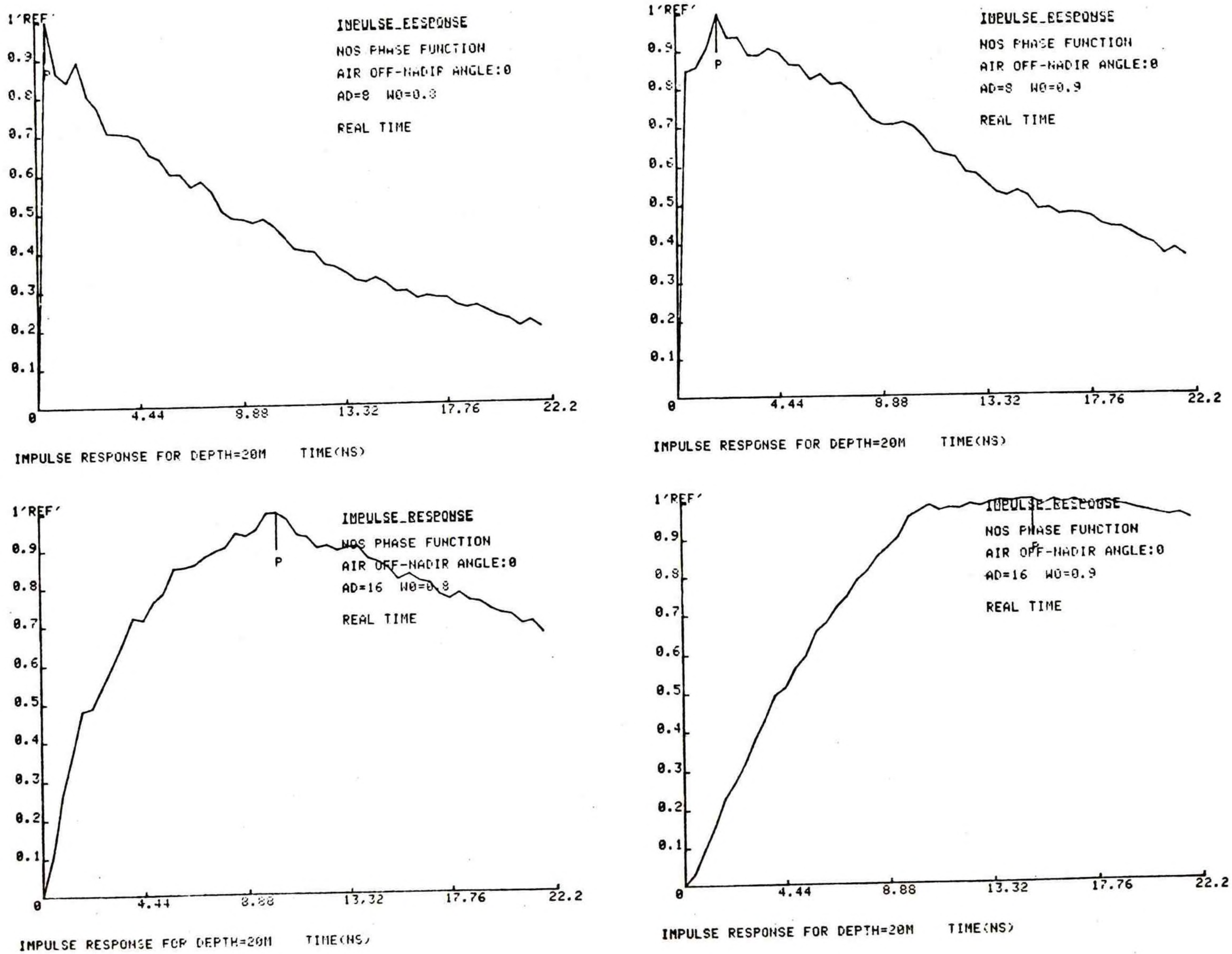

FIGURE 52. RESULTS FOR OPERATIONS AT THE NADIR

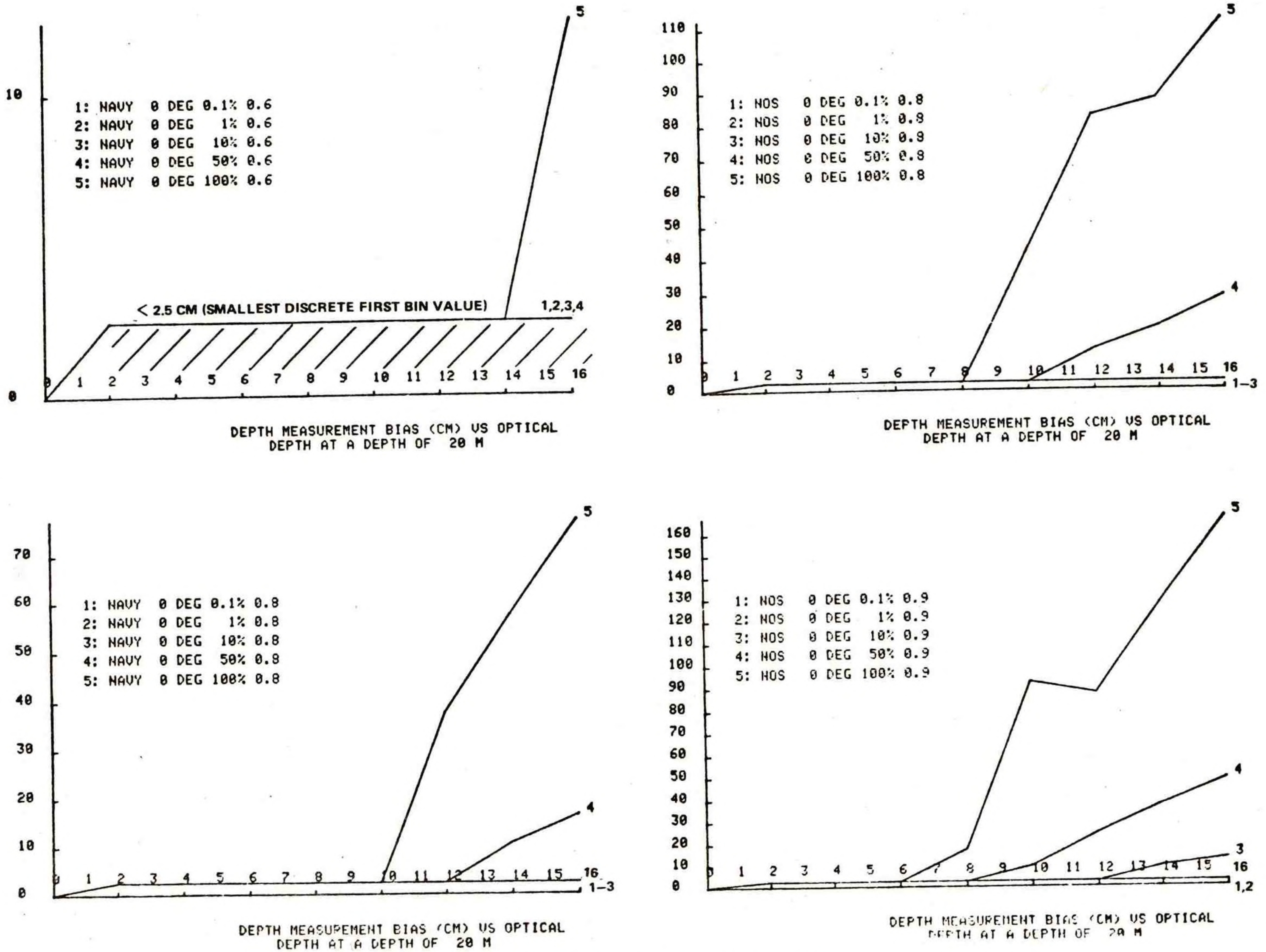

FIGURE 53. RESULTS FOR OPERATIONS AT THE NADIR

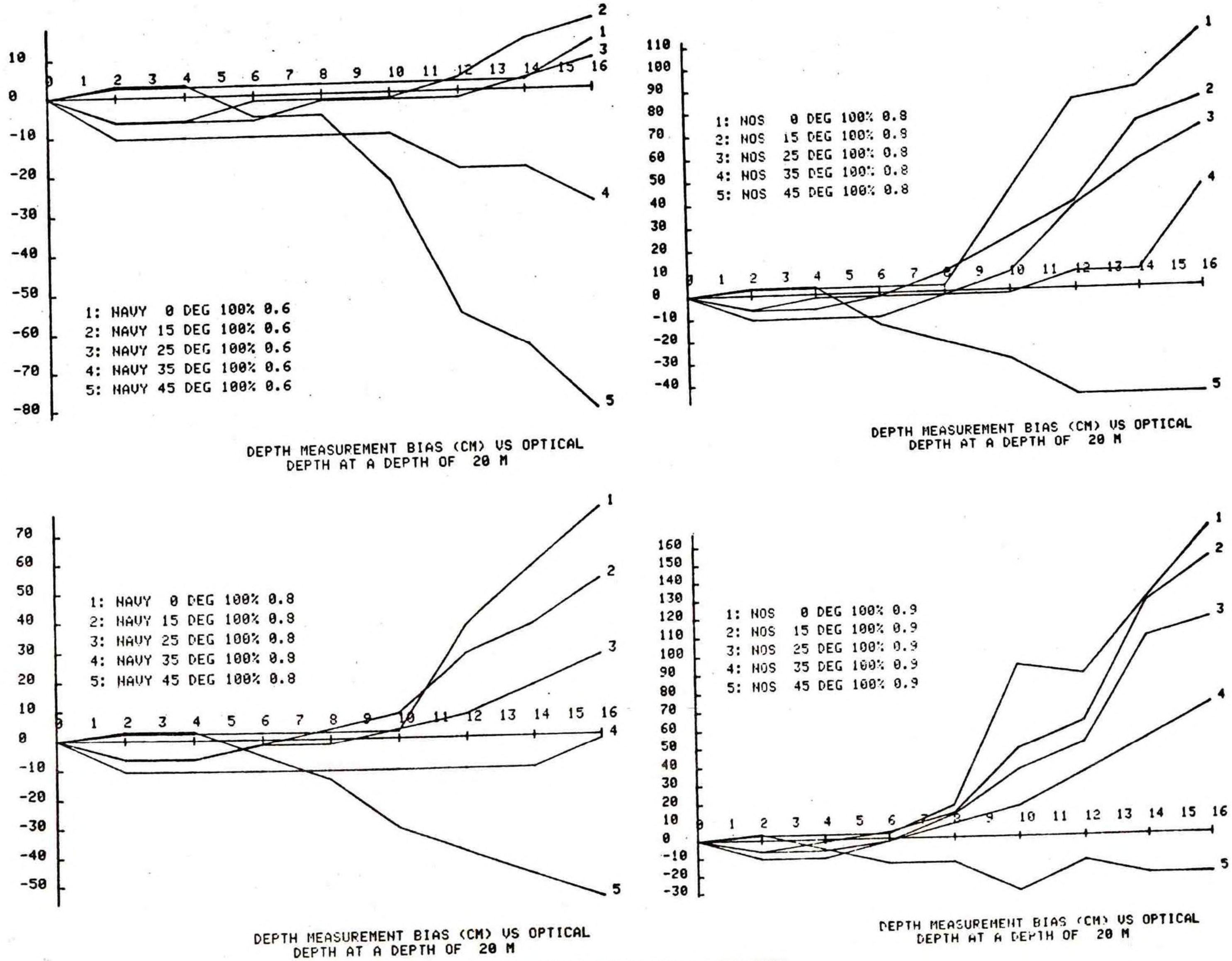

FIGURE 54. RESULTS FOR PEAK DETECTION

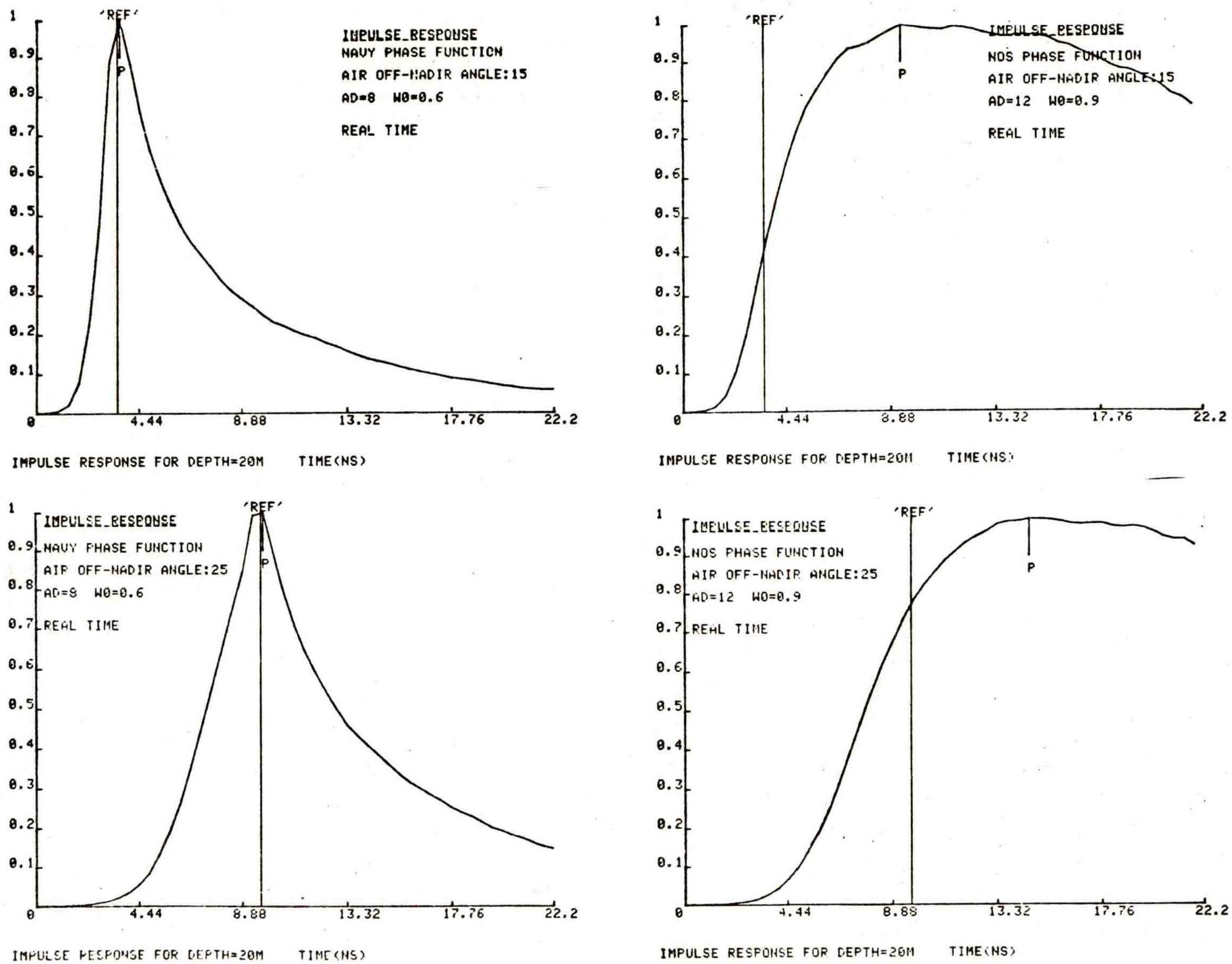

FIGURE 55. RESULTS FOR PRACTICAL CONDITIONS

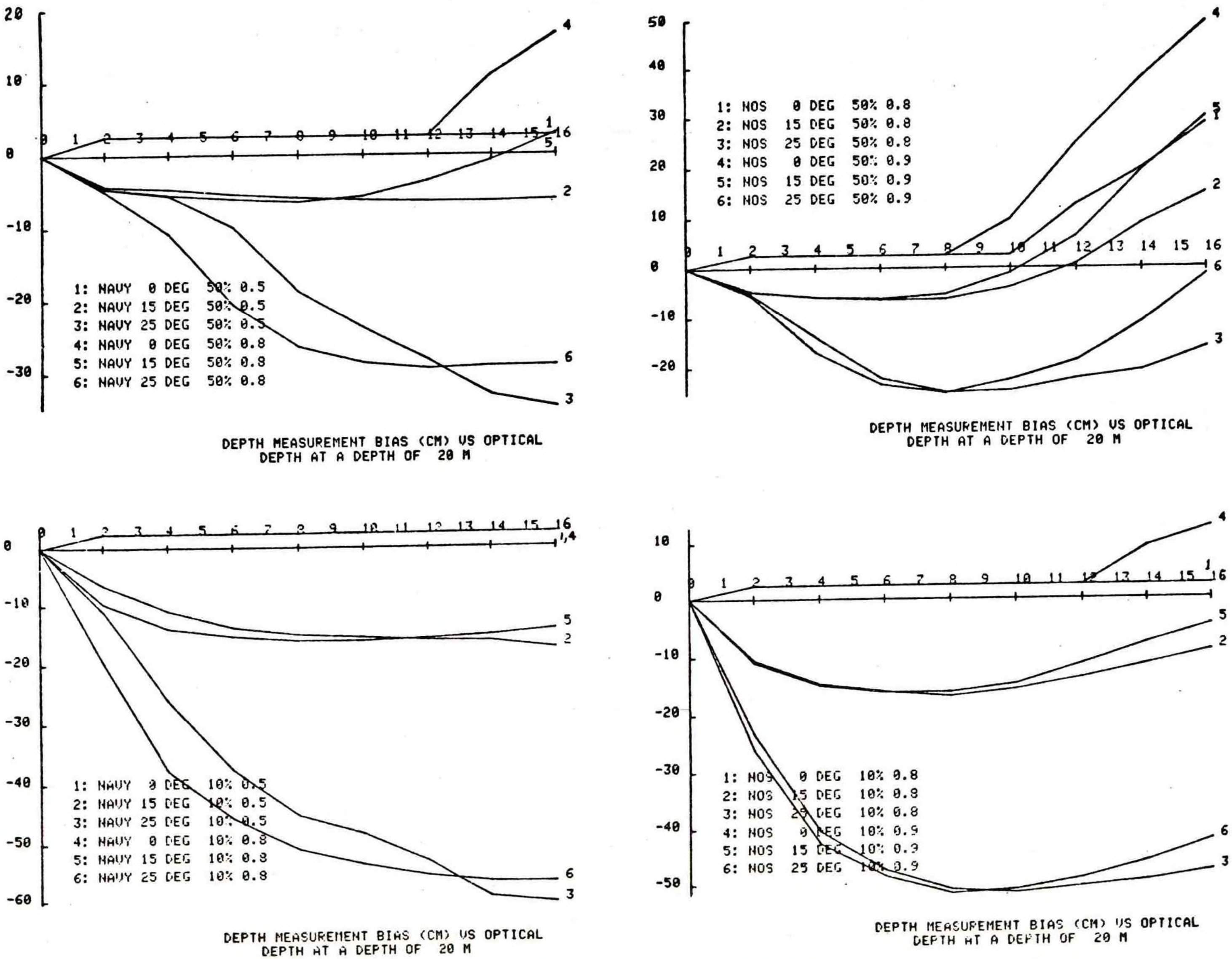

FIGURE 56. RESULTS FOR PRACTICAL CONDITIONS

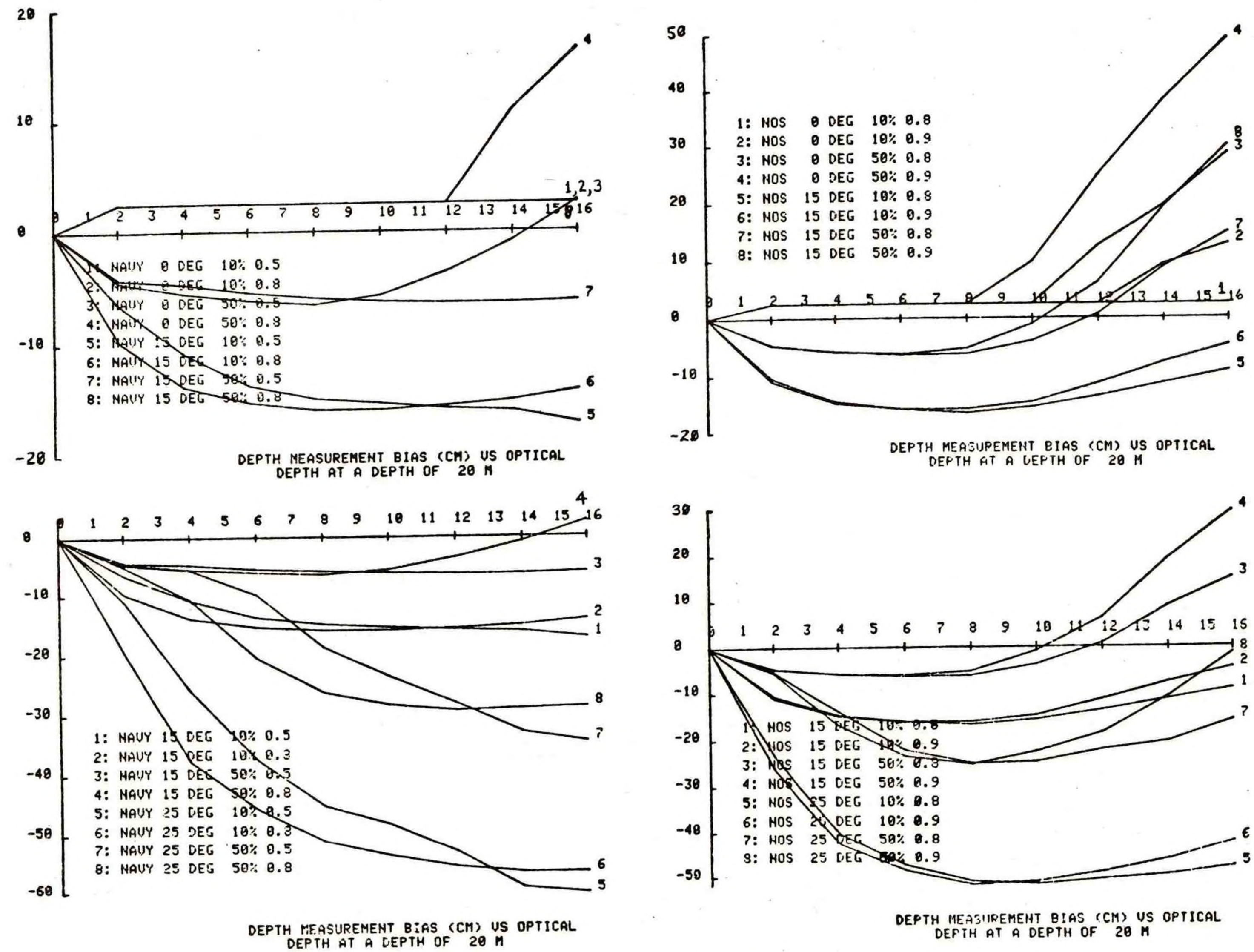

FIGURE 57. RESULTS FOR PRACTICAL CONDITIONS

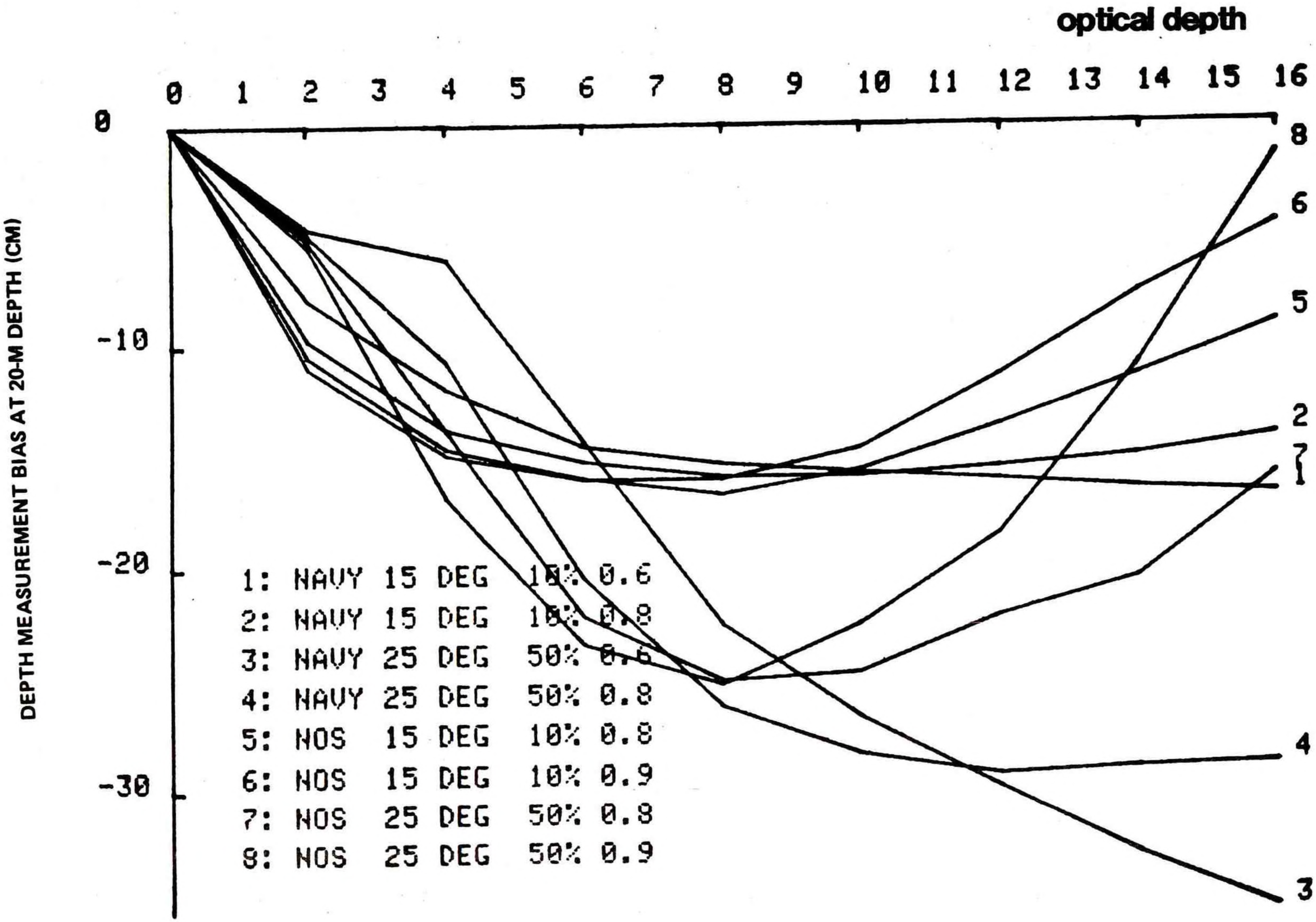

FIGURE 58. DEPTH MEASUREMENT BIAS (CM) VS. OPTICAL DEPTH AT A DEPTH OF 20 M

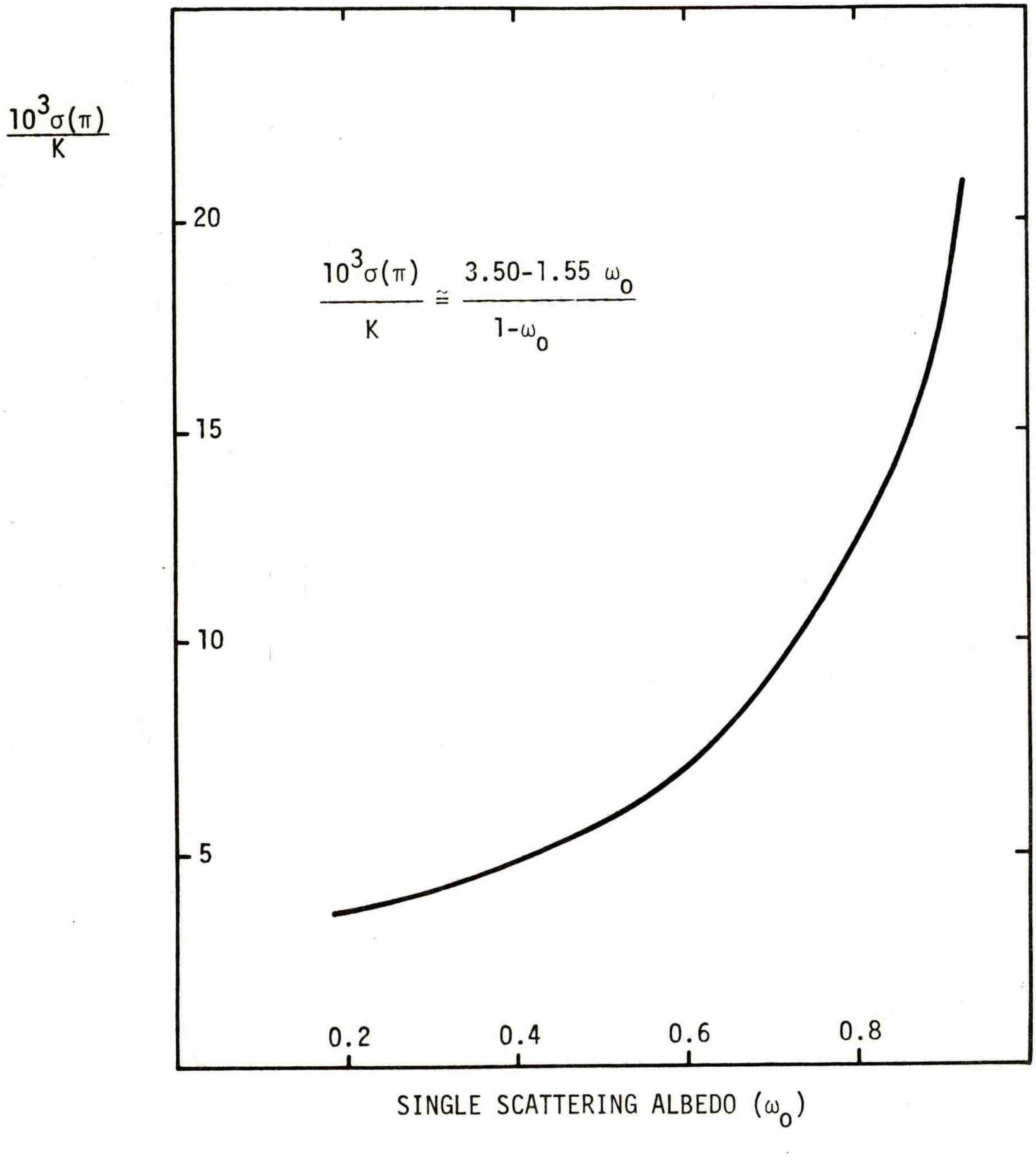

FIGURE 59. RATIO OF VOLUME SCATTERING FUNCTION AT 180° TO DIFFUSE ATTENUATION COEFFICIENT AS FUNCTION OF SINGLE-SCATTERING ALBEDO

APPENDIX A

FORMAT FOR ASCII IMPULSE RESPONSE DATA BASE

RECORD 1. FORMAT (A4, 3F8.2, E11.4)

IALPHA,ZEN,TOR(J),ALB(K),TEMP(J,K)

where

IALPHA	=	'NAVY' or 'NOS'
ZEN	=	nadir angle in air (degrees)
TOR(J)	=	value of αD
ALB(K)	=	albedo of single scattering
TEMP(J,K)	=	ln (flux at bottom)

RECORD 2. FORMAT (50E10.3)

(TDIST(I),I=1,50)

where

TDIST(I) = sampled return in Ith time bin

NOTE: Time bin duration = 0.005 t_w for ψ_{AIR} = 0^o, 15^o, and 25^o
= 0.01 t_w for ψ_{AIR} = 35^o and 45^o
where t_w = depth transit time for unscattered radiation

APPENDIX B
NUMERICAL VALUES FOR COMPUTED BIASES

convolution summary for navy water

zenith angle of entry= 0.00 degrees

bias in .1 percent point (PERCENT)

alpha*d=	2.000	4.000	6.000	8.000	10.000	12.000	14.000	16.000
albedo								
0.90	0.125	0.125	0.125	0.125	0.125	0.125	0.125	0.125
0.80	0.125	0.125	0.125	0.125	0.125	0.125	0.125	0.125
0.70	0.125	0.125	0.125	0.125	0.125	0.125	0.125	0.125
0.60	0.125	0.125	0.125	0.125	0.125	0.125	0.125	0.125
0.50	0.125	0.125	0.125	0.125	0.125	0.125	0.125	0.125
0.40	0.125	0.125	0.125	0.125	0.125	0.125	0.125	0.125
0.30	0.125	0.125	0.125	0.125	0.125	0.125	0.125	0.125
0.20	0.125	0.125	0.125	0.125	0.125	0.125	0.125	0.125

bias in 1 percent point (PERCENT)

alpha*d=	2.000	4.000	6.000	8.000	10.000	12.000	14.000	16.000
albedo								
0.90	0.125	0.125	0.125	0.125	0.125	0.125	0.125	0.125
0.80	0.125	0.125	0.125	0.125	0.125	0.125	0.125	0.125
0.70	0.125	0.125	0.125	0.125	0.125	0.125	0.125	0.125
0.60	0.125	0.125	0.125	0.125	0.125	0.125	0.125	0.125
0.50	0.125	0.125	0.125	0.125	0.125	0.125	0.125	0.125
0.40	0.125	0.125	0.125	0.125	0.125	0.125	0.125	0.125
0.30	0.125	0.125	0.125	0.125	0.125	0.125	0.125	0.125
0.20	0.125	0.125	0.125	0.125	0.125	0.125	0.125	0.125

bias in 10 percent point (PERCENT)

alpha*d=	2.000	4.000	6.000	8.000	10.000	12.000	14.000	16.000
albedo								
0.90	0.125	0.125	0.125	0.125	0.125	0.125	0.125	0.125
0.80	0.125	0.125	0.125	0.125	0.125	0.125	0.125	0.125
0.70	0.125	0.125	0.125	0.125	0.125	0.125	0.125	0.125
0.60	0.125	0.125	0.125	0.125	0.125	0.125	0.125	0.125
0.50	0.125	0.125	0.125	0.125	0.125	0.125	0.125	0.125
0.40	0.125	0.125	0.125	0.125	0.125	0.125	0.125	0.125
0.30	0.125	0.125	0.125	0.125	0.125	0.125	0.125	0.125
0.20	0.125	0.125	0.125	0.125	0.125	0.125	0.125	0.125

bias in 20 percent point (PERCENT)

alpha*d=	2.000	4.000	6.000	8.000	10.000	12.000	14.000	16.000
albedo								
0.90	0.125	0.125	0.125	0.125	0.125	0.125	0.125	0.605
0.80	0.125	0.125	0.125	0.125	0.125	0.125	0.125	0.125
0.70	0.125	0.125	0.125	0.125	0.125	0.125	0.125	0.125
0.60	0.125	0.125	0.125	0.125	0.125	0.125	0.125	0.125
0.50	0.125	0.125	0.125	0.125	0.125	0.125	0.125	0.125
0.40	0.125	0.125	0.125	0.125	0.125	0.125	0.125	0.125
0.30	0.125	0.125	0.125	0.125	0.125	0.125	0.125	0.125
0.20	0.125	0.125	0.125	0.125	0.125	0.125	0.125	0.125

convolution summary for navy water

zenith angle of entry= 0.00 degrees

bias in 50 percent point (PERCENT)

alpha*d=	2.000	4.000	6.000	8.000	10.000	12.000	14.000	16.000
albedo								
0.90	0.125	0.125	0.125	0.125	0.125	0.527	0.945	1.402
0.80	0.125	0.125	0.125	0.125	0.125	0.125	0.540	0.826
0.70	0.125	0.125	0.125	0.125	0.125	0.125	0.125	0.443
0.60	0.125	0.125	0.125	0.125	0.125	0.125	0.125	0.125
0.50	0.125	0.125	0.125	0.125	0.125	0.125	0.125	0.125
0.40	0.125	0.125	0.125	0.125	0.125	0.125	0.125	0.125
0.30	0.125	0.125	0.125	0.125	0.125	0.125	0.125	0.125
0.20	0.125	0.125	0.125	0.125	0.125	0.125	0.125	0.125

bias in 80 percent point (PERCENT)

alpha*d=	2.000	4.000	6.000	8.000	10.000	12.000	14.000	16.000
albedo								
0.90	0.125	0.125	0.125	0.125	0.462	1.283	1.994	2.609
0.80	0.125	0.125	0.125	0.125	0.125	0.686	1.258	1.742
0.70	0.125	0.125	0.125	0.125	0.125	0.125	0.653	0.909
0.60	0.125	0.125	0.125	0.125	0.125	0.125	0.125	0.391
0.50	0.125	0.125	0.125	0.125	0.125	0.125	0.125	0.125
0.40	0.125	0.125	0.125	0.125	0.125	0.125	0.125	0.125
0.30	0.125	0.125	0.125	0.125	0.125	0.125	0.125	0.125
0.20	0.125	0.125	0.125	0.125	0.125	0.125	0.125	0.125

results for bias in peak (PERCENT)

alpha*d=	2.000	4.000	6.000	8.000	10.000	12.000	14.000	16.000
albedo								
0.90	0.125	0.125	0.125	0.125	1.625	3.375	3.875	4.625
0.80	0.125	0.125	0.125	0.125	0.125	1.875	2.875	3.875
0.70	0.125	0.125	0.125	0.125	0.125	0.625	1.875	2.375
0.60	0.125	0.125	0.125	0.125	0.125	0.125	0.125	0.625
0.50	0.125	0.125	0.125	0.125	0.125	0.125	0.125	0.125
0.40	0.125	0.125	0.125	0.125	0.125	0.125	0.125	0.125
0.30	0.125	0.125	0.125	0.125	0.125	0.125	0.125	0.125
0.20	0.125	0.125	0.125	0.125	0.125	0.125	0.125	0.125

rise time from one percent point to peak (ns) for 20 meter water

alpha*d=	2.000	4.000	6.000	8.000	10.000	12.000	14.000	16.000
albedo								
0.90	0.000	0.000	0.000	0.000	2.667	5.778	6.667	8.001
0.80	0.000	0.000	0.000	0.000	0.000	3.111	4.890	6.667
0.70	0.000	0.000	0.000	0.000	0.000	0.889	3.111	4.000
0.60	0.000	0.000	0.000	0.000	0.000	0.000	0.000	0.889
0.50	0.000	0.000	0.000	0.000	0.000	0.000	0.000	0.000
0.40	0.000	0.000	0.000	0.000	0.000	0.000	0.000	0.000
0.30	0.000	0.000	0.000	0.000	0.000	0.000	0.000	0.000
0.20	0.000	0.000	0.000	0.000	0.000	0.000	0.000	0.000

convolution summary for navy water

zenith angle of entry= 15.00 degrees

bias in .1 percent point (PERCENT)

alpha*ds= albedo	2.000	4.000	6.000	8.000	10.000	12.000	14.000	16.000
0.90	-1.212	-1.437	-1.501	-1.516	-1.513	-1.490	-1.475	-1.435
0.80	-1.168	-1.403	-1.493	-1.516	-1.519	-1.502	-1.502	-1.484
0.70	-1.101	-1.349	-1.481	-1.512	-1.519	-1.508	-1.513	-1.506
0.60	-1.049	-1.290	-1.461	-1.502	-1.513	-1.506	-1.513	-1.515
0.50	-1.037	-1.253	-1.414	-1.484	-1.496	-1.497	-1.497	-1.510
0.40	-1.022	-1.178	-1.313	-1.438	-1.456	-1.474	-1.440	-1.486
0.30	-0.998	-1.049	-1.247	-1.308	-1.320	-1.420	-1.284	-1.379
0.20	-0.953	-1.022	-1.067	-1.191	-1.203	-1.289	-1.073	-1.270

bias in 1 percent point (PERCENT)

alpha*ds= albedo	2.000	4.000	6.000	8.000	10.000	12.000	14.000	16.000
0.90	-0.927	-1.081	-1.210	-1.245	-1.240	-1.211	-1.176	-1.120
0.80	-0.894	-1.045	-1.190	-1.241	-1.249	-1.234	-1.226	-1.202
0.70	-0.852	-1.026	-1.159	-1.227	-1.246	-1.246	-1.249	-1.242
0.60	-0.805	-1.000	-1.113	-1.201	-1.231	-1.246	-1.255	-1.259
0.50	-0.786	-0.964	-1.045	-1.155	-1.193	-1.234	-1.236	-1.257
0.40	-0.757	-0.909	-1.014	-1.051	-1.117	-1.199	-1.175	-1.239
0.30	-0.711	-0.814	-0.965	-1.005	-1.023	-1.117	-1.029	-1.180
0.20	-0.620	-0.752	-0.870	-0.914	-0.928	-0.987	-0.806	-1.045

bias in 10 percent point (PERCENT)

alpha*ds= albedo	2.000	4.000	6.000	8.000	10.000	12.000	14.000	16.000
0.90	-0.515	-0.720	-0.777	-0.800	-0.784	-0.738	-0.663	-0.559
0.80	-0.485	-0.692	-0.765	-0.799	-0.800	-0.781	-0.754	-0.710
0.70	-0.447	-0.652	-0.750	-0.787	-0.802	-0.803	-0.800	-0.790
0.60	-0.396	-0.596	-0.731	-0.770	-0.792	-0.806	-0.828	-0.842
0.50	-0.323	-0.540	-0.687	-0.748	-0.769	-0.794	-0.805	-0.864
0.40	-0.312	-0.484	-0.609	-0.701	-0.735	-0.760	-0.758	-0.878
0.30	-0.307	-0.395	-0.523	-0.606	-0.644	-0.697	-0.644	-0.872
0.20	-0.302	-0.312	-0.410	-0.462	-0.514	-0.562	-0.464	-0.815

bias in 20 percent point (PERCENT)

alpha*ds= albedo	2.000	4.000	6.000	8.000	10.000	12.000	14.000	16.000
0.90	-0.324	-0.546	-0.616	-0.642	-0.595	-0.514	-0.403	-0.256
0.80	-0.311	-0.519	-0.598	-0.645	-0.632	-0.583	-0.529	-0.458
0.70	-0.304	-0.484	-0.574	-0.630	-0.645	-0.636	-0.612	-0.578
0.60	-0.297	-0.437	-0.553	-0.606	-0.636	-0.653	-0.658	-0.654
0.50	-0.291	-0.370	-0.513	-0.572	-0.603	-0.644	-0.650	-0.683
0.40	-0.285	-0.311	-0.451	-0.520	-0.557	-0.595	-0.584	-0.714
0.30	-0.281	-0.297	-0.348	-0.412	-0.489	-0.520	-0.485	-0.752
0.20	-0.276	-0.286	-0.299	-0.302	-0.365	-0.384	-0.296	-0.777

convolution summary for navy water

zenith angle of entry= 15.00 degrees

bias in 50 percent point (PERCENT)

alpha*d=	2.000	4.000	6.000	8.000	10.000	12.000	14.000	16.000
albedo								
0.90	-0.226	-0.286	-0.310	-0.308	-0.216	-0.036	0.221	0.536
0.80	-0.222	-0.271	-0.303	-0.324	-0.283	-0.179	-0.042	0.136
0.70	-0.217	-0.257	-0.297	-0.316	-0.315	-0.272	-0.203	-0.120
0.60	-0.213	-0.244	-0.291	-0.304	-0.324	-0.313	-0.295	-0.255
0.50	-0.209	-0.232	-0.270	-0.292	-0.311	-0.317	-0.317	-0.309
0.40	-0.206	-0.222	-0.248	-0.266	-0.299	-0.278	-0.284	-0.344
0.30	-0.203	-0.213	-0.229	-0.237	-0.264	-0.210	-0.199	-0.305
0.20	-0.200	-0.206	-0.214	-0.216	-0.232	-0.095	-0.032	-0.680

bias in 80 percent point (PERCENT)

alpha*d=	2.000	4.000	6.000	8.000	10.000	12.000	14.000	16.000
albedo								
0.90	-0.134	-0.158	-0.107	-0.032	0.172	0.583	1.124	1.688
0.80	-0.132	-0.152	-0.121	-0.090	0.040	0.281	0.582	0.952
0.70	-0.130	-0.146	-0.138	-0.109	-0.058	0.076	0.256	0.429
0.60	-0.129	-0.141	-0.158	-0.127	-0.106	-0.026	0.057	0.148
0.50	-0.127	-0.136	-0.151	-0.150	-0.129	-0.073	-0.024	0.032
0.40	-0.126	-0.132	-0.143	-0.150	-0.159	-0.039	-0.027	-0.081
0.30	-0.125	-0.129	-0.135	-0.138	-0.149	0.018	0.037	-0.113
0.20	-0.124	-0.126	-0.129	-0.130	-0.136	0.069	0.203	-0.583

results for bias in peak (PERCENT)

alpha*d=	2.000	4.000	6.000	8.000	10.000	12.000	14.000	16.000
albedo								
0.90	-0.318	-0.318	-0.073	0.173	0.908	1.889	2.870	3.851
0.80	-0.318	-0.318	-0.073	0.173	0.418	1.399	1.889	2.625
0.70	-0.318	-0.318	-0.073	-0.073	0.173	0.663	1.153	1.644
0.60	-0.318	-0.318	-0.073	-0.073	-0.073	0.173	0.663	0.908
0.50	-0.318	-0.318	-0.318	-0.073	-0.073	-0.073	0.173	0.418
0.40	-0.318	-0.318	-0.318	-0.318	-0.073	-0.073	0.173	0.418
0.30	-0.318	-0.318	-0.318	-0.318	-0.318	-0.073	0.173	-0.073
0.20	-0.318	-0.318	-0.318	-0.318	-0.318	-0.073	2.380	-0.073

rise time from one percent point to peak (ns) for 20 meter water

alpha*d=	2.000	4.000	6.000	8.000	10.000	12.000	14.000	16.000
albedo								
0.90	1.104	1.383	2.062	2.569	3.894	5.619	7.333	9.010
0.80	1.045	1.317	2.025	2.562	3.021	4.773	5.646	6.936
0.70	0.967	1.283	1.970	2.092	2.572	3.461	4.355	5.232
0.60	0.883	1.237	1.886	2.045	2.100	2.571	3.476	3.928
0.50	0.848	1.172	1.318	1.961	2.031	2.105	2.554	3.036
0.40	0.797	1.072	1.262	1.329	1.893	2.042	2.442	3.004
0.30	0.713	0.900	1.172	1.246	1.279	1.892	2.178	2.007
0.20	0.548	0.786	1.002	1.080	1.106	1.658	5.774	1.763

convolution summary for navy water

zenith angle of entry= 25.00 degrees

bias in .1 percent point (PERCENT)

alpha*d=	2.000	4.000	6.000	8.000	10.000	12.000	14.000	16.000
albedo								
0.90	-3.272	-3.974	-4.195	-4.259	-4.250	-4.231	-4.241	-4.173
0.80	-3.132	-3.885	-4.158	-4.262	-4.266	-4.277	-4.330	-4.274
0.70	-2.976	-3.800	-4.107	-4.254	-4.272	-4.306	-4.422	-4.322
0.60	-2.804	-3.652	-4.046	-4.228	-4.258	-4.315	-4.475	-4.331
0.50	-2.660	-3.471	-3.919	-4.160	-4.183	-4.291	-4.500	-4.294
0.40	-2.571	-3.210	-3.736	-4.045	-4.048	-4.167	-4.508	-4.101
0.30	-2.442	-2.858	-3.408	-3.830	-3.784	-4.018	-4.496	-3.684
0.20	-2.343	-2.534	-2.919	-3.555	-3.178	-3.556	-4.387	-2.691

bias in 1 percent point (PERCENT)

alpha*d=	2.000	4.000	6.000	8.000	10.000	12.000	14.000	16.000
albedo								
0.90	-2.389	-3.103	-3.471	-3.631	-3.672	-3.672	-3.658	-3.614
0.80	-2.303	-2.978	-3.399	-3.616	-3.682	-3.731	-3.778	-3.756
0.70	-2.204	-2.831	-3.321	-3.581	-3.665	-3.763	-3.854	-3.838
0.60	-2.109	-2.655	-3.173	-3.513	-3.623	-3.767	-3.921	-3.865
0.50	-1.968	-2.489	-2.985	-3.389	-3.522	-3.715	-3.960	-3.839
0.40	-1.812	-2.349	-2.703	-3.192	-3.309	-3.583	-3.944	-3.642
0.30	-1.597	-2.160	-2.464	-2.871	-2.917	-3.260	-3.814	-2.967
0.20	-1.164	-1.866	-2.264	-2.481	-2.382	-2.579	-3.030	-2.311

bias in 10 percent point (PERCENT)

alpha*d=	2.000	4.000	6.000	8.000	10.000	12.000	14.000	16.000
albedo								
0.90	-1.127	-1.995	-2.365	-2.602	-2.689	-2.717	-2.680	-2.633
0.80	-0.980	-1.892	-2.285	-2.554	-2.683	-2.780	-2.828	-2.834
0.70	-0.849	-1.754	-2.188	-2.473	-2.645	-2.796	-2.918	-2.972
0.60	-0.709	-1.591	-2.062	-2.383	-2.565	-2.762	-2.975	-3.051
0.50	-0.548	-1.295	-1.876	-2.260	-2.417	-2.650	-2.964	-3.015
0.40	-0.400	-1.015	-1.624	-2.064	-2.210	-2.415	-2.875	-2.647
0.30	-0.319	-0.704	-1.227	-1.719	-1.852	-2.015	-2.763	-2.178
0.20	-0.311	-0.399	-0.718	-1.396	-1.261	-1.462	-2.169	-1.276

bias in 20 percent point (PERCENT)

alpha*d=	2.000	4.000	6.000	8.000	10.000	12.000	14.000	16.000
albedo								
0.90	-0.645	-1.539	-1.933	-2.160	-2.237	-2.256	-2.203	-2.145
0.80	-0.526	-1.388	-1.854	-2.119	-2.236	-2.326	-2.368	-2.380
0.70	-0.415	-1.199	-1.743	-2.053	-2.201	-2.340	-2.461	-2.533
0.60	-0.320	-0.999	-1.592	-1.953	-2.133	-2.304	-2.509	-2.608
0.50	-0.309	-0.769	-1.370	-1.799	-1.983	-2.203	-2.474	-2.553
0.40	-0.300	-0.523	-1.033	-1.561	-1.769	-1.970	-2.365	-2.336
0.30	-0.293	-0.321	-0.672	-1.316	-1.377	-1.702	-2.198	-1.395
0.20	-0.286	-0.301	-0.325	-0.651	-0.920	-1.291	-1.256	-1.246

convolution summary for navy water

zenith angle of entry= 25.00 degrees

bias in 50 percent point (PERCENT)

alpha*d=	2.000	4.000	6.000	8.000	10.000	12.000	14.000	16.000
albedo								
0.90	-0.259	-0.673	-1.122	-1.354	-1.394	-1.349	-1.209	-1.070
0.80	-0.249	-0.537	-1.026	-1.315	-1.423	-1.467	-1.452	-1.443
0.70	-0.240	-0.406	-0.905	-1.244	-1.404	-1.511	-1.587	-1.662
0.60	-0.232	-0.306	-0.720	-1.132	-1.340	-1.496	-1.648	-1.777
0.50	-0.226	-0.274	-0.495	-0.940	-1.187	-1.408	-1.650	-1.737
0.40	-0.220	-0.251	-0.309	-0.624	-0.927	-1.170	-1.526	-1.408
0.30	-0.215	-0.233	-0.264	-0.322	-0.522	-0.577	-1.213	-1.204
0.20	-0.211	-0.220	-0.235	-0.265	-0.292	-0.250	-1.173	-1.167

bias in 80 percent point (PERCENT)

alpha*d=	2.000	4.000	6.000	8.000	10.000	12.000	14.000	16.000
albedo								
0.90	-0.156	-0.239	-0.448	-0.634	-0.602	-0.442	-0.136	0.236
0.80	-0.152	-0.213	-0.370	-0.603	-0.669	-0.650	-0.551	-0.420
0.70	-0.148	-0.191	-0.299	-0.532	-0.670	-0.736	-0.756	-0.789
0.60	-0.145	-0.174	-0.243	-0.423	-0.622	-0.728	-0.838	-1.026
0.50	-0.142	-0.162	-0.203	-0.292	-0.481	-0.611	-0.817	-1.166
0.40	-0.140	-0.152	-0.175	-0.222	-0.304	-0.308	-0.664	-1.167
0.30	-0.138	-0.145	-0.157	-0.181	-0.214	-0.197	-1.050	-1.102
0.20	-0.136	-0.140	-0.146	-0.158	-0.169	-0.152	-1.090	-1.087

results for bias in peak (PERCENT)

alpha*d=	2.000	4.000	6.000	8.000	10.000	12.000	14.000	16.000
albedo								
0.90	-0.324	-0.324	-0.087	-0.087	0.388	1.099	1.810	2.995
0.80	-0.324	-0.324	-0.087	-0.087	0.151	0.388	0.862	1.336
0.70	-0.324	-0.324	-0.324	-0.087	-0.087	0.151	0.151	0.388
0.60	-0.324	-0.324	-0.324	-0.087	-0.087	-0.087	0.151	0.388
0.50	-0.324	-0.324	-0.324	-0.324	-0.324	-0.324	-0.087	-0.324
0.40	-0.324	-0.324	-0.324	-0.324	-0.324	-0.324	-0.087	-1.272
0.30	-0.324	-0.324	-0.324	-0.324	-0.324	-0.324	-0.087	-1.272
0.20	-0.324	-0.324	-0.324	-0.324	-0.324	-0.324	-1.272	-1.272

rise time from one percent point to peak (ns) for 20 meter water

alpha*d=	2.000	4.000	6.000	8.000	10.000	12.000	14.000	16.000
albedo								
0.90	3.872	5.212	6.346	6.647	7.613	8.945	10.252	12.394
0.80	3.712	4.978	6.211	6.618	7.186	7.723	8.700	9.548
0.70	3.525	4.703	5.621	6.553	6.711	7.338	7.510	7.923
0.60	3.347	4.372	5.343	6.426	6.631	6.901	7.636	7.975
0.50	3.085	4.061	4.991	5.748	5.998	6.360	7.263	6.591
0.40	2.790	3.798	4.461	5.379	5.598	6.113	7.233	4.445
0.30	2.388	3.444	4.013	4.777	4.863	5.507	6.989	3.179
0.20	1.576	2.892	3.639	4.045	3.860	4.229	3.296	1.949

convolution summary for navy water

zenith angle of entry=   35.00 degrees

bias in .1 percent point (PERCENT)

alpha*d=	2.000	4.000	6.000	8.000	10.000	12.000	14.000	16.000
albedo								
0.90	-6.315	-7.751	-8.194	-8.311	-8.376	-8.343	-8.222	-8.155
0.80	-6.055	-7.649	-8.171	-8.324	-8.441	-8.454	-8.337	-8.238
0.70	-5.761	-7.479	-8.125	-8.325	-8.499	-8.556	-8.398	-8.379
0.60	-5.407	-7.226	-8.034	-8.310	-8.544	-8.645	-8.431	-8.481
0.50	-5.027	-6.878	-7.849	-8.261	-8.567	-8.890	-8.446	-8.546
0.40	-4.865	-6.399	-7.574	-8.167	-8.545	-9.552	-8.423	-8.569
0.30	-4.586	-5.735	-7.078	-7.977	-8.433	-9.552	-8.258	-8.512
0.20	-4.391	-4.919	-6.019	-7.416	-8.122	-9.552	-7.596	-7.955

bias in 1 percent point (PERCENT)

alpha*d=	2.000	4.000	6.000	8.000	10.000	12.000	14.000	16.000
albedo								
0.90	-4.542	-6.173	-6.977	-7.275	-7.377	-7.429	-7.400	-7.344
0.80	-4.403	-5.921	-6.869	-7.268	-7.441	-7.542	-7.548	-7.565
0.70	-4.223	-5.636	-6.733	-7.236	-7.491	-7.641	-7.641	-7.707
0.60	-4.055	-5.266	-6.492	-7.161	-7.523	-7.734	-7.700	-7.883
0.50	-3.879	-4.889	-6.130	-6.998	-7.517	-7.904	-7.730	-8.018
0.40	-3.574	-4.535	-5.579	-6.672	-7.433	-8.093	-7.681	-8.045
0.30	-2.972	-4.245	-4.925	-5.926	-7.205	-8.217	-7.279	-7.241
0.20	-2.294	-3.809	-4.313	-4.956	-6.690	-7.611	-5.859	-5.387

bias in 10 percent point (PERCENT)

alpha*d=	2.000	4.000	6.000	8.000	10.000	12.000	14.000	16.000
albedo								
0.90	-2.105	-3.986	-4.803	-5.322	-5.611	-5.779	-5.826	-5.798
0.80	-1.817	-3.790	-4.639	-5.242	-5.627	-5.889	-6.030	-6.082
0.70	-1.552	-3.523	-4.459	-5.088	-5.597	-5.974	-6.197	-6.297
0.60	-1.257	-3.149	-4.214	-4.880	-5.496	-6.038	-6.308	-6.465
0.50	-0.945	-2.690	-3.922	-4.569	-5.301	-6.065	-6.341	-6.516
0.40	-0.740	-2.061	-3.487	-4.270	-4.932	-5.937	-6.097	-6.005
0.30	-0.525	-1.317	-2.473	-3.804	-4.466	-5.739	-5.002	-4.892
0.20	-0.509	-0.783	-1.390	-2.806	-3.964	-4.802	-3.920	-3.358

bias in 20 percent point (PERCENT)

alpha*d=	2.000	4.000	6.000	8.000	10.000	12.000	14.000	16.000
albedo								
0.90	-1.108	-3.075	-3.991	-4.473	-4.793	-4.965	-5.032	-5.008
0.80	-0.906	-2.794	-3.853	-4.395	-4.792	-5.080	-5.267	-5.339
0.70	-0.745	-2.427	-3.655	-4.262	-4.738	-5.156	-5.430	-5.566
0.60	-0.549	-1.991	-3.357	-4.071	-4.609	-5.177	-5.540	-5.710
0.50	-0.510	-1.426	-2.868	-3.807	-4.420	-5.137	-5.541	-5.668
0.40	-0.491	-0.943	-2.144	-3.388	-4.109	-4.983	-5.021	-5.137
0.30	-0.475	-0.594	-1.296	-2.075	-3.756	-4.789	-4.413	-3.992
0.20	-0.462	-0.494	-0.529	-1.229	-3.123	-3.800	-3.309	-1.743

convolution summary for navy water

zenith angle of entry= 35.00 degrees

bias in 50 percent point (PERCENT)

alpha*dz=	2.000	4.000	6.000	8.000	10.000	12.000	14.000	16.000
albedo								
0.90	-0.416	-1.267	-2.365	-2.949	-3.268	-3.405	-3.439	-3.348
0.80	-0.395	-0.959	-2.155	-2.860	-3.284	-3.560	-3.729	-3.787
0.70	-0.377	-0.727	-1.849	-2.680	-3.236	-3.647	-3.912	-4.056
0.60	-0.362	-0.512	-1.424	-2.346	-3.101	-3.671	-3.986	-4.189
0.50	-0.348	-0.448	-0.937	-1.809	-2.846	-3.646	-3.945	-4.138
0.40	-0.337	-0.400	-0.508	-1.202	-2.085	-3.513	-3.714	-3.748
0.30	-0.327	-0.365	-0.417	-0.664	-1.104	-3.209	-2.678	-1.673
0.20	-0.318	-0.338	-0.360	-0.457	-0.502	-1.671	-1.473	-1.127

bias in 80 percent point (PERCENT)

alpha*dz=	2.000	4.000	6.000	8.000	10.000	12.000	14.000	16.000
albedo								
0.90	-0.214	-0.387	-1.033	-1.576	-1.886	-1.922	-1.855	-1.625
0.80	-0.205	-0.330	-0.819	-1.482	-1.917	-2.153	-2.275	-2.263
0.70	-0.198	-0.286	-0.554	-1.262	-1.847	-2.292	-2.543	-2.645
0.60	-0.192	-0.252	-0.401	-0.892	-1.598	-2.297	-2.686	-2.870
0.50	-0.186	-0.226	-0.309	-0.520	-0.982	-2.139	-2.696	-2.794
0.40	-0.182	-0.207	-0.250	-0.364	-0.512	-1.704	-2.400	-2.341
0.30	-0.178	-0.193	-0.214	-0.279	-0.332	-1.482	-1.317	-0.331
0.20	-0.174	-0.182	-0.191	-0.230	-0.248	0.115	-1.173	-0.216

results for bias in peak (PERCENT)

alpha*dz=	2.000	4.000	6.000	8.000	10.000	12.000	14.000	16.000
albedo								
0.90	-0.530	-0.530	-0.530	-0.530	-0.530	-0.079	0.373	0.824
0.80	-0.530	-0.530	-0.530	-0.530	-0.530	-0.530	-0.530	-0.079
0.70	-0.530	-0.530	-0.530	-0.530	-0.530	-0.981	-0.981	-0.981
0.60	-0.530	-0.530	-0.530	-0.530	-0.530	-0.981	-0.981	-1.432
0.50	-0.530	-0.530	-0.530	-0.530	-0.530	-0.981	-0.530	-1.432
0.40	-0.530	-0.530	-0.530	-0.530	-0.530	-0.530	-0.530	-0.530
0.30	-0.530	-0.530	-0.530	-0.530	-0.530	-0.079	-0.530	-0.530
0.20	-0.530	-0.530	-0.530	-0.530	-0.530	0.824	-1.432	-0.530

rise time from one percent point to peak (ns) for 20 meter water

alpha*dz=	2.000	4.000	6.000	8.000	10.000	12.000	14.000	16.000
albedo								
0.90	7.908	11.120	12.705	13.293	13.494	14.485	15.316	16.096
0.80	7.632	10.625	12.493	13.279	13.620	13.818	13.832	14.754
0.70	7.279	10.064	12.224	13.216	13.719	13.126	13.126	13.255
0.60	6.947	9.333	11.749	13.068	13.781	13.309	13.242	12.712
0.50	6.600	8.591	11.036	12.747	13.769	13.643	14.189	12.979
0.40	5.999	7.892	9.950	12.104	13.603	14.904	14.092	14.811
0.30	4.813	7.322	8.661	10.634	13.155	16.039	13.302	13.226
0.20	3.476	6.462	7.455	8.722	12.141	16.622	8.724	9.572

convolution summary for navy water

zenith angle of entry= 45.00 degrees

bias in .1 percent point (PERCENT)

alpha*ds	2.000	4.000	6.000	8.000	10.000	12.000	14.000	16.000
albedo								
0.90	-10.089	-12.326	-12.937	-13.207	-13.337	-13.384	-13.341	-13.269
0.80	-9.689	-12.189	-12.928	-13.251	-13.429	-13.591	-13.498	-13.380
0.70	-9.209	-11.973	-12.890	-13.267	-13.553	-13.795	-13.632	-13.530
0.60	-8.661	-11.622	-12.800	-13.244	-13.642	-14.113	-13.700	-13.627
0.50	-8.027	-11.131	-12.577	-13.146	-13.678	-14.411	-13.723	-13.656
0.40	-7.432	-10.380	-12.142	-12.919	-13.584	-14.584	-13.680	-13.574
0.30	-7.084	-9.251	-11.452	-12.410	-13.226	-14.621	-13.286	-13.373
0.20	-6.661	-7.722	-10.192	-11.722	-12.510	-14.579	-11.635	-13.199

bias in 1 percent point (PERCENT)

alpha*ds	2.000	4.000	6.000	8.000	10.000	12.000	14.000	16.000
albedo								
0.90	-7.133	-9.958	-11.184	-11.715	-12.018	-12.117	-12.196	-12.220
0.80	-6.873	-9.676	-11.086	-11.722	-12.102	-12.322	-12.429	-12.463
0.70	-6.575	-9.242	-10.907	-11.682	-12.181	-12.516	-12.612	-12.708
0.60	-6.225	-8.659	-10.644	-11.587	-12.243	-12.793	-12.806	-12.990
0.50	-5.904	-7.901	-10.180	-11.386	-12.246	-13.047	-12.920	-13.215
0.40	-5.272	-7.171	-9.426	-11.005	-12.120	-13.270	-12.841	-13.272
0.30	-4.178	-6.633	-8.254	-10.298	-11.665	-14.027	-11.889	-13.066
0.20	-2.758	-5.597	-6.918	-8.885	-10.835	-13.969	-9.598	-9.021

bias in 10 percent point (PERCENT)

alpha*ds	2.000	4.000	6.000	8.000	10.000	12.000	14.000	16.000
albedo								
0.90	-3.289	-6.533	-7.984	-8.935	-9.525	-9.870	-10.091	-10.222
0.80	-2.779	-6.277	-7.769	-8.860	-9.614	-10.073	-10.409	-10.610
0.70	-2.256	-5.966	-7.455	-8.694	-9.649	-10.257	-10.668	-10.939
0.60	-1.661	-5.275	-7.073	-8.391	-9.614	-10.435	-10.827	-11.245
0.50	-1.084	-4.345	-6.609	-7.908	-9.461	-10.643	-10.852	-11.707
0.40	-0.656	-3.086	-5.934	-7.282	-8.977	-10.743	-10.687	-11.743
0.30	-0.281	-1.766	-4.684	-6.465	-7.854	-10.644	-8.925	-8.878
0.20	-0.121	-0.682	-2.859	-5.213	-6.535	-9.467	-5.011	-6.244

bias in 20 percent point (PERCENT)

alpha*ds	2.000	4.000	6.000	8.000	10.000	12.000	14.000	16.000
albedo								
0.90	-1.687	-5.203	-6.702	-7.637	-8.287	-8.723	-9.011	-9.161
0.80	-1.229	-4.802	-6.513	-7.545	-8.367	-8.944	-9.360	-9.609
0.70	-0.862	-4.238	-6.252	-7.363	-8.362	-9.102	-9.610	-9.951
0.60	-0.559	-3.413	-5.877	-7.053	-8.263	-9.227	-9.789	-10.288
0.50	-0.268	-2.441	-5.200	-6.653	-8.003	-9.354	-9.845	-10.590
0.40	-0.156	-1.369	-4.229	-6.112	-7.480	-9.429	-9.630	-9.922
0.30	-0.002	-0.584	-2.540	-5.163	-6.620	-9.198	-6.561	-6.551
0.20	0.167	-0.154	-0.827	-2.581	-5.530	-7.427	-3.489	-2.222

convolution summary for navy water

zenith angle of entry= 45.00 degrees

bias in 50 percent point (PERCENT)

alpha*dz	2.000	4.000	6.000	8.000	10.000	12.000	14.000	16.000
albedo								
0.90	-0.177	-2.438	-4.353	-5.346	-5.951	-6.423	-6.751	-6.953
0.80	-0.079	-1.940	-4.095	-5.284	-6.067	-6.679	-7.179	-7.547
0.70	0.025	-1.318	-3.656	-5.122	-6.085	-6.846	-7.466	-7.974
0.60	0.145	-0.744	-3.067	-4.825	-6.016	-6.943	-7.642	-8.302
0.50	0.208	-0.318	-2.097	-4.191	-5.784	-7.050	-7.671	-8.433
0.40	0.254	-0.080	-0.998	-2.871	-5.359	-7.114	-6.925	-7.642
0.30	0.291	0.158	-0.212	-1.272	-3.177	-6.088	-3.470	-2.177
0.70	0.320	0.260	0.125	-0.205	-1.766	-3.787	0.350	0.361

bias in 80 percent point (PERCENT)

alpha*dz	2.000	4.000	6.000	8.000	10.000	12.000	14.000	16.000
albedo								
0.90	0.281	-0.593	-2.176	-3.258	-3.832	-4.288	-4.564	-4.741
0.80	0.334	-0.395	-1.816	-3.187	-4.039	-4.682	-5.159	-5.555
0.70	0.374	-0.160	-1.335	-2.922	-4.107	-4.929	-5.535	-6.101
0.60	0.405	0.020	-0.811	-2.430	-4.031	-5.050	-5.793	-6.437
0.50	0.429	0.206	-0.303	-1.590	-3.511	-5.146	-5.879	-6.502
0.40	0.447	0.339	0.015	-0.768	-2.304	-4.884	-5.175	-6.271
0.30	0.462	0.409	0.275	-0.056	-0.789	-3.004	0.454	0.481
0.20	0.474	0.449	0.401	0.298	-0.435	-0.421	0.485	0.490

results for bias in peak (PERCENT)

alpha*dz	2.000	4.000	6.000	8.000	10.000	12.000	14.000	16.000
albedo								
0.90	0.152	-0.271	-0.271	-0.695	-1.118	-1.118	-1.542	-1.542
0.80	0.152	0.152	-0.271	-0.695	-1.542	-1.965	-2.388	-2.812
0.70	0.152	0.152	-0.271	-0.695	-1.542	-2.388	-3.235	-4.082
0.60	0.152	0.152	-0.271	-0.271	-1.118	-2.812	-3.235	-4.082
0.50	0.152	0.152	0.152	-0.271	-0.695	-2.812	-3.659	-5.353
0.40	0.152	0.152	0.152	-0.271	-0.695	-1.118	-3.659	-2.388
0.30	0.152	0.152	0.152	0.152	0.152	-0.271	0.152	0.152
0.20	0.152	0.152	0.152	0.152	0.152	-0.271	0.152	0.152

rise time from one percent point to peak (ns) for 20 meter water

alpha*dz	2.000	4.000	6.000	8.000	10.000	12.000	14.000	16.000
albedo								
0.90	15.295	20.335	22.909	23.135	22.881	23.091	22.367	22.416
0.80	14.748	20.633	22.704	23.150	22.169	21.742	21.078	20.261
0.70	14.123	19.721	22.327	23.066	22.335	21.261	19.683	18.108
0.60	13.388	18.498	21.777	23.756	23.354	20.952	20.091	18.699
0.50	12.714	16.907	21.690	23.334	24.249	21.487	19.441	16.504
0.40	11.386	15.374	20.107	22.534	23.985	25.511	19.276	22.848
0.30	9.091	14.244	17.647	21.938	24.809	28.878	25.278	27.750
0.20	6.110	12.071	14.844	18.973	23.066	28.755	20.468	19.257

convolution summary for NOS water

zenith angle of entry= 0.00 degrees

bias in .1 percent point (PERCENT)

alpha*dz albedo	2.000	4.000	6.000	8.000	10.000	12.000	14.000	16.000
0.90	0.125	0.125	0.125	0.125	0.125	0.125	0.125	0.125
0.80	0.125	0.125	0.125	0.125	0.125	0.125	0.125	0.125
0.70	0.125	0.125	0.125	0.125	0.125	0.125	0.125	0.125
0.60	0.125	0.125	0.125	0.125	0.125	0.125	0.125	0.125
0.50	0.125	0.125	0.125	0.125	0.125	0.125	0.125	0.125
0.40	0.125	0.125	0.125	0.125	0.125	0.125	0.125	0.125
0.30	0.125	0.125	0.125	0.125	0.125	0.125	0.125	0.125
0.20	0.125	0.125	0.125	0.125	0.125	0.125	0.125	0.125

bias in 1 percent point (PERCENT)

alpha*dz albedo	2.000	4.000	6.000	8.000	10.000	12.000	14.000	16.000
0.90	0.125	0.125	0.125	0.125	0.125	0.125	0.125	0.125
0.80	0.125	0.125	0.125	0.125	0.125	0.125	0.125	0.125
0.70	0.125	0.125	0.125	0.125	0.125	0.125	0.125	0.125
0.60	0.125	0.125	0.125	0.125	0.125	0.125	0.125	0.125
0.50	0.125	0.125	0.125	0.125	0.125	0.125	0.125	0.125
0.40	0.125	0.125	0.125	0.125	0.125	0.125	0.125	0.125
0.30	0.125	0.125	0.125	0.125	0.125	0.125	0.125	0.125
0.20	0.125	0.125	0.125	0.125	0.125	0.125	0.125	0.125

bias in 10 percent point (PERCENT)

alpha*dz albedo	2.000	4.000	6.000	8.000	10.000	12.000	14.000	16.000
0.90	0.125	0.125	0.125	0.125	0.125	0.125	0.463	0.638
0.80	0.125	0.125	0.125	0.125	0.125	0.125	0.125	0.125
0.70	0.125	0.125	0.125	0.125	0.125	0.125	0.125	0.125
0.60	0.125	0.125	0.125	0.125	0.125	0.125	0.125	0.125
0.50	0.125	0.125	0.125	0.125	0.125	0.125	0.125	0.125
0.40	0.125	0.125	0.125	0.125	0.125	0.125	0.125	0.125
0.30	0.125	0.125	0.125	0.125	0.125	0.125	0.125	0.125
0.20	0.125	0.125	0.125	0.125	0.125	0.125	0.125	0.125

bias in 20 percent point (PERCENT)

alpha*dz albedo	2.000	4.000	6.000	8.000	10.000	12.000	14.000	16.000
0.90	0.125	0.125	0.125	0.125	0.125	0.447	0.745	1.014
0.80	0.125	0.125	0.125	0.125	0.125	0.125	0.415	0.523
0.70	0.125	0.125	0.125	0.125	0.125	0.125	0.125	0.125
0.60	0.125	0.125	0.125	0.125	0.125	0.125	0.125	0.125
0.50	0.125	0.125	0.125	0.125	0.125	0.125	0.125	0.125
0.40	0.125	0.125	0.125	0.125	0.125	0.125	0.125	0.125
0.30	0.125	0.125	0.125	0.125	0.125	0.125	0.125	0.125
0.20	0.125	0.125	0.125	0.125	0.125	0.125	0.125	0.125

convolution summary for NOS water

zenith angle of entry= 0.00 degrees

bias in 50 percent point (PERCENT)

alpha*dz	2.000	4.000	6.000	8.000	10.000	12.000	14.000	16.000
albedo								
0.90	0.125	0.125	0.125	0.125	0.486	1.230	1.877	2.449
0.80	0.125	0.125	0.125	0.125	0.125	0.624	0.973	1.424
0.70	0.125	0.125	0.125	0.125	0.125	0.125	0.444	0.479
0.60	0.125	0.125	0.125	0.125	0.125	0.125	0.125	0.125
0.50	0.125	0.125	0.125	0.125	0.125	0.125	0.125	0.125
0.40	0.125	0.125	0.125	0.125	0.125	0.125	0.125	0.125
0.30	0.125	0.125	0.125	0.125	0.125	0.125	0.125	0.125
0.20	0.125	0.125	0.125	0.125	0.125	0.125	0.125	0.125

bias in 80 percent point (PERCENT)

alpha*dz	2.000	4.000	6.000	8.000	10.000	12.000	14.000	16.000
albedo								
0.90	0.125	0.125	0.125	0.125	1.587	2.585	3.809	4.487
0.80	0.125	0.125	0.125	0.125	0.533	1.437	2.467	3.180
0.70	0.125	0.125	0.125	0.125	0.125	0.586	0.909	0.845
0.60	0.125	0.125	0.125	0.125	0.125	0.125	0.449	0.472
0.50	0.125	0.125	0.125	0.125	0.125	0.125	0.125	0.125
0.40	0.125	0.125	0.125	0.125	0.125	0.125	0.125	0.125
0.30	0.125	0.125	0.125	0.125	0.125	0.125	0.125	0.125
0.20	0.125	0.125	0.125	0.125	0.125	0.125	0.125	0.125

results for bias in peak (PERCENT)

alpha*dz	2.000	4.000	6.000	8.000	10.000	12.000	14.000	16.000
albedo								
0.90	0.125	0.125	0.125	0.875	4.625	4.375	6.375	8.375
0.80	0.125	0.125	0.125	0.125	2.125	4.125	4.375	5.625
0.70	0.125	0.125	0.125	0.125	0.375	2.375	3.875	3.125
0.60	0.125	0.125	0.125	0.125	0.375	0.125	0.375	0.875
0.50	0.125	0.125	0.125	0.125	0.125	0.125	0.125	0.125
0.40	0.125	0.125	0.125	0.125	0.125	0.125	0.125	0.125
0.30	0.125	0.125	0.125	0.125	0.125	0.125	0.125	0.125
0.20	0.125	0.125	0.125	0.125	0.125	0.125	0.125	0.125

rise time from one percent point to peak (ns) for 20 meter water

alpha*dz	2.000	4.000	6.000	8.000	10.000	12.000	14.000	16.000
albedo								
0.90	0.000	0.000	0.000	1.334	8.001	7.556	11.112	14.669
0.80	0.000	0.000	0.000	0.000	3.556	7.112	7.556	9.779
0.70	0.000	0.000	0.000	0.000	0.444	4.000	6.667	5.334
0.60	0.000	0.000	0.000	0.000	0.444	0.000	0.444	1.334
0.50	0.000	0.000	0.000	0.000	0.000	0.000	0.000	0.000
0.40	0.000	0.000	0.000	0.000	0.000	0.000	0.000	0.000
0.30	0.000	0.000	0.000	0.000	0.000	0.000	0.000	0.000
0.20	0.000	0.000	0.000	0.000	0.000	0.000	0.000	0.000

convolution summary for NOS water

zenith angle of entry= 15.00 degrees

bias in .1 percent point (PERCENT)

alpha*ds=	2.000	4.000	6.000	8.000	10.000	12.000	14.000	16.000
albedo								
0.90	-1.265	-1.479	-1.528	-1.530	-1.523	-1.467	-1.402	-1.291
0.80	-1.237	-1.462	-1.527	-1.541	-1.538	-1.514	-1.511	-1.437
0.70	-1.196	-1.432	-1.523	-1.789	-1.789	-1.789	-1.789	-1.492
0.60	-1.131	-1.373	-1.517	-1.789	-1.789	-1.789	-1.789	-1.505
0.50	-1.051	-1.291	-1.504	-1.789	-1.789	-1.789	-1.789	-1.492
0.40	-1.040	-1.245	-1.472	-1.789	-1.789	-1.789	-1.789	-1.446
0.30	-1.024	-1.136	-1.397	-1.789	-1.789	-1.789	-1.789	-1.298
0.20	-0.998	-1.034	-1.262	-1.789	-1.789	-1.789	-1.072	-1.292

bias in 1 percent point (PERCENT)

alpha*ds=	2.000	4.000	6.000	8.000	10.000	12.000	14.000	16.000
albedo								
0.90	-0.976	-1.158	-1.259	-1.264	-1.230	-1.112	-1.015	-0.908
0.80	-0.953	-1.120	-1.255	-1.280	-1.261	-1.199	-1.150	-1.027
0.70	-0.924	-1.055	-1.242	-1.294	-1.277	-1.259	-1.226	-1.175
0.60	-0.887	-1.032	-1.224	-1.299	-1.294	-1.332	-1.253	-1.250
0.50	-0.837	-1.001	-1.187	-1.285	-1.338	-1.452	-1.247	-1.265
0.40	-0.794	-0.954	-1.095	-1.245	-1.374	-1.789	-1.189	-1.265
0.30	-0.755	-0.868	-1.027	-1.127	-1.356	-1.789	-1.039	-1.258
0.20	-0.676	-0.780	-0.970	-1.034	-1.112	-1.789	-0.988	-1.227

bias in 10 percent point (PERCENT)

alpha*ds=	2.000	4.000	6.000	8.000	10.000	12.000	14.000	16.000
albedo								
0.90	-0.550	-0.748	-0.804	-0.803	-0.737	-0.570	-0.386	-0.232
0.80	-0.525	-0.733	-0.802	-0.839	-0.784	-0.684	-0.572	-0.458
0.70	-0.493	-0.708	-0.794	-0.876	-0.804	-0.754	-0.693	-0.669
0.60	-0.451	-0.666	-0.784	-0.889	-0.834	-0.810	-0.753	-0.742
0.50	-0.393	-0.605	-0.766	-0.864	-0.869	-0.887	-0.776	-0.749
0.40	-0.317	-0.538	-0.722	-0.826	-0.896	-0.950	-0.732	-0.742
0.30	-0.310	-0.465	-0.647	-0.748	-0.906	-0.989	-0.418	-0.724
0.20	-0.303	-0.327	-0.508	-0.452	-0.900	-1.007	-0.284	-0.648

bias in 20 percent point (PERCENT)

alpha*ds=	2.000	4.000	6.000	8.000	10.000	12.000	14.000	16.000
albedo								
0.90	-0.393	-0.574	-0.646	-0.633	-0.511	-0.317	-0.023	0.217
0.80	-0.347	-0.556	-0.650	-0.669	-0.581	-0.451	-0.306	-0.193
0.70	-0.313	-0.533	-0.641	-0.702	-0.621	-0.530	-0.459	-0.314
0.60	-0.305	-0.493	-0.630	-0.713	-0.650	-0.598	-0.529	-0.614
0.50	-0.297	-0.438	-0.602	-0.675	-0.676	-0.658	-0.526	-0.659
0.40	-0.290	-0.356	-0.536	-0.579	-0.687	-0.750	-0.415	-0.663
0.30	-0.283	-0.306	-0.436	-0.448	-0.632	-0.873	-0.272	-0.636
0.20	-0.278	-0.291	-0.307	-0.301	-0.309	-0.939	-0.234	0.285

convolution summary for NOS water

zenith angle of entry= 15.00 degrees

bias in 50 percent point (PERCENT)

alpha*d=	2.000	4.000	6.000	8.000	10.000	12.000	14.000	16.000
albedo								
0.90	-0.236	-0.290	-0.304	-0.259	-0.049	0.310	0.951	1.490
0.80	-0.229	-0.286	-0.315	-0.308	-0.195	0.036	0.433	0.739
0.70	-0.223	-0.275	-0.311	-0.364	-0.252	-0.114	0.043	0.226
0.60	-0.218	-0.258	-0.307	-0.382	-0.285	-0.195	-0.150	-0.147
0.50	-0.213	-0.243	-0.294	-0.322	-0.297	-0.218	-0.194	-0.149
0.40	-0.208	-0.230	-0.265	-0.278	-0.283	-0.224	-0.162	-0.108
0.30	-0.204	-0.219	-0.239	-0.242	-0.251	-0.221	-0.108	0.395
0.20	-0.201	-0.209	-0.219	-0.215	-0.220	-0.215	-0.082	0.821

bias in 80 percent point (PERCENT)

alpha*d=	2.000	4.000	6.000	8.000	10.000	12.000	14.000	16.000
albedo								
0.90	-0.138	-0.133	-0.045	0.102	0.597	1.253	2.486	3.560
0.80	-0.135	-0.148	-0.098	-0.036	0.231	0.686	1.280	2.400
0.70	-0.133	-0.154	-0.120	-0.143	0.086	0.360	0.859	0.880
0.60	-0.131	-0.147	-0.146	-0.186	-0.046	0.145	0.726	0.768
0.50	-0.129	-0.141	-0.161	-0.171	-0.122	0.086	0.071	0.812
0.40	-0.127	-0.136	-0.149	-0.155	-0.148	0.037	0.034	0.839
0.30	-0.125	-0.131	-0.139	-0.140	-0.144	-0.032	0.060	0.854
0.20	-0.124	-0.127	-0.131	-0.130	-0.132	-0.097	0.071	1.837

results for bias in peak (PERCENT)

alpha*d=	2.000	4.000	6.000	8.000	10.000	12.000	14.000	16.000
albedo								
0.90	-0.318	-0.073	0.173	0.663	2.380	3.115	6.303	7.529
0.80	-0.318	-0.073	-0.073	0.418	1.153	1.889	3.606	4.096
0.70	-0.318	-0.318	-0.073	0.173	0.418	1.399	1.889	4.096
0.60	-0.318	-0.318	-0.073	-0.073	0.418	0.663	0.908	1.644
0.50	-0.318	-0.318	-0.318	-0.318	0.173	0.418	0.908	0.663
0.40	-0.318	-0.318	-0.318	-0.318	-0.073	0.418	-0.073	0.663
0.30	-0.318	-0.318	-0.318	-0.318	-0.318	0.418	-0.073	1.644
0.20	-0.318	-0.318	-0.318	-0.318	-0.318	0.418	-0.073	1.644

rise time from one percent point to peak (ns) for 20 meter water

alpha*d=	2.000	4.000	6.000	8.000	10.000	12.000	14.000	16.000
albedo								
0.90	1.193	1.968	2.595	3.493	6.544	7.662	13.265	15.294
0.80	1.151	1.899	2.143	3.078	4.376	5.598	8.620	9.287
0.70	1.099	1.336	2.120	2.658	3.072	4.817	5.646	9.554
0.60	1.031	1.294	2.086	2.224	3.102	3.617	3.918	5.246
0.50	0.941	1.239	1.575	1.753	2.739	3.389	3.906	3.494
0.40	0.863	1.153	1.409	1.681	2.359	4.000	2.023	3.494
0.30	0.792	0.997	1.286	1.467	1.882	4.000	1.752	5.260
0.20	0.649	0.838	1.182	1.298	1.440	4.000	1.659	5.203

convolution summary for NOS water

zenith angle of entry= 25.00 degrees

bias in .1 percent point (PERCENT)

alpha*d=	2.000	4.000	6.000	8.000	10.000	12.000	14.000	16.000
albedo								
0.90	-3.374	-4.024	-4.135	-4.231	-4.276	-4.258	-4.046	-3.865
0.80	-3.235	-3.953	-4.109	-4.231	-4.295	-4.348	-4.114	-4.001
0.70	-3.077	-3.851	-4.080	-4.209	-4.281	-4.390	-4.185	-4.058
0.60	-2.888	-3.725	-4.026	-4.147	-4.235	-4.372	-4.194	-4.079
0.50	-2.682	-3.547	-3.931	-4.091	-4.126	-4.256	-4.104	-4.082
0.40	-2.559	-3.285	-3.822	-4.049	-3.988	-3.974	-3.679	-4.071
0.30	-2.410	-2.917	-3.594	-3.989	-3.716	-3.803	-3.032	-4.018
0.20	-2.260	-2.458	-3.009	-3.312	-3.539	-3.630	-2.310	-2.690

bias in 1 percent point (PERCENT)

alpha*d=	2.000	4.000	6.000	8.000	10.000	12.000	14.000	16.000
albedo								
0.90	-2.450	-3.237	-3.529	-3.670	-3.636	-3.557	-3.380	-3.265
0.80	-2.373	-3.125	-3.495	-3.665	-3.665	-3.616	-3.498	-3.430
0.70	-2.267	-2.979	-3.430	-3.632	-3.636	-3.627	-3.545	-3.572
0.60	-2.145	-2.786	-3.321	-3.564	-3.585	-3.606	-3.522	-3.679
0.50	-1.985	-2.562	-3.123	-3.391	-3.491	-3.558	-3.381	-3.665
0.40	-1.821	-2.336	-2.801	-3.137	-3.327	-3.474	-2.885	-3.226
0.30	-1.566	-2.111	-2.424	-2.669	-3.023	-2.925	-2.322	-2.669
0.20	-1.351	-1.913	-2.167	-2.450	-2.492	-2.749	-1.120	-2.621

bias in 10 percent point (PERCENT)

alpha*d=	2.000	4.000	6.000	8.000	10.000	12.000	14.000	16.000
albedo								
0.90	-1.308	-2.123	-2.422	-2.583	-2.555	-2.448	-2.303	-2.109
0.80	-1.169	-2.018	-2.364	-2.549	-2.584	-2.528	-2.477	-2.389
0.70	-1.007	-1.903	-2.270	-2.470	-2.539	-2.533	-2.559	-2.522
0.60	-0.844	-1.763	-2.149	-2.368	-2.445	-2.497	-2.544	-2.561
0.50	-0.679	-1.486	-2.013	-2.213	-2.335	-2.474	-2.357	-2.510
0.40	-0.491	-1.214	-1.828	-2.098	-2.194	-2.492	-1.869	-2.434
0.30	-0.321	-0.778	-1.165	-1.833	-2.044	-2.547	-1.012	-1.573
0.20	-0.313	-0.456	-0.684	-0.981	-1.848	-2.605	0.504	-1.229

bias in 20 percent point (PERCENT)

alpha*d=	2.000	4.000	6.000	8.000	10.000	12.000	14.000	16.000
albedo								
0.90	-0.778	-1.697	-1.984	-2.140	-2.071	-1.953	-1.768	-1.529
0.80	-0.663	-1.561	-1.940	-2.122	-2.117	-2.044	-1.993	-1.884
0.70	-0.528	-1.405	-1.874	-2.069	-2.089	-2.042	-2.103	-2.086
0.60	-0.393	-1.207	-1.772	-1.981	-2.031	-1.967	-2.076	-2.227
0.50	-0.316	-0.927	-1.507	-1.820	-1.937	-1.891	-1.881	-2.236
0.40	-0.305	-0.624	-1.082	-1.460	-1.760	-1.839	-1.228	-1.662
0.30	-0.295	-0.370	-0.679	-1.028	-1.579	-1.828	-0.852	-1.205
0.20	-0.288	-0.303	-0.314	-0.691	-1.218	-2.503	0.630	-1.168

convolution summary for NOS water

zenith angle of entry= 25.00 degrees

bias in 50 percent point (PERCENT)

alpha*dz	2.000	4.000	6.000	8.000	10.000	12.000	14.000	16.000
albedo								
0.90	-0.275	-0.845	-1.173	-1.264	-1.130	-0.929	-0.545	-0.074
0.80	-0.261	-0.693	-1.111	-1.256	-1.240	-1.115	-1.028	-0.798
0.70	-0.249	-0.520	-0.995	-1.184	-1.222	-1.154	-1.226	-1.143
0.60	-0.238	-0.363	-0.794	-1.038	-1.164	-1.116	-1.247	-1.299
0.50	-0.230	-0.291	-0.605	-0.804	-1.087	-1.050	-1.055	-1.192
0.40	-0.223	-0.260	-0.315	-0.653	-0.913	-0.975	-0.830	-1.041
0.30	-0.217	-0.237	-0.259	-0.479	-0.773	-0.916	0.661	-1.004
0.20	-0.212	-0.222	-0.229	-0.286	-0.752	-1.301	0.833	-1.002

bias in 80 percent point (PERCENT)

alpha*dz	2.000	4.000	6.000	8.000	10.000	12.000	14.000	16.000
albedo								
0.90	-0.162	-0.278	-0.505	-0.537	-0.209	0.252	1.310	2.524
0.80	-0.156	-0.239	-0.464	-0.578	-0.461	-0.203	0.247	0.752
0.70	-0.151	-0.209	-0.377	-0.552	-0.497	-0.341	-0.328	-0.172
0.60	-0.147	-0.186	-0.277	-0.468	-0.493	-0.347	-0.437	-0.722
0.50	-0.144	-0.168	-0.217	-0.356	-0.478	-0.338	-0.132	-0.876
0.40	-0.141	-0.156	-0.178	-0.258	-0.395	-0.313	0.677	-0.894
0.30	-0.139	-0.147	-0.156	-0.200	-0.333	-0.334	0.848	-0.880
0.20	-0.137	-0.141	-0.143	-0.166	-0.359	-0.387	2.234	-0.879

results for bias in peak (PERCENT)

alpha*dz	2.000	4.000	6.000	8.000	10.000	12.000	14.000	16.000
albedo								
0.90	-0.324	-0.324	-0.087	0.625	1.810	2.521	5.365	5.840
0.80	-0.324	-0.324	-0.087	-0.087	0.388	1.810	2.758	3.469
0.70	-0.324	-0.324	-0.324	-0.087	0.151	0.625	2.047	3.232
0.60	-0.324	-0.324	-0.324	-0.324	0.151	0.625	1.099	0.388
0.50	-0.324	-0.324	-0.324	-0.324	0.151	0.625	0.625	0.388
0.40	-0.324	-0.324	-0.324	-0.324	-0.324	0.151	2.047	-1.035
0.30	-0.324	-0.324	-0.324	-0.324	-0.324	0.151	2.047	-1.035
0.20	-0.324	-0.324	-0.324	-0.324	-0.324	0.151	2.047	-1.035

rise time from one percent point to peak (ns) for 20 meter water

alpha*dz	2.000	4.000	6.000	8.000	10.000	12.000	14.000	16.000
albedo								
0.90	3.987	5.463	6.456	8.054	10.212	11.396	16.400	17.073
0.80	3.843	5.253	6.392	6.710	7.599	10.174	11.731	12.936
0.70	3.645	4.980	5.826	6.648	7.100	7.973	10.486	12.759
0.60	3.415	4.618	5.620	6.076	7.006	7.933	8.665	7.626
0.50	3.116	4.198	5.250	5.752	6.828	7.843	7.512	7.600
0.40	2.808	3.774	4.646	5.275	5.632	6.797	9.248	4.109
0.30	2.330	3.353	3.939	4.399	5.061	5.767	8.193	3.065
0.20	1.926	2.981	3.457	3.987	4.066	5.438	5.939	2.975

convolution summary for NOS water

zenith angle of entry= 35.00 degrees

bias in .1 percent point (PERCENT)

alpha*d=	2.000	4.000	6.000	8.000	10.000	12.000	14.000	16.000
albedo								
0.90	-6.693	-7.868	-8.143	-8.127	-7.928	-7.745	-7.712	-7.732
0.80	-6.458	-7.728	-8.103	-8.145	-7.950	-7.937	-7.983	-8.088
0.70	-6.187	-7.584	-8.024	-8.141	-7.896	-8.054	-8.231	-8.408
0.60	-5.831	-7.303	-7.867	-8.100	-7.744	-8.128	-8.500	-8.541
0.50	-5.416	-6.951	-7.649	-7.989	-7.680	-8.171	-8.588	-8.586
0.40	-4.982	-6.376	-7.280	-7.699	-7.531	-8.165	-8.618	-8.535
0.30	-4.597	-5.623	-6.627	-6.916	-6.839	-8.014	-8.625	-7.741
0.20	-4.503	-4.813	-5.657	-6.133	-6.472	-7.600	-8.619	-7.719

bias in 1 percent point (PERCENT)

alpha*d=	2.000	4.000	6.000	8.000	10.000	12.000	14.000	16.000
albedo								
0.90	-4.775	-6.365	-6.990	-7.150	-7.114	-7.036	-6.938	-6.893
0.80	-4.570	-6.162	-6.884	-7.159	-7.165	-7.161	-7.161	-7.222
0.70	-4.466	-5.855	-6.743	-7.121	-7.150	-7.243	-7.296	-7.556
0.60	-4.346	-5.453	-6.504	-6.973	-7.047	-7.289	-7.508	-7.697
0.50	-4.197	-4.995	-6.144	-6.705	-6.807	-7.285	-7.624	-7.730
0.40	-3.857	-4.580	-5.592	-6.233	-6.595	-7.205	-8.331	-7.717
0.30	-3.177	-4.251	-4.768	-5.166	-5.903	-6.981	-8.402	-7.665
0.20	-2.587	-3.423	-4.173	-4.270	-4.970	-6.258	-8.342	-7.466

bias in 10 percent point (PERCENT)

alpha*d=	2.000	4.000	6.000	8.000	10.000	12.000	14.000	16.000
albedo								
0.90	-2.611	-4.165	-4.998	-5.347	-5.421	-5.362	-5.347	-5.218
0.80	-2.308	-3.974	-4.871	-5.303	-5.516	-5.517	-5.667	-5.723
0.70	-1.875	-3.704	-4.646	-5.181	-5.517	-5.630	-5.824	-6.164
0.60	-1.560	-3.370	-4.384	-4.930	-5.420	-5.657	-5.926	-6.666
0.50	-1.227	-2.916	-4.024	-4.508	-5.155	-5.563	-6.009	-7.377
0.40	-0.879	-2.215	-3.510	-3.986	-4.695	-5.376	-6.029	-7.388
0.30	-0.528	-1.577	-2.632	-3.004	-3.966	-4.999	-6.975	-6.804
0.20	-0.511	-0.887	-1.961	-2.445	-3.053	-4.648	-7.000	-6.801

bias in 20 percent point (PERCENT)

alpha*d=	2.000	4.000	6.000	8.000	10.000	12.000	14.000	16.000
albedo								
0.90	-1.432	-3.332	-4.168	-4.497	-4.563	-4.530	-4.489	-4.366
0.80	-1.179	-3.096	-4.051	-4.450	-4.675	-4.731	-4.797	-4.866
0.70	-0.916	-2.780	-3.861	-4.319	-4.673	-4.839	-4.928	-5.271
0.60	-0.691	-2.290	-3.579	-4.069	-4.561	-4.872	-5.003	-5.965
0.50	-0.519	-1.759	-3.173	-3.754	-4.257	-4.814	-5.188	-6.728
0.40	-0.497	-1.226	-2.496	-3.029	-3.901	-4.670	-5.591	-6.771
0.30	-0.478	-0.784	-1.815	-2.391	-3.115	-4.409	-5.704	-6.758
0.20	-0.463	-0.509	-0.523	-0.529	-1.759	-3.555	-5.754	-6.755

convolution summary for NOS water

zenith angle of entry= 35.00 degrees

bias in 50 percent point (PERCENT)

alpha*d= albedo	2.000	4.000	6.000	8.000	10.000	12.000	14.000	16.000
0.90	-0.441	-1.623	-2.666	-2.894	-2.972	-2.993	-2.646	-2.359
0.80	-0.413	-1.335	-2.546	-2.891	-3.141	-3.164	-3.131	-3.184
0.70	-0.390	-0.967	-2.321	-2.793	-3.172	-3.319	-3.343	-3.711
0.60	-0.370	-0.744	-2.002	-2.582	-3.108	-3.384	-3.553	-4.110
0.50	-0.354	-0.516	-1.435	-2.098	-2.950	-3.330	-3.811	-6.433
0.40	-0.340	-0.440	-0.657	-1.144	-2.333	-3.186	-3.925	-6.630
0.30	-0.328	-0.386	-0.424	-0.442	-1.195	-3.046	-3.940	-6.622
0.20	-0.319	-0.348	-0.356	-0.360	-0.367	-2.928	-3.946	-6.620

bias in 80 percent point (PERCENT)

alpha*d= albedo	2.000	4.000	6.000	8.000	10.000	12.000	14.000	16.000
0.90	-0.223	-0.519	-1.315	-1.424	-1.425	-1.239	-0.630	0.041
0.80	-0.212	-0.426	-1.203	-1.439	-1.700	-1.662	-1.485	-1.330
0.70	-0.203	-0.352	-0.957	-1.348	-1.760	-1.936	-1.973	-2.148
0.60	-0.195	-0.295	-0.539	-1.116	-1.595	-2.072	-2.100	-2.637
0.50	-0.189	-0.253	-0.362	-0.445	-1.213	-1.951	-2.171	-3.413
0.40	-0.183	-0.223	-0.268	-0.295	-0.343	-1.678	-2.176	-6.488
0.30	-0.178	-0.201	-0.217	-0.224	-0.240	-1.494	-3.700	-6.485
0.20	-0.175	-0.186	-0.190	-0.191	-0.194	-1.322	-3.791	-6.484

results for bias in peak (PERCENT)

alpha*d= albedo	2.000	4.000	6.000	8.000	10.000	12.000	14.000	16.000
0.90	-0.530	-0.530	-0.079	0.373	0.824	1.726	2.628	3.530
0.80	-0.530	-0.530	-0.530	-0.079	-0.079	0.373	0.373	2.177
0.70	-0.530	-0.530	-0.530	-0.079	-0.530	-0.530	-0.530	-0.079
0.60	-0.530	-0.530	-0.530	-0.530	-0.530	-0.530	-0.530	-0.981
0.50	-0.530	-0.530	-0.530	-0.530	-0.530	-1.432	-0.530	-2.785
0.40	-0.530	-0.530	-0.530	-0.530	-0.530	-1.432	-2.334	-6.845
0.30	-0.530	-0.530	-0.530	-0.530	-0.530	-1.432	-2.334	-6.845
0.20	-0.530	-0.530	-0.530	-0.530	-0.530	-1.432	-4.139	-6.845

rise time from one percent point to peak (ns) for 20 meter water

alpha*d= albedo	2.000	4.000	6.000	8.000	10.000	12.000	14.000	16.000
0.90	8.367	11.499	13.620	14.824	15.643	17.266	18.853	20.541
0.80	7.962	11.099	12.521	13.953	13.964	14.847	14.847	18.522
0.70	7.758	10.495	12.245	13.878	13.047	13.229	13.334	14.736
0.60	7.520	9.703	11.773	12.698	12.843	13.320	13.752	13.235
0.50	7.227	8.799	11.064	12.170	12.370	11.535	13.981	9.744
0.40	6.556	7.982	9.977	11.240	11.952	11.377	11.817	1.719
0.30	5.217	7.334	8.353	9.136	10.590	10.935	11.959	1.615
0.20	4.055	5.702	7.179	7.371	8.750	9.511	8.284	1.223

convolution summary for NOS water

zenith angle of entry= 45.00 degrees

bias in .1 percent point (PERCENT)

alpha*d=	2.000	4.000	6.000	8.000	10.000	12.000	14.000	16.000
albedo								
0.90	-10.764	-12.373	-12.995	-13.051	-13.055	-12.938	-13.045	-12.860
0.80	-10.401	-12.260	-12.996	-13.138	-13.156	-13.094	-13.253	-13.079
0.70	-9.945	-12.086	-12.969	-13.189	-13.208	-13.211	-13.370	-13.302
0.60	-9.390	-11.895	-12.921	-13.215	-13.231	-13.265	-13.437	-13.372
0.50	-8.697	-11.591	-12.826	-13.219	-13.234	-13.284	-13.462	-13.371
0.40	-7.894	-11.088	-12.602	-13.186	-13.209	-13.272	-13.397	-13.354
0.30	-7.302	-9.993	-12.219	-13.093	-13.109	-13.205	-13.393	-13.278
0.20	-6.530	-8.397	-11.545	-12.833	-12.910	-11.547	-13.388	-11.697

bias in 1 percent point (PERCENT)

alpha*d=	2.000	4.000	6.000	8.000	10.000	12.000	14.000	16.000
albedo								
0.90	-7.668	-10.429	-11.440	-11.845	-11.901	-11.854	-11.839	-11.718
0.80	-7.297	-10.229	-11.423	-12.017	-12.041	-12.015	-12.011	-11.958
0.70	-6.925	-9.883	-11.349	-12.177	-12.156	-12.111	-12.097	-12.041
0.60	-6.529	-9.385	-11.194	-12.315	-12.264	-12.118	-12.114	-12.036
0.50	-6.177	-8.672	-10.851	-12.403	-12.336	-11.872	-13.200	-11.974
0.40	-5.904	-7.773	-10.142	-12.401	-12.336	-11.555	-13.299	-11.778
0.30	-4.857	-6.761	-9.068	-12.299	-12.195	-10.934	-13.319	-11.666
0.20	-3.267	-6.049	-7.338	-11.655	-10.817	-9.940	-13.283	-11.604

bias in 10 percent point (PERCENT)

alpha*d=	2.000	4.000	6.000	8.000	10.000	12.000	14.000	16.000
albedo								
0.90	-4.164	-7.038	-8.465	-9.181	-9.559	-9.604	-9.584	-9.616
0.80	-3.547	-6.768	-8.342	-9.258	-9.717	-9.800	-9.777	-9.878
0.70	-2.984	-6.417	-8.152	-9.273	-9.786	-9.867	-9.827	-10.099
0.60	-2.227	-5.998	-7.827	-9.229	-9.784	-9.803	-9.788	-10.176
0.50	-1.569	-5.447	-7.344	-9.087	-9.709	-9.614	-9.547	-10.137
0.40	-0.933	-4.161	-6.628	-8.420	-9.136	-9.078	-9.400	-11.357
0.30	-0.503	-2.567	-5.790	-7.473	-8.783	-8.556	-10.889	-9.950
0.20	-0.176	-1.580	-2.932	-6.295	-7.530	-6.935	-8.306	-9.935

bias in 20 percent point (PERCENT)

alpha*d=	2.000	4.000	6.000	8.000	10.000	12.000	14.000	16.000
albedo								
0.90	-2.376	-5.855	-7.166	-7.914	-8.393	-8.485	-8.495	-8.491
0.80	-1.816	-5.600	-7.045	-7.962	-8.573	-8.728	-8.732	-8.759
0.70	-1.278	-5.204	-6.869	-7.921	-8.638	-8.825	-8.819	-8.754
0.60	-0.823	-4.462	-6.578	-7.806	-8.613	-8.752	-8.877	-8.587
0.50	-0.509	-3.401	-6.173	-7.595	-8.531	-8.580	-8.954	-9.801
0.40	-0.232	-2.180	-5.527	-7.126	-8.388	-8.327	-8.939	-9.885
0.30	-0.061	-1.019	-3.695	-6.406	-7.493	-7.109	-8.276	-9.861
0.20	0.161	-0.208	-1.367	-5.699	-6.515	-6.037	-8.171	-9.854

convolution summary for NOS water

zenith angle of entry= 45.00 degrees

bias in 50 percent point (PERCENT)

alpha*d=	2.000	4.000	6.000	8.000	10.000	12.000	14.000	16.000
albedo								
0.90	-0.380	-3.282	-4.874	-5.613	-6.166	-6.243	-6.273	-6.248
0.80	-0.203	-2.856	-4.770	-5.730	-6.407	-6.663	-6.702	-6.723
0.70	-0.069	-2.225	-4.544	-5.761	-6.521	-6.860	-6.804	-6.780
0.60	0.074	-1.606	-4.114	-5.712	-6.518	-6.865	-6.724	-6.530
0.50	0.187	-0.723	-3.492	-5.508	-6.409	-6.723	-6.530	-6.450
0.40	0.241	-0.185	-2.293	-4.022	-6.234	-6.088	-6.090	-6.459
0.30	0.284	0.133	-0.546	-3.394	-5.910	-5.655	-5.870	-9.595
0.20	0.317	0.256	0.126	-0.041	-4.048	-5.044	-3.065	-9.612

bias in 80 percent point (PERCENT)

alpha*d=	2.000	4.000	6.000	8.000	10.000	12.000	14.000	16.000
albedo								
0.90	0.215	-1.200	-2.812	-3.509	-4.077	-4.073	-4.117	-4.073
0.80	0.296	-0.863	-2.702	-3.716	-4.482	-4.698	-4.770	-4.764
0.70	0.351	-0.445	-2.464	-3.742	-4.677	-5.073	-4.970	-4.770
0.60	0.391	-0.100	-1.976	-3.659	-4.718	-5.190	-4.892	-4.300
0.50	0.420	0.162	-1.299	-3.284	-4.645	-5.138	-4.274	-2.672
0.40	0.442	0.323	-0.195	-1.374	-4.383	-4.863	-3.827	-6.301
0.30	0.459	0.403	0.243	-0.051	-3.862	-4.219	-2.963	-6.289
0.20	0.472	0.448	0.403	0.317	-2.483	-3.840	-2.913	-6.285

results for bias in peak (PERCENT)

alpha*d=	2.000	4.000	6.000	8.000	10.000	12.000	14.000	16.000
albedo								
0.90	0.152	-0.271	-0.695	-0.695	-1.542	-0.695	-1.118	-1.118
0.80	0.152	0.152	-0.695	-1.118	-1.542	-2.388	-2.388	-2.388
0.70	0.152	0.152	-0.271	-1.542	-2.388	-2.388	-3.235	-2.812
0.60	0.152	0.152	-0.271	-1.542	-2.812	-3.235	-3.235	-2.812
0.50	0.152	0.152	0.152	-0.271	-2.812	-4.082	-3.235	-2.812
0.40	0.152	0.152	0.152	-0.271	-2.388	-4.082	-3.235	-2.812
0.30	0.152	0.152	0.152	0.152	-2.812	-4.082	-3.235	-6.623
0.20	0.152	0.152	0.152	0.152	-0.271	0.999	-3.235	-6.623

rise time from one percent point to peak (ns) for 20 meter water

alpha*d=	2.000	4.000	6.000	8.000	10.000	12.000	14.000	16.000
albedo								
0.90	16.418	21.324	22.558	23.408	21.747	23.427	22.507	22.252
0.80	15.638	21.793	22.522	22.879	22.041	20.208	20.201	20.090
0.70	14.858	21.068	23.257	22.327	20.506	20.410	18.602	19.374
0.60	14.026	20.022	22.931	22.617	19.843	18.648	18.639	19.364
0.50	13.287	18.524	23.099	25.469	19.993	16.353	20.918	19.233
0.40	12.714	16.637	21.611	25.464	20.884	15.688	21.126	18.822
0.30	10.516	14.513	19.357	26.140	19.698	14.384	21.168	10.586
0.20	7.178	13.019	15.724	24.787	22.140	22.964	21.093	10.455

3 8398 1000 8690 3
N.O.A.A. CENTRAL LIBRARY

NOAA SCIENTIFIC AND TECHNICAL PUBLICATIONS

The National Oceanic and Atmospheric Administration was established as part of the Department of Commerce on October 3, 1970. The mission responsibilities of NOAA are to assess the socioeconomic impact of natural and technological changes in the environment and to monitor and predict the state of the solid Earth, the oceans and their living resources, the atmosphere, and the space environment of the Earth.

The major components of NOAA regularly produce various types of scientific and technical information in the following kinds of publications:

PROFESSIONAL PAPERS — Important definitive research results, major techniques, and special investigations.

CONTRACT AND GRANT REPORTS — Reports prepared by contractors or grantees under NOAA sponsorship.

ATLAS — Presentation of analyzed data generally in the form of maps showing distribution of rainfall, chemical and physical conditions of oceans and atmosphere, distribution of fishes and marine mammals, ionospheric conditions, etc.

TECHNICAL SERVICE PUBLICATIONS — Reports containing data, observations, instructions, etc. A partial listing includes data serials; prediction and outlook periodicals; technical manuals, training papers, planning reports, and information serials; and miscellaneous technical publications.

TECHNICAL REPORTS — Journal quality with extensive details, mathematical developments, or data listings.

TECHNICAL MEMORANDUMS — Reports of preliminary, partial, or negative research or technology results, interim instructions, and the like.

NATIONAL OCEANIC AND ATMOSPHERIC ADMINISTRATION
NOAA
U.S. DEPARTMENT OF COMMERCE

Information on availability of NOAA publications can be obtained from:

ENVIRONMENTAL SCIENCE INFORMATION CENTER (D822)
ENVIRONMENTAL DATA AND INFORMATION SERVICE
NATIONAL OCEANIC AND ATMOSPHERIC ADMINISTRATION
U.S. DEPARTMENT OF COMMERCE

6009 Executive Boulevard
Rockville, MD 20852

NOAA--S/T 81-153